mTORC2 promotes tumor growth via lipid synthesis

Inauguraldissertation

zur

Erlangung der Würde eines Doktors der Philosophie

vorgelegt der

Philosophisch-Naturwissenschaftlichen Fakultät

der Universität Basel

von

Yakir Guri

aus Israel

Basel, 2016

Genehmigt von der Philosophisch-Naturwissenschaftlichen Fakultät auf Antrag von

Prof. Dr. Michael N. Hall und Prof. Dr. Markus H. Heim.

Basel, den 18.10.2016

Prof. Dr. Jörg Schibler, Dekan

There are no complex lipids, just lipids.

H. Riezman

יגעת ומצאת, האמן

Dedicated to my family

1.2. Table of Contents

1.3. List of diagrams and figures

Introduction

Manuscript

Supplemental Figures

Supplemental Findings

1.4. Summary

mTOR (mammalian target of rapamycin) regulates cell growth and metabolism. mTOR forms two independent complexes, termed mTORC1 (mTOR complex 1) and mTORC2, both are frequently activated in tumors. TSC1 and PTEN are two tumor suppressors and upstream regulators of the mTOR pathway.

To investigate the role of mTOR in liver tumor development, we used mice in which *Tsc1* and *Pten* are deleted in the liver (hereafter referred to as, L-dKO mice). L-dKO mice exhibited sustained mTORC1 and mTORC2 activation, and invariably developed liver tumors. To identify mechanisms governing tumor development, we performed longitudinal unbiased quantitative proteomic and phosphoproteomic analyses on livers from L-dKO mice and littermate controls. Most prominently, fatty acid (FA) and lipid synthesis pathways were up-regulated in L-dKO mice. Indeed, L-dKO mice displayed enhanced hepatic de novo FA synthesis, hepatosteatosis followed by the appearance of tumors. Longitudinal lipidomic analyses of livers from L-dKO mice revealed increased accumulation of sphingolipid (SL) and glycerophospholipid (PL), particularly of cardiolipin (CL). CL accumulation correlated with hyper-tubular mitochondria in hepatocytes and improved oxidative phosphorylation (OxPhos). Inhibition of de novo FA or SL synthesis reduced tumor burden. Furthermore, L-dKO mice preferentially synthesized and accumulated the SL glucosylceramide (GlcCer). To examine whether GlcCer are necessary for tumor development, we knocked down GCS (Glucosylceramide Synthase), the rate-limiting enzyme of GlcCer synthesis. GCS inhibition in hepatocytes reduced tumor burden. Together these data indicates that FA and lipids are required for tumor development.

Lastly, we investigated whether mTORC1 and/or mTORC2 promoted FA and lipid synthesis. Pharmacological inhibition studies indicated that mTORC2 promoted FA synthesis, via SREBP1c. Indeed, genetic deletion of *Rictor*, an essential component of mTORC2, in L-dKO mice (L-TriKO) reduced hepatic FA, CL and SL (GlcCer) accumulation. Importantly, L-TriKO mice also exhibited reduced liver tumor number and size, compared to L-dKO

mice. Thus, mTORC2 promotes FA and lipid accumulation and ultimately tumor development.

Collectively, this thesis provides mechanistic insights for the role of mTORC2 in promoting tumor development, via FA and lipid synthesis. Lipids are required for tumor growth, as macromolecules, but also to support mitochondrial function to match increased energy demand. Inhibition of FA or lipid synthesis pathways kills cancer cells, thus exposing a cancer-specific vulnerability that can be exploited for the rational design of targeted cancer drugs.

1.5. Novel findings

1. Oncogenic mTORC2 promotes fatty acid and lipid synthesis.
2. Cancer cells require fatty acids for growth and proliferation.
3. Cancer cells require sphingolipid, particularly glucosylceramide for growth.
4. mTORC2, via fatty acid and lipids, increases cancer cell biomass and improves mitochondrial function.

Graphical Abstract

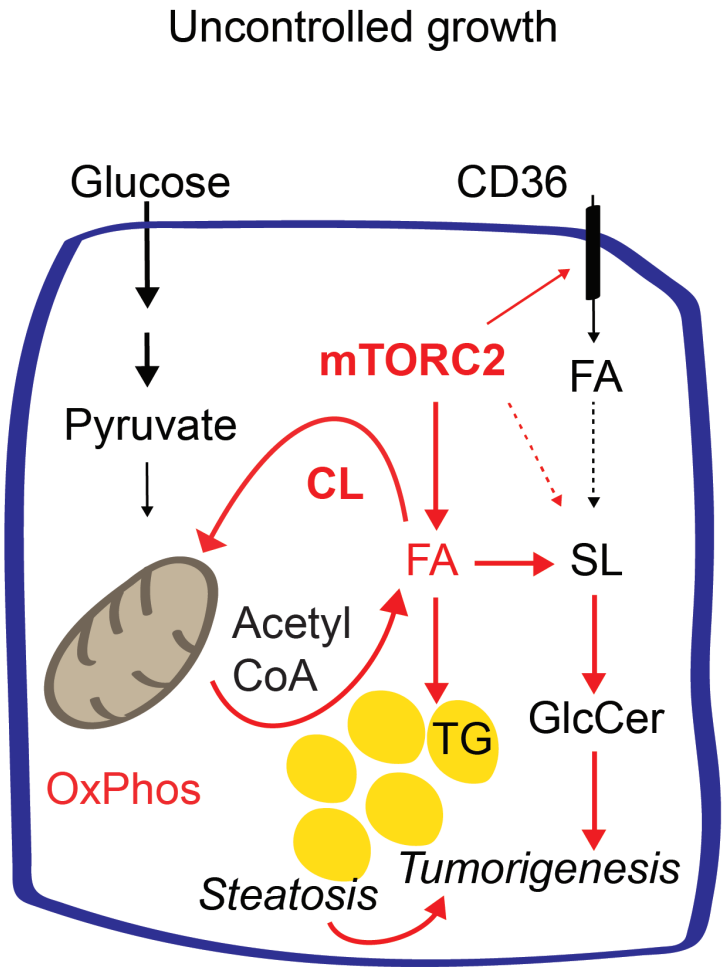

Abbreviation: FA, fatty acid; SL, sphingolipid; GlcCer, glucosylceramide; CL, cardiolipin; TG, triglyceride; OxPhos, oxidative phosphorylation; CD36, fatty acid translocase.

1.6. Acronyms

4E-BP1	Eukaryotic translation initiation factor 4E binding protein 1
ACC	Acetyl-coA carboxylase
ACLY	ATP-Citrate Lyase
ACSL4	Long-chain-fatty-acid-CoA ligase 4
AGC	Protein kinase A, G, and C families
AKT	Rac protein kinase alpha
ALB-Cre	Albumin promoter driven Cre recombinase
ATP	Adenosine triphosphate
CC	Choleangiocarcinoma
CDS	CDP-DAG synthase (CDS 1 or 2)
CL	Cardiolipin (s) a.k.a. diphosphatidylglycerol (s)
CMD-HFD	Choline-methionine deficient high-fat diet
CRLS1	Cardiolipin synthase
CoA	Co-enzyme A (As in Acetyl-CoA)
CDP	Cytidine pyrophosphate
Cer	Ceramide (s)
CerS	Ceramide synthase (isoforms 1 to 6)
DAG	Diacylglycerol or diglyceride
ELOV	Elongation of very long chain fatty acids
ER	Endoplasmic reticulum
ERMES	ER-mitochondrion encounter structure
FASN	Fatty acid synthase
FKBP12	FK506-binding protein 12
FOXO	Forkhead box protein O
FRB	FKBP12 rapamycin binding domain
GBA	Glucosylceramidase beta
GlcCer	Glucosylceramide or glucosylsphingolipid
GPAT	Glycerol 3-phosphate acyltransferase
GCS	Glucosylceramide synthase
HCC	Hepatocellular carcinoma
IMM	Inner mitochondrial membrane
KO	Knockout (genetic)
LCB(s)	long-chain base(s) (SL synthesis)
LIPIN-1	Phosphatidic-acid phosphatase
LKB1	Liver kinase B1
LPA	Lysophosphatidic acid
MAM(s)	Mitochondria associated ER membrane(s)
MFN	Mitofusin (MFN 1 or 2)
mLST8	Mammalian lethal with SEC13 protein 8
mTOR	Mammalian (mechanistic) target of rapamycin
mTORC1	mTOR complex 1
mTORC2	mTOR complex 2
NADPH	Nicotinamide adenine dinucleotide phosphate
NAFLD	Non-alcoholic fatty liver disease
NASH	Non-alcoholic steatohepatitis
NDGR1	N-myc downstream regulated
PA	Phosphatidic acid
PDHC	Pyruvate dehydrogenase complex
PDHK1	Pyruvate dehydrogenase complex kinase 1
PDK1	Phosphoinositide-dependent kinase 1
PE	Phosphatidylethanolamine

PI	Phosphatidylinositol
PI3K	Phosphatidylinositol 3-kinase
PI3P	Phosphatidylinositol 3-phosphate
PL	Phospholipid (also glycerophospholipids)
PLD	Phospholipase D
PPARγ	Peroxisome proliferator-activated receptor gamma
PPP	Pentose phosphate pathway
PS	Phosphatidylserine
PSS1	Phosphatidylserine Synthase-1
PTEN	Phosphatase and tensin homolog deleted on chromosome ten
qPCR	Quantitative PCR
RAG	RAS-related GTP-binding protein
REHB	RAS homologue enriched in brain
RAPTOR	Regulatory associated protein of mTOR complex 1
RICTOR	Rapamycin insensitive companion of mTOR
RTK	Receptor tyrosine kinase(s)
S6K	Ribosomal protein S6 kinase
SCD1	Stearoyl-CoA Desaturase 1
SGK1	Serum/glucocorticoid regulated kinase 1
SIN1	SAPK (stress-activated protein kinase)-interacting protein 1
SM	Sphingomyelin (s)
SMase	Sphingomyelinase (neutral or a lysosomal)
SPT	Serine palmitoyltransferase (a.k.a. long chain base subunit 1)
SREBP-1	Sterol regulatory element binding protein-1
TCA	Tricarboxylic acid cycle or citric acid cycle
TG	Triacylglyceride or Triglyceride
TSC	Tuberous sclerosis complex
ULK1	Unc-51-like kinase 1
WT	wild type or control (genetic)
UDP	Uridine diphosphate (pyrimidine nucleotide)
VLCFA(s)	Very long chain fatty acid(s)

2.0. Introduction

2.1. Fatty acids

2.1.1. Fatty acid synthesis

Fatty acid (FA) synthesis is induced by growth factors, through the transcription factor SREBP-1c (Sterol Regulatory Element-Binding Protein-1). SREBP-1c is produced as inactive precursor, upon cleavage (SREBP-1c mature) it translocates to the nucleus (Wang, Sato et al. 1994). Mature SREBP-1c stimulates the expression of genes involved in FA biosynthesis, including *Acac, Fasn*, *Scd1* and *Elovl6* (Jeon and Osborne 2012) (Diagram 1). FA synthesis requires acetyl groups that are derived from the tricarboxylic (TCA) cycle, in the form of citrate. Citrate exits the mitochondrion to the cytoplasm via a 'citrate shuttle'. ACLY (ATP-Citrate Lyase) converts cytoplasmic citrate into acetyl-CoA and oxaloacetate. Oxaloacetate can be converted into pyruvate, generating NADPH that replenishes reducing power for lipid synthesis. ACC (Acetyl-CoA Carboxylase) converts acetyl-CoA to malonyl-CoA. Acetyl and malonyl groups are then coupled to the acyl-carrier protein domain of FASN (Fatty Acid Synthase). FASN by repeated condensation steps generates palmitate (basic 16 carbon unit). Palmitate is introduced with a double bond in the Δ9 position by SCD1 (Stearoyl-CoA Desaturase 1), thereby generating mono-unsaturated FAs (MUFA). Other FA desaturases (FADS) generate highly polyunsaturated fatty acids (PUFA) mainly from dietary essential PUFA (Lee, Lee et al. 2016). FAs can be further elongated by ELOVL (Elongation Of Very Long Chain Fatty Acids), a family of seven enzymes (ELOVL1-7) with different chain length and saturation affinities (Guillou, Zadravec et al. 2010). The ER localized ELOVL1-7 synthesize long chain fatty acids (VLCFAs), by adding two carbons in each cycle. Once generated, the various FAs have many fates, including being stored for energy, incorporated into membrane or signaling.

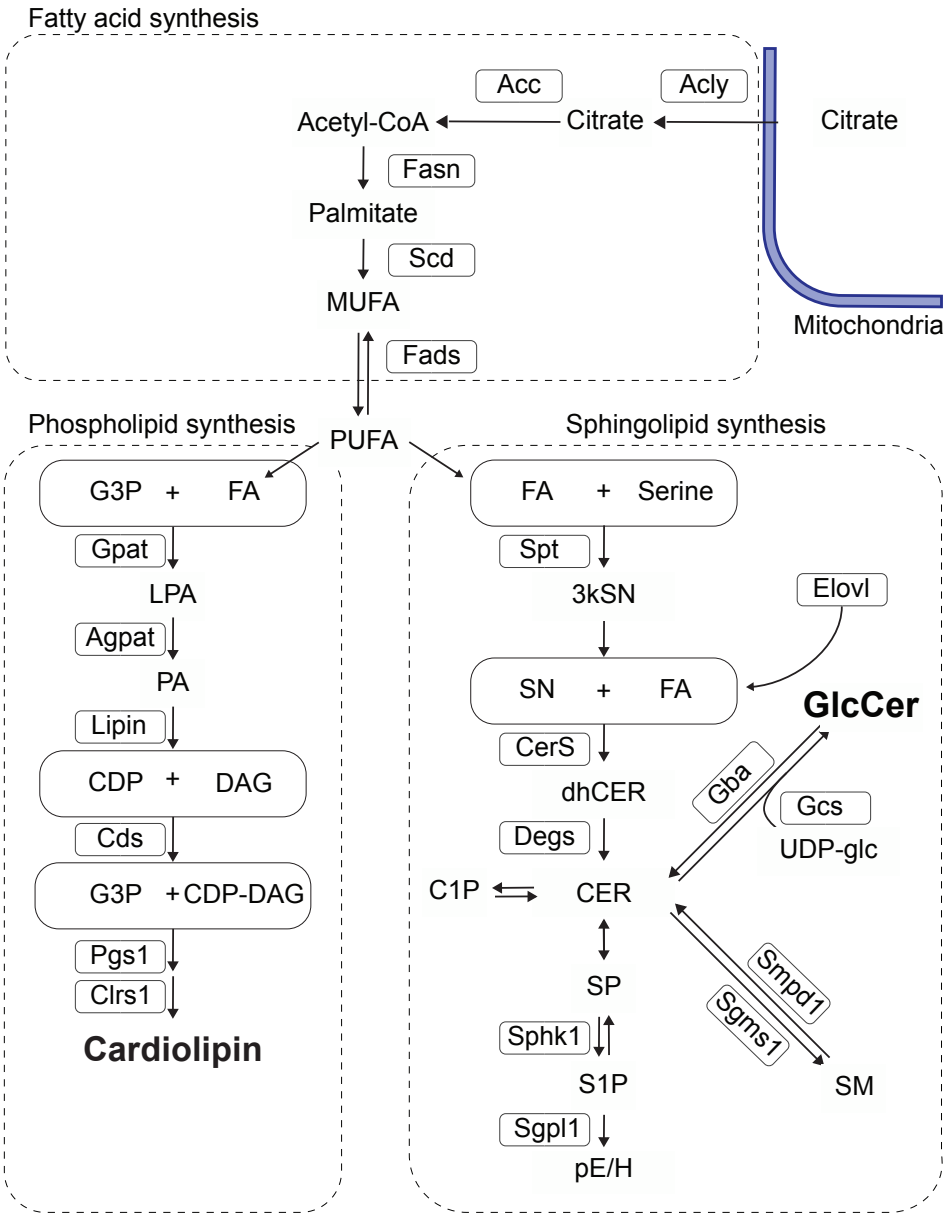

Diagram 1. De novo fatty acid and lipid synthesis. For simplification selected enzymes are depicted.

2.2. Lipids

2.2.1. Lipid synthesis: Sphingolipids

Sphingolipid (SL) is a group of lipids in which FAs are linked via amide bonds to a long-chain base (LCB), also called sphingoid (Christie 2013). SL requires the amino acid serine as the backbone to which acyl chains are attached (Diagram 2). The synthesis of SL begins at the ER, where two important precursors: LCB and VLCFA are produced (the latter described above). Generation of LCB is the rate-limiting reaction for de novo SL biosynthesis, catalyzed by SPT (Serine Palmitoyltransferase) (Breslow 2013). SPT condense serine and palmitoyl-CoA to generate 3-keto-dihydrosphingosine (also known as 3-keto-sphinganine, 3kSN), which is then reduced to yield the LCB dihydrosphingosine (also known as sphinganine, SN). LCB is N-acylated, with fatty acids of different lengths, by CerS (Ceramide Synthase, isoforms 1 to 6) to produce dihydroceramide (dhCER). CerS1-6 exhibits different FA specificities, hence the structural heterogeneity among SL species. Fatty acids used for sphingolipid synthesis are produced by ELOVL (see above). Ceramides undergo headgroup modifications in the Golgi apparatus to yield Sphingomyelin (SM) or glucosylceramide (GlcCer). GCS (glucosylceramide synthase) catalyzes the rate-limiting step of GlcCer synthesis, adding glucose (obtained from UDP-glucose) to ceramide.

The reverse reactions of most steps described above delineates the SL catabolism (Diagram 1). SM hydrolysis by membrane bound nSMase (neutral-Sphingomyelinase, a.k.a SMPD2 or 3) or lysosomal aSMAse (acid-SMase, a.k.a SMPD1) yields in ceramide and phosphocholine. Similarly, glycohydrolases such as GBA (glucosylceramidase beta) and GBA2 remove head group from GlcCer, thereby counteracting the action of GCS. Sphingolipid production is tuned in response to metabolic needs. For example, alterations in cellular serine concentration affect SPT activity, while sphingolipid level may reduce that of serine (Cowart and Hannun 2007). Another mode of regulation is via the ORMDL (mammalian homologues of the yeast ORM) that inhibit SPT activity (Siow, Sunkara et al. 2015, Siow, Sunkara et al. 2015).

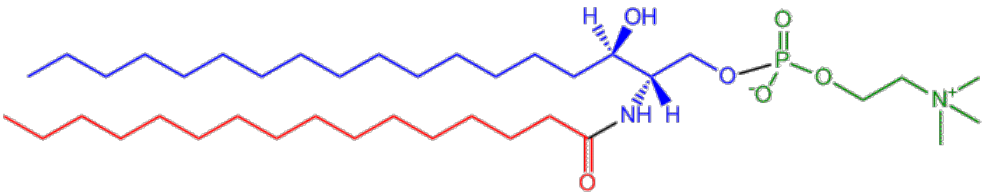

Diagram 2. Sphingolipid Structure. Sphingoid Base, N-Acyl group, Headgroup. Adapted from LIPID MAPS, www.lipidmaps.org.

2.2.2. Lipid synthesis: Glycerophospholipids

Glycerophospholipid (PL) contain fatty acids esterified (*sn*-1 - 2) to a glycerol backbone and a head group connected by a phosphate (*sn*-3) (Diagram 3) (Aguilera-Romero, Gehin et al. 2014). GPAT (glycerol 3-phosphate acyltransferase, isoforms GPAT1 to 3) generates lysophosphatidic acid (LPA), adding a fatty acid to glycerol 3-phosphate on the sn-1 position (Diagram 1). LPA is then converted by AGPAT (Acylglycerol-3-Acyltransferase) to a phosphatidic acid (PA). PA can be used for the synthesis of PL in two mechanisms that require nucleotides (described below). PAP (Phosphatidic Acid Phosphatase), also known as lipin (isoforms 1 to 3), converts PA to diacylglycerol (DAG). DAG is covalently connected to a long chain fatty acid by DAGT (Diglyceride Acyltransferase 1 or 2), generating triacylglyceride (TG) that can be stored in lipid droplets. Alternatively, DAG is connected choline or ethanolamine (from a nucleotide cytidine pyrophosphate carrier, CDP-choline or -ethanolamine), thereby generating phosphatidylcholine (PC) or phosphatidylethanolamine (PE), respectively (Gibellini and Smith 2010). Instead, DAG is connected to CDP yielding the liponucleotide, CDP-DAG (Diagram 1). CDP-DAG generated by CDS (CDP-DAG synthase 1 or 2), is required for the synthesis of the glycerophospholipids phosphatidylinositol (PI), phosphatidylserine (PS) and cardiolipin (CL, a.k.a. diphosphatidylglycerol).

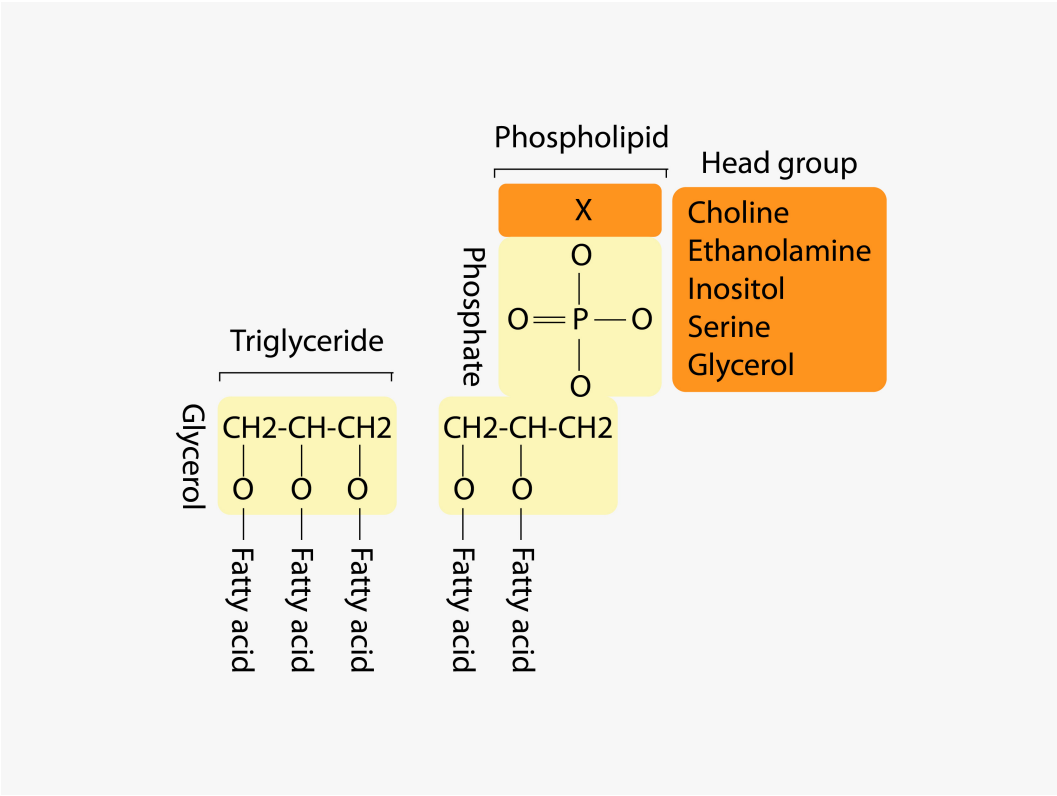

Diagram 3. Glycerophospholipid structure. PL can be divided into different subgroups (defined by the head-group). The head group can consist of choline, ethanolamine, inositol, serine or glycerol. Modified from (Burri, Hoem et al. 2012).

2.2.3. Cardiolipin

CLs are exclusively synthesized in the mitochondria (Schlame and Haldar 1993, Schlame, Rua et al. 2000). The rate-liming step in CL biosynthesis is catalyzed by PGS1 (Phosphatidylglycerol-phosphate Synthase 1). PGS1 condenses the liponucleotide CDP-DAG and glycerol-3-phosphate (releasing a CMP), producing a short-lived phosphatidylglycerol-phosphate (PGP). PGP is dephosphorylated by the PTEN-like mitochondrial phosphatase PTPMT1, generating a phosphatidylglycerol (PG) (Zhang, Guan et al. 2011). Cardiolipin synthase (CRLS1) links PG to a CDP-DAG (yet another liponucleotide molecule), synthesizing an immature CL. CL is then remodeled into a mature tetralinoleoyl-CL (4 linoleolic acid chains (C18:2)), by several enzymes. The catalytic center of the mitochondrial protein CRLS1 is exposed to the matrix side of the inner mitochondrial membrane (IMM) (Schlame and Haldar 1993, Schlame, Rua et al. 2000). CL lodged in the IMM,

providing stability for the enzyme complexes involved in energy production (Houtkooper and Vaz 2008, Duncan, Robinson et al. 2016). Furthermore, CLs appears to be important for mitochondrial fusion (Joshi, Thompson et al. 2012), which is associated with improved mitochondrial function (van der Bliek, Shen et al. 2013, Yu-Wai-Man, Carelli et al. 2014). Thus, FAs are used also for CL synthesis, which is required for mitochondria function.

2.3. The TOR signaling pathway

2.3.1. mTORC1 and mTORC2 components

The evolutionarily conserved serine/threonine kinase Target of Rapamycin (TOR) integrates various stimuli to control the metabolic pathways that drive cell growth. TOR forms two structurally and functionally separate protein complexes termed TOR Complex 1 (TORC1) and TORC2 (Wullschleger, Loewith et al. 2006, Laplante and Sabatini 2012). Mammalian TORC1 (mTORC1) contains mTOR, mLST8 (mammalian lethal with sec-13 protein 8), and RAPTOR (regulatory associated protein of mammalian target of rapamycin). mTORC2 contains mTOR, mLST8, mSIN1 (mammalian stress-activated map kinase-interacting protein 1), and RICTOR (rapamycin-insensitive companion of mTOR) (Diagram 4).

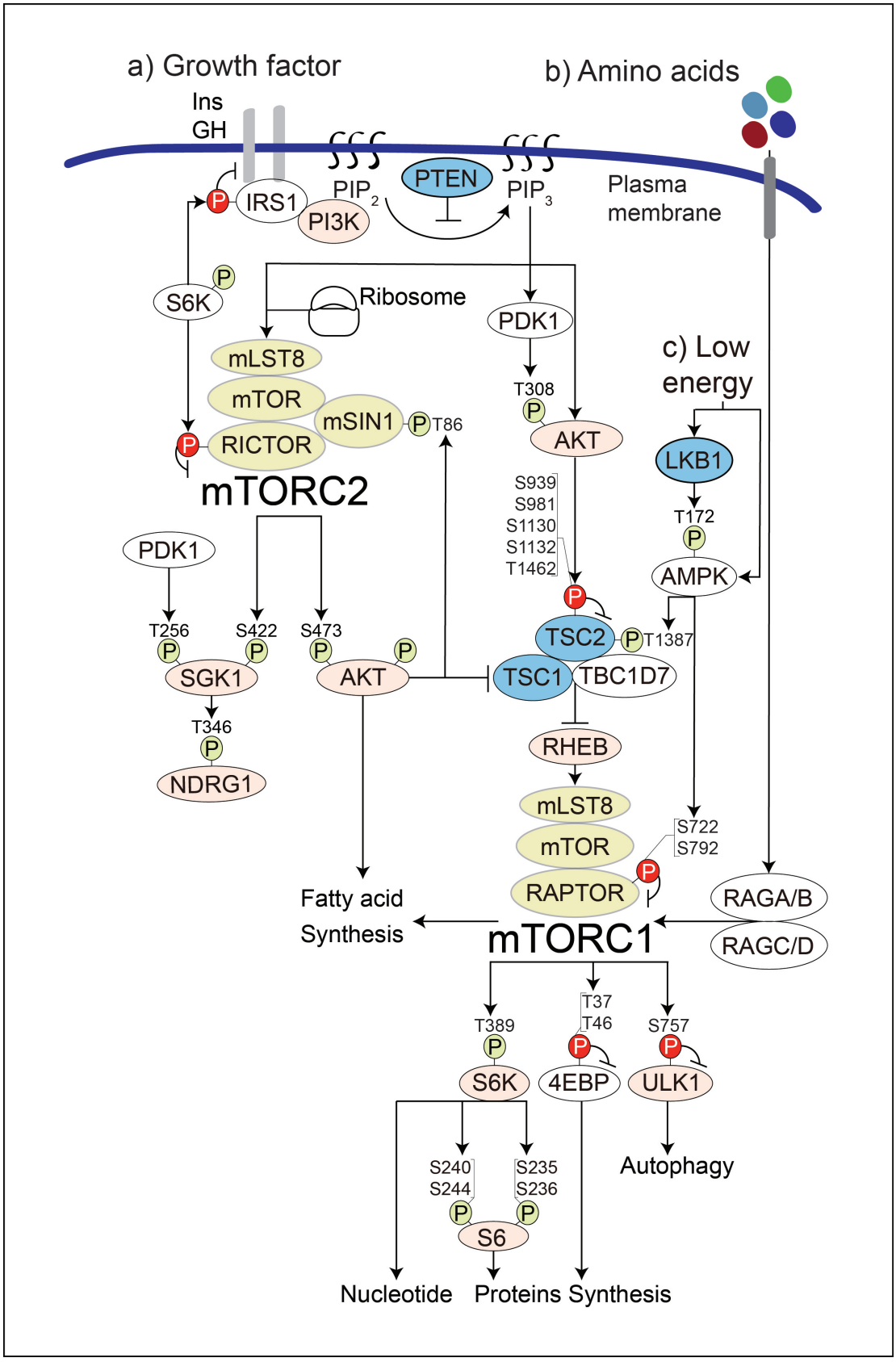

Diagram 4. The mTOR-signaling pathway. mTOR promotes anabolic and inhibits catabolic processes and ultimately leads to cell growth (Yakir Guri 2016).

2.3.2. Upstream of mTORC1 and mTORC2

mTORC1 is activated by amino acids, cellular energy and growth factors (Dibble and Manning 2013, Shimobayashi and Hall 2014). Growth factors and cellular energy stimulate mTORC1 via inhibition of a heterotrimeric protein complex consisting of tuberous sclerosis complex 1 (TSC1), TSC2 and TBC1D7 (TRE2-BUB2-CDC16 domain family member 7) (Inoki, Li et al. 2002, Kenerson, Aicher et al. 2002, Manning, Tee et al. 2002, Tee, Manning et al. 2003, Sancak, Peterson et al. 2008), referred to as the TSC complex. mTORC1 is activated by amino acids through the RAG (RAS-related GTP-binding protein) family of small GTPases (Long, Lin et al. 2005, Kim, Goraksha-Hicks et al. 2008). RAGA or RAGB forms heterodimer with either RAGC or RAGD. Amino acids stimulate the conversion of the RAG heterodimers to the active conformation, in which RAGA or RAGB is loaded with GTP and RAGC or RAGD is loaded with GDP. Once activated, RAG heterodimer recruits mTORC1 to the surface of the lysosome to bind GTP-loaded RHEB (RAS homologue enriched in brain), thereby activating mTORC1 (Dibble and Cantley 2015).

Growth factors bind RTK (Receptor Tyrosine Kinases) to activate phosphatidylinositol-4,5-bisphosphate 3-kinase (PI3K). PI3K generates phosphatidylinositol-3,4,5-trisphosphate (PIP3) by phosphorylating the membrane phospholipid phosphatidylinositol-4,5-bisphosphate (PIP2) (Pearce, Komander et al. 2010). PIP3 recruits PDK1 (Phosphoinositide-Dependent Kinase 1) and AKT to the plasma membrane, where PDK1 phosphorylates AKT at Thr308 (Alessi, James et al. 1997). PTEN (Phosphatase and Tensin Homolog Deleted on Chromosome 10) negatively regulated the mTOR signaling, by converting PIP3 to PIP2, thereby counteracting the activity of PI3K. AKT inhibits the TSC complex by phosphorylating TSC2, of the TSC complex (Menon, Dibble et al. 2014). The TSC complex is a GAP (GTPase-Activating Protein) for RHEB (RAS Homologue Enriched in Brain). High AMP/ATP ratio (low cellular energy level) activates AMPK (AMP-Activated Protein Kinase). AMPK phosphorylates TSC2, thereby stimulating the GAP activity of the TSC complex towards RHEB, to inhibit mTORC1 (Corradetti, Inoki et al. 2004,

Inoki, Ouyang et al. 2006). AMPK also inhibits mTORC1 via phosphorylation of RAPTOR. When intracellular ATP level are high, AMPK is inactive, relieving the mTORC1 inhibition.

Mechanisms of mTORC2 activation are less defined (Sparks and Guertin 2010, Shimobayashi and Hall 2014). Growth factors activate mTORC2 by promoting its association with ribosomes, in a PI3K dependent manner (Frias, Thoreen et al. 2006, Yang, Inoki et al. 2006, Zinzalla, Stracka et al. 2011). Recently, PI3K was suggested to trigger mTORC2 activation via PIP_3 interaction with the PH domain of mSIN1 (Liu, Gan et al. 2015).

2.3.3. Downstream of mTORC1 and mTORC2

mTOR signaling promotes anabolic and inhibits catabolic processes. mTORC1 controls protein synthesis via S6K (ribosomal protein S6 kinase) and 4E-BPs (4E binding proteins). mTORC1 phosphorylates 4E-BPs, which is then dissociated from eIF4E (eukaryotic translation initiator factor 4E). eIF4E in its free form bind eIF4G at the 5' end of mRNAs, thereby promoting cap-dependent translation initiation. mTORC1 phosphorylates S6K at the Thr389 leading to its activation. Active pS6K phosphorylates and activates S6 ribosomal protein on several residues (Ser235, Ser236, Ser240 and Ser244) (Ben-Sahra, Howell et al. 2013, Robitaille, Christen et al. 2013). S6, in turn, stimulates the expression of several genes involved in ribosome biosynthesis (Chauvin, Koka et al. 2014). S6K also regulates protein biosynthesis via direct phosphorylation of other proteins involved in translation or mRNA processing, including eIF4B, eIF2K and PDCD4 (reviewed in (Shimobayashi and Hall 2014)). mTORC1-S6K phosphorylates and inhibits the autophagy activating Unc-51-like kinase 1 (ULK1) [Reviewed in (Mamane, Petroulakis et al. 2006, Ma and Blenis 2009, Kim, Kundu et al. 2011)]. Thus, mTORC1 regulates protein synthesis on multiple levels and inhibits autophagy.

mTORC2 regulates several cellular processes via the AGC kinase family members AKT, protein kinase C α (PKCα), and serum/glucocorticoid-regulated kinase (SGK) [reviewed in (Cybulski and Hall 2009, Sparks and Guertin 2010)]. mTORC2 controls the actin cytoskeleton organization

through PKCα, paxilin and the small GTPases RHO and RAC (Jacinto, Loewith et al. 2004, Sarbassov, Ali et al. 2004).

In a positive feedback loop, AKT phosphorylates mSIN1-Thr86 in mTORC2 (Yang, Murashige et al. 2015). In a negative feedback loop, mTORC1 via S6K phosphorylates and inhibits the IRS-1 (Insulin Receptor Substrate 1), thereby dampening PI3K-AKT signaling (Takano, Usui et al. 2001, Um, Frigerio et al. 2004). The macrolide rapamycin acutely inhibits mTORC1. The ATP-site competitive inhibitor, INK128 inhibits both mTORC1 and mTORC2 (Benjamin, Colombi et al. 2011). mTOR, often in the context of positive and negative feedback loops, is a node for convergence and crosstalk of several oncogenic pathways (Diagram 4) (Efeyan and Sabatini 2010, Chandarlapaty, Sawai et al. 2011, Shimobayashi and Hall 2014, Eltschinger and Loewith 2016).

2.3.4. mTOR promotes fatty acid and nucleotide synthesis

mTOR promotes FA synthesis (Ricoult and Manning 2013, Albert and Hall 2015, Caron, Richard et al. 2015). However, conflicting evidences exist regarding the specific contribution of mTORC1 and mTORC2. As mentioned above, FA synthesis is activated by the transcription factor SREBP-1c. AKT transcriptionally regulates SREBP-1c (Porstmann, Griffiths et al. 2005). In retinal pigment cells and mouse derived embryonic fibroblasts, mTORC1 induced SREBP-1c processing via S6K (S6 kinase) (Porstmann, Santos et al. 2008, Duvel, Yecies et al. 2010) (Diagram 5). In rat liver, SREBP-1c expression was blocked by rapamycin, but this appeared to be independent of S6K (Li, Brown et al. 2010). In another mechanism, mTORC1 phosphorylates the phosphatidic-acid phosphatase, lipin-1. Lipin-1 is an inhibitor of SREBP-1, once phosphorylated lipin-1 is excluded from the nucleus, thereby allowing SREBP-1 to induce FA synthesis (Peterson, Sengupta et al. 2011). Together, these studies suggest that mTORC1 promotes de novo lipogenesis via SREBP-1c.

Several lines of evidences question the role of mTORC1 in promoting hepatic de novo lipogenesis. First, liver-specific *Tsc1* knockout mice (exhibiting constitutive active mTORC1) do not exhibit increased SREBP-1c

expression or de novo lipogenesis. Moreover, these mice are protected from age and diet induced hepatosteatosis (Yecies, Zhang et al. 2011, Cornu, Oppliger et al. 2014). This was suggested being due to mTORC1-S6K mediated negative feedback loop, and reduced PI3K-AKT-mTORC2 signaling. However, as recently demonstrated, *Tsc1* and *S6K* double knockout mice fed high-fat diet displayed increased hepatic TG content, but exhibited unchanged mTORC2 signaling (Kenerson, Subramanian et al. 2015). Although more experiments are required, the latter study suggests that the effect of mTORC1 on hepatic TG content is independent of the negative feedback loop. Furthermore, rapamycin treatment failed to prevent hepatic steatosis in liver-specific *Pten* knockout mice, in which both mTORC1 and mTORC2 are ectopically activated (Kenerson, Yeh et al. 2011), also suggesting the hepatosteatosis in these mice is independent of mTORC1. Lastly, adenovirus-mediated hepatic *Raptor* knockdown did not alter hepatic triglyceride (TG) content in mice; reduction of hepatic TG was observed only when mice were fed high fat diet (Peterson, Sengupta et al. 2011). More recently, liver-specific *Raptor* knockout mice were generated (driven by an albumin promoter), and exhibited no change in hepatic TG content even when are fed with high-fat diet (Umemura, Park et al. 2014). In contrast, liver-specific *Rictor* knockout mice (abrogated mTORC2 activity) exhibited reduced SREBP-1c expression and hepatic TG content (Hagiwara, Cornu et al. 2012, Liu, Gan et al. 2013), indicating that mTORC2 promotes hepatic de novo synthesis, and probably not mTORC1.

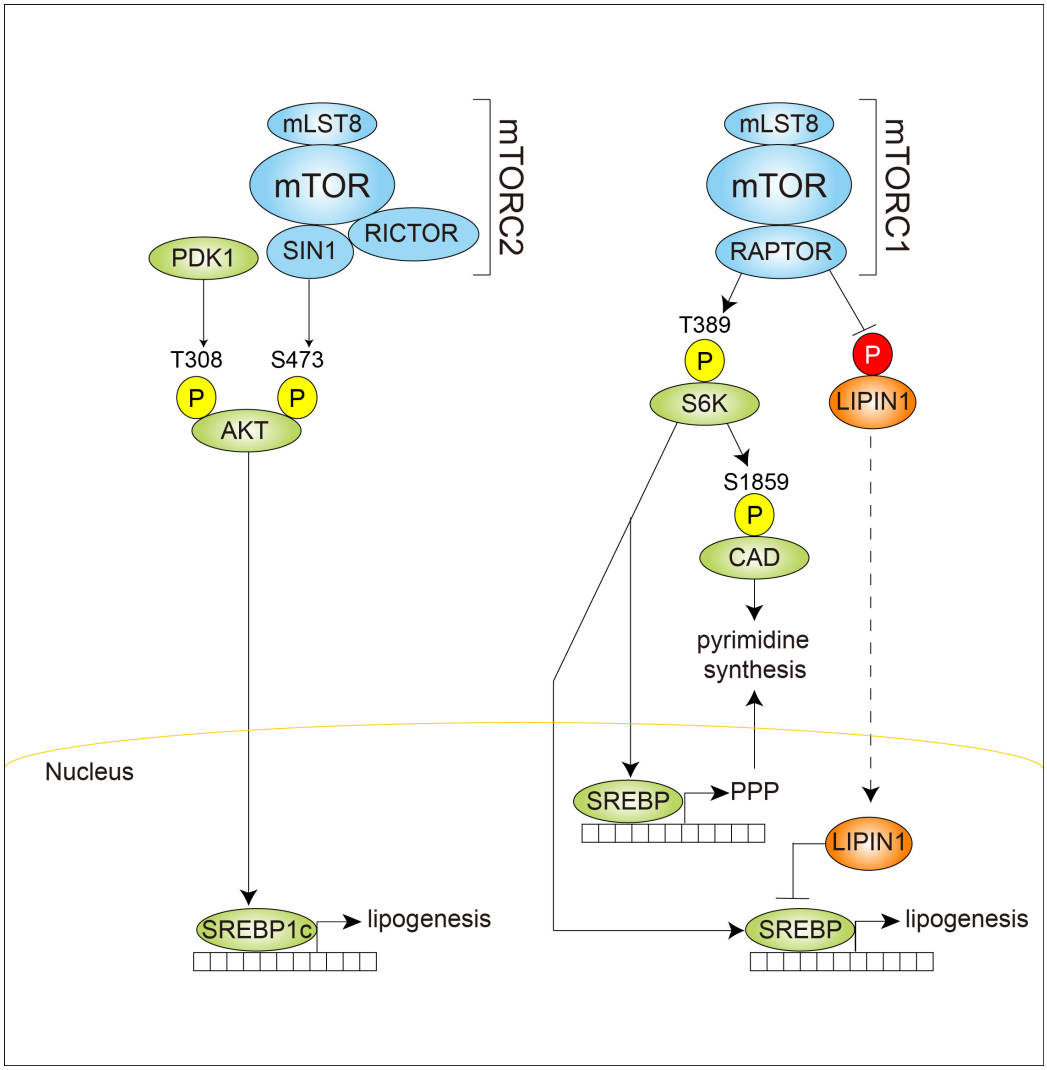

Diagram 5. mTOR promotes lipid synthesis via SREBP. (Shimobayashi and Hall 2014).

FA provides essential building block for lipid synthesis. Except, lipid synthesis requires other constituents, such as nucleotides, and reducing power in the form of NADPH. Such constituents can be obtained from the pentose phosphate pathway (PPP) and nucleotide synthesis pathways. In that regard, mTOR provides another mode of regulation for lipid synthesis.

mTORC1 activates PPP, thereby stimulating synthesis of precursors for nucleotide biosynthesis and generates NADPH (Duvel, Yecies et al. 2010). Furthermore, mTORC1 phosphorylates (Ser1859) and activates CAD (Carbamoyl Phosphate Synthetase 2, Aspartate Transcarbamylase, and Dihydroorotase) (Ben-Sahra, Howell et al. 2013, Robitaille, Christen et al. 2013). CAD is a tri-functional enzyme that catalyzes the first three steps in

the de novo pyrimidine biosynthesis. Pyrimidines (uracil, thymine and cytosine) are high-energy molecules that drive molecular reactions. As described above, the rate-limiting steps of the lipids GlcCer and CL requires uridine and cytidine, respectively. mTORC1 promotes transcriptionally the expression of enzymes contributing to purine synthesis, also in cancer cell lines (Ben-Sahra, Hoxhaj et al. 2016). mTORC2 does not drive nucleotide biosynthesis, but might do so by stimulating the expression of the PPP via activation of SREBP-1c. Thus, mTOR signaling, FA, lipid and nucleotide synthesis are functionally related.

2.3.5. mTORC2 is functionally at MAM

mTORC2 is at the contact sites between mitochondria and endoplasmic reticulum (ER), also known as the mitochondria-associated membrane (MAM) (Vance 1990, Betz, Stracka et al. 2013). Tethering of mitochondria to the ER is mediated mainly by IP3R-Grp75-VDAC1 complex or the dimer MFN1 (Mitofusin 1) and MFN2 (Raturi and Simmen 2013). MAM is enriched in enzymes involved in calcium signaling and lipid metabolism (Dennis and Kennedy 1972). mTORC2 is necessary for efficient calcium transmission from the ER to the mitochondria (Bononi, Missiroli et al. 2012, Betz, Stracka et al. 2013). From lipid synthesis standpoint, several enzymes of the PL biosynthesis are at MAM, including DGAT 2, PEMT2 (Phosphatidylethanolamine N-Methyltransferase), ACSL4 (Acyl-CoA Synthetase Long-Chain Family Member 4) and PSS1 (Phosphatidylserine Synthase 1). Noteworthy, liver-specific *Rictor* knockout mice displayed reduced MAM formation (Betz, Stracka et al. 2013) and reduced TG synthesis (Hagiwara, Cornu et al. 2012). Thus, mTORC2 is functionally at MAM, an important site for lipid synthesis (Betz and Hall 2013, Betz, Stracka et al. 2013), and may account for its role in promoting lipid synthesis.

2.4. mTOR signaling in cancer

mTORC1 and mTORC2 are frequently activated in cancer (Dazert and Hall 2011, Yecies and Manning 2011, Zoncu, Efeyan et al. 2011, Laplante and Sabatini 2012, Bhat, Sonenberg et al. 2013, Cornu, Albert et al. 2013, Albert and Hall 2015, Mischel 2015). mTORC1 is aberrantly activated in human tumor syndromes, such as neurofibromatosis (NF1/2 mutations), Cowden's (PTEN mutation), Peutz-Jeghers and tuberous sclerosis complex (TSC1/2 mutations) and Lymphangioleiomyomatosis (LAM) (TSC2 mutations) (Inoki and Guan 2009, Mester and Charis 2015, Ngeow and Eng 2016). Mice with liver-specific deletion of *Tsc1* (Menon, Yecies et al. 2012) or *Pten* (Horie, Suzuki et al. 2004, Stiles, Wang et al. 2004) develop liver cancer at about one year of age. mTORC1 promotes tumor development by increasing protein synthesis via phosphorylation of 4E-BP1 and S6K1 (Dowling, Topisirovic et al. 2010). Possibly by stimulating selective translation of oncogenes (Hsieh, Liu et al. 2012) or by promoting translational elongation (Faller, Jackson et al. 2015) and c-Myc expression (Csibi, Lee et al. 2014) (Reviewed in (Hsieh and Ruggero 2010, Pelletier, Graff et al. 2015))

mTORC2 is also required for tumor development (Guertin, Stevens et al. 2009), but much less is known about the mechanism(s). In glioblastoma multiforme with EGFRvIII (Epidermal Growth Factor Receptor, variant III) amplification, RICTOR acetylation and enhanced mTORC2 activity was observed (Masui, Tanaka et al. 2013, Masui, Cavenee et al. 2014, Masui, Tanaka et al. 2015, Mischel 2015). mTORC2 appeared to promote cancer drugs resistance, via the nuclear factor NF-kappa-B (NF-κB) (Tanaka, Babic et al. 2011), or via transcriptional regulation of the oncoprotein c-MYC (Masui, Tanaka et al. 2013).

2.4.1. mTOR in metabolic reprogramming of cancer cells

Cancer cells sustain growth and proliferation by activating distinct metabolic features (Schulze and Harris 2012). As such, cancer cells adapt to changes in their microenvironment (oxygen, pH, glucose or nutrient concentrations), a process referred to as metabolic 'rewiring' or 'reprogramming' (DeBerardinis, Lum et al. 2008, Pavlova and Thompson 2016). mTOR is both central

controller of cellular metabolism and a convergence node for several oncogenic pathways (Mendoza, Er et al. 2011, Eltschinger and Loewith 2016). Therefore, metabolic flexibility in tumors might be a direct or indirect effect of cells displaying oncogenic mutation that activate mTOR.

In the presence of oxygen, non-cancerous cells transport cytosolic pyruvate into the mitochondria. Mitochondrial pyruvate is then decarboxylated to form acetyl-CoA (coenzyme A) by the pyruvate dehydrogenase (PDH) complex (PDHC). Acetyl-CoA is required for oxidative phosphorylation and lipid biosynthesis (Pietrocola, Galluzzi et al. 2015). In contrast, rapidly proliferating cells convert excess of pyruvate to lactate (aerobic glycolysis a.k.a 'Warburg effect') (Warburg 1956). As a result, rapidly proliferating cells exhibit compensatory increase in glucose uptake and lactate production. PDH kinase 1 (PDHK1) phosphorylates and inactivates mitochondrial PDH and consequently the PDHC, allowing glycolytic metabolites (carbon sources) be diverted to fuel anabolic processes including, de novo serine, pentose and lipid synthesis (Kim, Tchernyshyov et al. 2006, Papandreou, Cairns et al. 2006, Hitosugi, Fan et al. 2011, Olson, Schell et al. 2016).

Recent studies suggest a central role for mTOR signaling in controlling cancer cell metabolic reprogramming (Pavlova and Thompson 2016). For example, cancer cells exposed to the glycolysis inhibitor (2-DG) exhibited sustained mTORC1 activity and enhanced mitochondrial and growth (Pusapati, Daemen et al. 2016). mTORC1 activation appeared to be via glutaminolysis (Duran and Hall 2012, Duran, Oppliger et al. 2012), these data suggests that mTORC1 can be activated by the tumor-metabolic environment. Indeed, glutamine-activated mTORC1 was recently shown to underlie resistance to angiogenesis inhibitors (Allen, Mieville et al. 2016, Jimenez-Valerio, Martinez-Lozano et al. 2016, Pisarsky, Bill et al. 2016). mTORC2 addicted cancer cell lines also exhibited increased mitochondrial activity, probably in addition to aerobic glycolysis (Colombi, Molle et al. 2011). Collectively, the above indicates that mTOR promotes cancer, via activation of distinct metabolic pathways to increase cell mass and proliferation.

2.4.2. Lipids and cancer

Cancer cells display elevated FA synthesis, while non-cancer cells rely on exogenous sources (bloodstream) (Medes, Thomas et al. 1953, Spirtes, Medes et al. 1953). Enzymes involved in FA synthesis ACC, FASN, SCD1 and ELOVL6 are frequently upregulate, across cancer types (Medes, Thomas et al. 1953, Spirtes, Medes et al. 1953, Kuhajda, Jenner et al. 1994, Li, Ding et al. 1994, Menendez and Lupu 2007, Flavin, Peluso et al. 2010, Park, Lee et al. 2010, Santos and Schulze 2012, Baenke, Peck et al. 2013, Bae, Oh et al. 2016, Feng, Chen et al. 2016, Peck and Schulze 2016). However, to date, the regulation and function of lipid accumulation remains elusive.

As described above, under physiological conditions mTOR promotes FA synthesis. Whether mTOR can promote cancer via an increase of FAs is poorly defined. High-grade *Pten* mutated prostate tumors displayed cholesteryl-ester accumulation in lipid droplets, suggesting a role for PI3K-AKT in altering lipid droplet composition in tumors (Yue, Li et al. 2014). Breast cancer cell lines expressing oncogenic PI3K or K-RAS exhibit enhanced de novo FA synthesis, which appeared to be mediated by mTORC1 (Ricoult, Yecies et al. 2015). While others suggested that mTORC2 may promote tumor progression via the expression of FASN (Li, Pilo et al. 2016). Thus, further studies are required to elucidate the oncogenic role of mTORC1 and/or mTORC2 and FA synthesis.

FAs are the building blocks of lipids (described above). However, to our knowledge, no study examined the role of mTOR signaling in mediating lipid synthesis in tumors. Owing to technological advances, tumor lipid phenotype can be determined, in particular abundance, composition and spatial distribution (Beloribi-Djefaflia, Vasseur et al. 2016). Indeed, breast tumors, compared to adjacent non-tumor tissue, displayed a unique ‘phosphilipid signature’ (Hilvo, Denkert et al. 2011, Guenther, Muirhead et al. 2015). Similarly, invasive breast cancer cells displayed poly-unsaturated fatty acids incorporated to PI, as compared to in situ carcinoma (non-invasive). Thus, changes in lipid composition/accumulation are associated with cancer aggressiveness (Kawashima, Iwamoto et al. 2013). Unlike breast cancers, renal cell and hepatocellular carcinoma exhibited increased

phosphatidylglycerol (PG), a CL precursor. Altered CL composition was reported in mitochondria from different brain tumors (astrocytoma, ependymoblastoma and microglioma) (Kiebish, Han et al. 2008). Suggesting a cancer-specific alteration in CL composition. This data suggests that various oncogenic pathway induce changes in lipid abundance and composition.

In pancreatic tumors, enhanced cholesterol uptake appeared to activate ERK1/2 pathway (Guillaumond, Bidaut et al. 2015). Thus, not only oncogenic signaling alters lipid composition, but also lipids can activate oncogenic pathways, thereby amplifying oncogenic signaling.

Sphingolipids may promote or inhibit tumors. Ceramide is a potent 'tumor suppressor lipid', by inducing apoptosis or autophagy. Autophagy, however, can also yield cancer cell survival. Overall, cancer cell preferentially upregulate ceramide degrading enzymes, thereby escaping apoptosis. One such pathway, to promptly eliminate ceramide, is by ceramide glycosylation. Ceramide glycosylation is chiefly catalyzed by glucosylceramide synthase (GCS), thereby providing an escape route from ceramide-induced apoptosis (Liu, Han et al. 2000, Ogretmen and Hannun 2004, Gupta, Patwardhan et al. 2010, Gupta, Bhinge et al. 2012, Kartal Yandim, Apohan et al. 2013, Liu, Hill et al. 2013, Tyler, Johansson et al. 2015).

2.4.3. NAFLD and liver cancer

Liver cancer is the fifth most common cancer worldwide and has poor prognosis accounting for about 600.000 deaths annually (Llovet, Zucman-Rossi et al. 2016). One risk factor for liver cancer is Non-Alcoholic Fatty Liver Disease (NAFLD). NAFLD is the most prevalent liver disease western countries (Bellentani, Scaglioni et al. 2010, Baffy 2013, Fazel, Koenig et al. 2016, Lonardo, Byrne et al. 2016). NAFLD is characterized by excessive accumulation of FAs in hepatocytes, in about ~30% of patients it is due to enhanced de novo fatty acid (FA) synthesis. Tissue damage in NAFLD can be further amplified by inflammation (Wolf, Adili et al. 2014, Ma, Kesarwala et al. 2016), a condition referred to as non-alcoholic steatohepatitis (NASH) (Park, Lee et al. 2010, Scherer and Dufour 2016). NAFLD or NASH patients

may progress to HCC (even without developing liver cirrhosis) (Mittal, Sada et al. 2015).

Studies using high fat diet (HFD) or modified diet regimens (methionine-choline deficient) with or without parallel DEN (diethylnitrosamine) administration are frequently used as a model for NAFLD and NASH (Park, Lee et al. 2010, Wolf, Adili et al. 2014, Ma, Kesarwala et al. 2016). Although useful, in majority of cases mice are fed HFD, therefore examining the effect of hyper-nutrition, and not that of de novo FA and lipid synthesis. In this thesis we separate the contribution of hyper-nutrition from that of de novo fatty acid and lipid synthesis.

3.0. Aims of thesis

1. Full biochemical and histological characterization of L-dKO mice (liver cancer mouse model).
2. Examination of the effects of hepatic mTOR-activation on the whole-body.
3. Global analysis (proteome and phosphoproteome) of mTOR-driven tumors – to elucidate early oncogenic mechanisms downstream of mTOR signaling.

The above led to the discovery that L-dKO mice exhibit increased fatty acid and lipid synthesis and develop hepatosteatosis, prior to the appearance of liver tumors. I therefore set out to examine the following,

1. What lipid species are deregulated in L-dKO mice and are possibly controlled by mTOR signaling (lipidomics was performed in collaboration with the lab of Howard Riezman).
2. Is there a causal relationship between fatty acids and/or lipid accumulation and tumor development?
3. What is/are the function(s) of fatty acids and lipids in tumors.
4. To elucidate whether the above is mTORC1 or mTORC2 dependent.

Inspiration

Various oncogenic mutations lead to sustained mTOR activation (see appendix). The question that inspired me was (and still is), what are the mechanisms downstream of mTOR required for tumor development. Importantly, the basic (and key) trait of this thesis is the use of longitudinal studies. This approach allowed us to identify that fatty acid and lipid synthesis occur prior to tumor development and persist within tumors. In this thesis we provide evidence that mTOR-driven tumors require fatty acids and lipids for development. Moreover, we demonstrate that the above is primarily controlled by mTORC2. We hope that these studies provide a better understanding for the oncogenic role of mTOR and lipids, and will stimulate the usage of FA or lipid pathways inhibitors as (co-) therapy for cancer.

4. Results (manuscript)

mTORC2 promotes tumorigenesis via lipid synthesis

Yakir Guri[1], Marco Colombi[1], Sravanth K. Hindupur[1], Suzette Moes[1], Paul Jenoe[1], Isabelle Riezman[2], Howard Riezman[2] and Michael N. Hall[1*]

[1] Biozentrum, University of Basel

4056 Basel, Switzerland

[2] Department of Biochemistry, University of Geneva,

1211 Geneva, Switzerland

* Corresponding author: m.hall@unibas.ch

Keywords: mTOR, NAFLD, lipidome, proteome, serine, mitochondria, oxidative phosphorylation

Summary

Dysregulated mammalian TOR (mTOR) promotes cancer, but underlying mechanisms are poorly understood. We describe an mTOR-driven mouse model that displays hepatosteatosis progressing to hepatocellular carcinoma (HCC). Longitudinal proteomic, lipidomic and metabolomic analyses revealed that hepatic mTORC2 promotes de novo fatty acid and lipid synthesis, and thereby tumorigenesis. In particular, mTORC2 stimulated sphingolipid (glucoceramide) and glycerophospholipid (cardiolipin) synthesis. Inhibition of fatty acid or sphingolipid synthesis prevented tumor development. Increased levels of cardiolipin were associated with tubular mitochondria and enhanced oxidative phosphorylation. Thus, mTORC2 promotes cancer via formation of lipids essential for growth and energy production. Collectively, these findings illustrate a role for mTORC2 in lipid-mediated oncogenesis that could be exploited for targeted cancer therapies.

Introduction

Cancer is a disorder characterized by increased metabolic activity leading to enhanced cell growth and proliferation. Thus, cancer cells exhibit metabolic features that are distinct from non-cancerous cells (DeBerardinis, Lum et al. 2008, Schulze and Harris 2012, Pavlova and Thompson 2016). One such feature is elevated fatty acid (FA) synthesis, while non-cancerous cells rely on exogenous sources (Medes, Thomas et al. 1953, Spirtes, Medes et al. 1953). Various enzymes that mediate fatty acid and lipid synthesis are transcriptionally up-regulated in tumors (Kuhajda, Jenner et al. 1994, Li, Ding et al. 1994, Menendez and Lupu 2007, Flavin, Peluso et al. 2010, Park, Lee et al. 2010, Schulze and Downward 2011, Santos and Schulze 2012, Baenke, Peck et al. 2013, Bae, Oh et al. 2016, Feng, Chen et al. 2016, Peck and Schulze 2016). Although clinical trials for lipogenesis inhibitors are ongoing (Beloribi-Djefaflia, Vasseur et al. 2016), the regulation and function of lipids in tumors remain elusive.

Liver cancer is the fifth most common cancer worldwide and has poor prognosis, accounting for about 600,000 deaths annually (Llovet, Zucman-Rossi et al. 2016). One risk factor for liver cancer is Non-Alcoholic Fatty Liver Disease (NAFLD). NAFLD is characterized by excessive accumulation of triglycerides (TG) in hepatocytes (also known as hepatosteatosis), due in part to enhanced hepatic de novo FA synthesis (Lambert, Ramos-Roman et al. 2014, Sanders and Griffin 2016). NAFLD may progresses to Non-Alcoholic Steatohepatitis (NASH) and ultimately HCC (Postic and Girard 2008).

FA synthesis is induced by growth factors, through the transcription factor SREBP1c (Sterol Regulatory Element-Binding Protein-1c). Upon growth factor stimulation, precursor SREBP1c is proteolytically processed to yield mature SREBP1c, which is translocated into the nucleus to activate expression of the FA biosynthesis genes *Acc*, *Fasn*, *Scd1* and *Elovl6* (Horton, Goldstein et al. 2002).

FAs are assembled from acetyl groups derived mainly from citrate. Citrate produced by the TCA cycle in mitochondria is shuttled to the cytoplasm and converted, by ACLY (ATP-Citrate Lyase), to acetyl-CoA and oxaloacetate. Oxaloacetate is converted to pyruvate, generating NADPH that provides reducing power for lipid synthesis. Acetyl-CoA is converted to malonyl-CoA by ACC (Acetyl-CoA Carboxylase). FASN (Fatty Acid Synthase) then condenses malonyl-CoA and several molecules of acetyl-CoA to produce palmitate (16 carbon unit). SCD1 (Stearoyl-CoA Desaturase 1) desaturates palmitate thereby generating mono-unsaturated FA. Other FA desaturases (FADS) generate highly polyunsaturated fatty acids (PUFA) (Lee, Lee et al. 2016). FAs can be stored in the form of triacylglycerol (TG). Alternatively, FAs are utilized for the synthesis of sphingolipids (SLs) and glycerophospholipids (PLs) that are ultimately used as signaling molecules or membrane building blocks. PLs, including mitochondria-specific cardiolipin, are the major lipid constituent of cellular membranes.

The evolutionarily conserved Ser/Thr kinase Target of Rapamycin (TOR) controls metabolic pathways that mediate cell growth. TOR forms two structurally and functionally distinct protein complexes termed TOR Complex 1 (TORC1) and TORC2 (Loewith, Jacinto et al. 2002, Wullschleger, Loewith

et al. 2006). Mammalian TORC1 (mTORC1) is activated by nutrients, growth factors and cellular energy (Laplante and Sabatini 2012, Dibble and Manning 2013, Shimobayashi and Hall 2016). Growth factors stimulate mTORC1 via PI3K-PDK1-AKT mediated inhibition of the negative regulator and tumor suppressor TSC, consisting of TSC1 and TSC2 (Inoki, Li et al. 2002, Kenerson, Aicher et al. 2002, Kwiatkowski, Zhang et al. 2002, Manning, Tee et al. 2002, Tee, Fingar et al. 2002, Dibble, Elis et al. 2012). The tumor suppressor PTEN (Phosphatase and tensin homolog deleted on chromosome 10) negatively regulates both mTORC1 and mTORC2 signaling. mTORC1 directly or indirectly phosphorylates S6K (Ribosomal Protein S6 Kinase), ribosomal protein S6, CAD (Carbamoyl Phosphate Synthetase 2, Aspartate Transcarbamylase, and Dihydroorotase), and ULK (Unc-51 Like Autophagy Activating Kinase 1) among others. Growth factors activate mTORC2 via PI3K dependent association of mTORC2 with the ribosome (Zinzalla, Stracka et al. 2011). mTORC2 phosphorylates several members of the AGC kinase family, including AKT, to control various cellular process (Dibble and Manning 2013, Shimobayashi and Hall 2016). mTORC2 physiologically controls hepatic fatty acid synthesis via AKT and SREBP1c (Hagiwara, Cornu et al. 2012). mTORC2 is also tumorigenic (Guertin, Stevens et al. 2009, Masui, Tanaka et al. 2013, Masui, Tanaka et al. 2015), but little is known about the underling mechanism(s). Tumors frequently exhibit activated SREBP1c (Ricoult, Yecies et al. 2015, Li, Pilo et al. 2016). Rapamycin acutely inhibits only mTORC1 whereas INK128 inhibits both mTORC1 and mTORC2 (Benjamin, Colombi et al. 2011, Hsieh, Liu et al. 2012).

Here we demonstrate that, in liver-specific *Tsc1 Pten* double knockout (L-dKO) mice, mTORC2 promotes elevated hepatic fatty acid and lipid (sphingolipid, cardiolipin) synthesis, and thereby hepatosteatosis and hepatocellular carcinoma (HCC). Enhanced cardiolipin synthesis leads to increased mitochondrial activity and energy production. Thus, mTORC2 is oncogenic via lipogenesis.

Results

Liver specific activation of mTOR signaling promotes FA synthesis, hepatosteatosis, and HCC.

To study the role of mTOR signaling in cancer, we generated mice lacking both *Tsc1* and *Pten* specifically in the liver (termed L-dKO mice). The L-dKO *(Tsc1$^{loxP/loxP}$; Pten$^{loxP/loxP}$; Alb-CRE)* mice exhibited reduced expression of TSC1 and PTEN in the liver, and concomitant activation of mTORC1 and mTORC2 signaling, as compared to age-matched littermate control mice *(Tsc1$^{loxP/loxP}$; Pten$^{loxP/loxP}$)* (Figure 1A). The L-dKO mice displayed disproportionately increased liver weight (hepatomegaly), beginning at 4 weeks of age, which was independent of feeding behavior (Figure S1A-C). L-dKO mice also exhibited increased serum levels of the liver damage markers ALT, AST and LDH (Figure S1D), and elevated hepatic expression of the cancer-associated genes *Afp* and *Aldh* (Figure S1E). L-dKO mice invariably presented liver cancer, detected microscopically, at about 12 weeks of age and died at 20 weeks of age, at which time the liver was replete with tumors (Figure S1A). Histological analysis confirmed liver cancer, hepatocellular

carcinoma (HCC) and rarely (~10%) cholangiocarcinoma (CC) (Figure 1B H&E panel and Figure S1F). A fibrotic rim, indicative of NASH, demarcated the tumors (Figure S1G SR and PAS panel). To confirm that tumors correlate with increased proliferation, BrdU incorporation was assessed. L-dKO and control mice at 16 weeks of age (at which time tumor and non-tumor regions can be readily discriminated) were injected IP with BrdU (n=3). As expected, hepatocyte proliferation was higher in tumors (Figure S1H), compared to non-tumor regions and control liver. Collectively, and consistent with previous studies (Kenerson, Aicher et al. 2002, Kenerson, Yeh et al. 2013), the above indicates that dysregulated hepatic mTOR causes liver cancer.

To identify early, mTOR-dependent molecular events that promote liver cancer development, we performed longitudinal, unbiased quantitative proteomics and phosphoproteomics on liver samples from 4, 8 and 12 week-old L-dKO mice and age-matched littermates. Pathway enrichment analysis of proteins and phosphorylation events that were consistently and significantly (>2 fold) up- or down-regulated at all three ages (Figure S2A, B) revealed enrichment of FA and lipid synthesis pathways (Figures 1C and S2C, D). Importantly, FA and lipid synthesis pathways were up-regulated specifically in livers developing HCC, i.e., livers from L-dKO mice. Immunoblot analysis confirmed increased expression of FA synthesis enzymes ACC, FASN and SCD1 in liver lysates from L-dKO mice, compared to control mice (Figure 1A). Immunoblotting also showed increased levels of mature SREBP1c (Figure 1A) while quantitative PCR analysis revealed increased expression of the *Acc1*, *Fasn,* and *Scd1* genes (Figure S2E),

indicating that the increase in expression of FA synthesis enzymes was at the transcriptional level. Additionally, phosphoproteomics revealed increased ACLY-Ser455 phosphorylation (pACLY-Ser455) in livers of L-dKO mice, possibly leading to ACLY activation (Das, Morvan et al. 2015). pACLY-Ser455 was also validated by immunoblotting (Figure 1A). Expression of CD36, a long-chain fatty acid transporter that contributes to hepatosteatosis (Zhou, Febbraio et al. 2008, Steneberg, Sykaras et al. 2015), was also increased in liver of L-dKO mice (Figures 1A, S2F), suggesting enhanced FA uptake in addition to synthesis. Up-regulation of lipid biosynthesis pathways was also confirmed, as described further below. Isolated liver tumors from 20 week-old L-dKO mice (12 tumors, from 4 mice) also displayed increased expression of FA and lipid synthesis pathways, as determined by proteomic and RNA sequencing (RNAseq) analyses and confirmed by immunoblotting (Figure 1C and Table S1). We note that in biochemical experiments in which we use liver samples from 20 week-old mice, the samples are excised tumors, whereas samples from younger mice (4, 8 and 12 weeks) are whole liver.

We next investigated FA accumulation (hepatosteatosis) and its correlation with tumor development. Macroscopically, livers from L-dKO mice appeared fatty starting at 8 weeks of age (Figure S1A). Lipid droplet specific Oil-red-O (ORO) staining confirmed hepatosteatosis (Figure 1D and Figure S1F). H&E staining revealed enlarged hepatocytes, likely due to a combination of lipid droplet accumulation and mTOR driven cell growth (Figures S1F and S2G, H). Consistent with enhanced lipid droplet accumulation, hepatic TG levels were increased in 4, 8, 12 and 20 week-old L-dKO mice, compared to control mice (Figure 1D). Hepatic TG

accumulation was more pronounced in ad-libitum fed mice compared to mice starved overnight (Figure S2I). We note that all subsequent experiments were performed with ad-libitum fed mice. The above indicates that FA accumulation precedes HCC in L-dKO mice, as observed clinically.

To investigate the effect of activated hepatic mTOR signaling on whole-body metabolism, we performed indirect calorimetry on L-dKO and control mice at 12 and 20 weeks of age. The respiratory exchange ratio (RER) was lower in L-dKO, compared to control mice, despite little-to-no difference in feeding behavior or physical activity, suggesting that L-dKO mice are more reliant on FA oxidation for energy production (Figure S3A-C). L-dKO mice were unaltered in total fat or lean mass compared to controls, as determined by longitudinal whole-body fat composition analyses (EchoMRI) (Figure S3D). Since L-dKO mice displayed hepatosteatosis and hepatomegaly but did not exhibit an overall increase in fat or lean mass, we investigated whether L-dKO mice exhibit cancer cachexia (wasting syndrome) that may offset the increased liver mass. Cachexia is characterized by substantial tissue loss, in particular skeletal muscle and adipose tissue (Argiles, Busquets et al. 2014). Indeed, L-dKO mice exhibited reduced skeletal muscle and adipose tissue mass compared to control mice (Figure S3E, F). Hepatic expression of genes involved in lipid secretion (*Apob, Mttp*) or degradation (*Atgl, Acox1, Mcad, Cpt1*), as well as LDL and HDL levels were not changed (Figure S3G, H). Thus, L-dKO mice exhibit whole body cachexia-like effects.

FA synthesis is required for tumor development.

To determine whether FA synthesis is required for tumor development, 6 to 8 week-old L-dKO (n=4) and littermate control (n=5) mice were treated with the FASN inhibitor orlistat (120 mg/kg/bw) or drug vehicle alone (Kridel, Axelrod et al. 2004, Seguin, Carvalho et al. 2012, Sounni, Cimino et al. 2014) daily for 12 weeks. Orlistat treated L-dKO mice displayed significantly fewer hepatic lipid droplets and liver tumors, compared to L-dKO mice treated with drug vehicle alone (Figures 2A and S4A, B). Orlistat treatment did not reduce total liver or body weight (Figure S4C). Furthermore, Orlistat treatment had no effect on the phosphorylation status of AKT-Ser473 and S6-Ser235/6 (Figure S4D), indicating that drug action was not via inhibition of mTOR. Thus, FA synthesis required for tumor development.

To determine if FA synthesis in the liver is required for tumor development, we used adenovirus associated virus (AAV) to knockdown FASN specifically in hepatocytes. Importantly, to achieve hepatocyte specific knockdown, we used an AAV with high liver tropism and expressing *shFASN* from the albumin promoter (AAV-DJ-Albumin-*shFASN-RFP,* hereafter referred to as AAV-*shFASN*) (Figure S4E). AAV-*shFASN* or the control virus AAV-*shScrmbl* (AAV-DJ-Albumin-*shScrmbl-RFP)* was injected into the tail vein of 6 to 8 week-old L-dKO (n=4) and control (n=3) mice. FASN knockdown was confirmed by immunoblotting, qPCR and immunofluorescence (Figure S4F-I). Tumor burden was assessed in mice sacrificed at 20 weeks of age. L-dKO mice infected with AAV-*shFASN* exhibited significantly reduced hepatocyte proliferation and tumor burden, compared to L-dKO mice treated with AAV-*shScrmbl* (Figure 2B).

Importantly, AAV-*shFASN* did not have a detrimental effect in wild-type mice, indicating that in contrast to transformed hepatocytes, normal hepatocytes are not dependent on FASN expression. Control mice lacking tumors presumably obtain sufficient FAs from the diet. Collectively, these data indicate that hepatic FA synthesis is required for tumor development in mTOR driven HCC.

mTOR promotes do novo sphingolipid synthesis: Glucosylceramide.

The transcriptomic and proteomic analyses described above suggested that mTOR promotes lipid synthesis in addition to FA synthesis. In particular, enzymes mediating sphingolipid (SL) and glycerophospholipid (PL) synthesis were up-regulated in the liver of young L-dKO mice (4, 8, or 12 weeks) and in tumors of 20 week-old L-dKO mice (Figure 1C).

The rate-limiting reaction in de novo SL biosynthesis is the condensation of serine and palmitate catalyzed by SPT (Serine Palmitoyltransferase) to generate 3-keto-sphinganine (3kSN) (Aguilera-Romero, Gehin et al. 2014, Garcia-Barros, Coant et al. 2014) (Figure 1C). 3kSN is then reduced to yield the long chain base (LCB) sphinganine (SN). LCB is N-acylated, with fatty acid chains of different lengths, by CerS (Ceramide Synthase, isoforms 1 to 6) to produce dihydroceramide (dhCer). The fatty acids used for sphingolipid synthesis are produced by ELOVL (Elongation of Very Long Chain Fatty Acids), comprising a family of seven isoforms. DES (Dihydroceramide Desaturase, isoforms 1 and 2) adds a double bond to complete the synthesis of ceramide. Ceramide undergoes head group modifications in the golgi to yield sphingomyelin (SM) or glucosylceramide (GlcCer). GlcCer synthesis is

catalyzed by GCS (Glucosylceramide Synthase) that transfers glucose from uridine diphosphate (UDP) glucose to ceramide. Ceramide can also be converted to sphingosine (SP) by ceramidases. SL biosynthetic enzymes, including SPT and CerS, are implicated in NAFLD (Pagadala, Kasumov et al. 2012) and cancer (Ogretmen and Hannun 2004, Levy and Futerman 2010). L-dKO mice exhibited increased expression (mRNA and protein) of sphingolipid anabolic enzymes, in particular SPT, ELOVL (isoforms 1, 4, 6 and 7), CerS (isoforms 2, 3, 5 and 6), DES (isoforms 1 and 2), and GCS (Figures 1C). Expression of enzymes that mediate reverse, catabolic steps was not altered, with the exception of SMPD (isoforms 1 to 4) and GBA (isoforms 1 to 2) that were increased and decreased, respectively (Figure 1C). Importantly, increased SMPD and decreased GBA expression suggests that GlcCer synthesis is favored in L-dKO mice. SPK1 (Sphingosine Kinase 1) and SPL1 (Sphingosine Lyase 1) that mediate sphingosine 1 phosphate (S1P) metabolism downstream of ceramide were also up-regulated (see Discussion). Altered expression of SPT, GCS, SMPD (isoforms 1 and 3), and SPK1 was confirmed by immunoblotting or qPCR (Figures 1A, 3A and S5A). Immunofluorescence on perfused livers from 8 week-old L-dKO and control mice indicated that increased SPT expression was specific to hepatocytes (Figure S5B). These findings suggest that de novo SL synthesis is increased in hepatocytes from L-dKO mice, likely leading to GlcCer accumulation.

To determine whether the above changes in expression lead to changes in lipid accumulation, we performed longitudinal unbiased semi-quantitative lipidomic analysis on liver samples from 4, 8, 12 and 20 (tumors) week-old L-dKO mice and age-matched littermates (n=6, per time point). Lipid

enrichment analysis revealed that L-dKO mice exhibit enhanced accumulation of dhCer, ceramide, and GlcCer (Figure 4A; Table S2). As suggested by the above transcriptomic and proteomic analyses (Figure 1C), the most pronounced accumulation was of GlcCer. The observed GluCer accumulation in livers of L-dKO mice was validated by immunofluorescence analysis on frozen liver sections (Figure S5C). Thus, liver of L-dKO mice accumulates sphingolipids, preferentially GlcCer.

To confirm that de novo SL synthesis, as opposed to SL salvage pathways that can also produce elevated levels of GlcCer, was high in L-dKO mice we performed metabolomic analysis on liver samples from 4, 8, 12 and 20 week-old L-dKO mice and control littermates. Indeed, sphinganine (SN), an intermediate of de novo synthesis, was increased in liver samples from L-dKO mice (Figure 3B). Moreover, metabolomic analysis indicated that the level of the amino acid serine, which is required for the rate-limiting step in de novo SL synthesis, was consistently reduced in liver samples from L-dKO mice (Figure 3C). Alanine and glutamine levels were not similarly depleted (Figure S5D), suggesting that the reduction in serine is due to consumption by de novo SL synthesis. Thus, consistent with the observed increase in fatty acid synthesis, L-dKO mice display increased hepatic de novo SL synthesis.

Sphingolipid (GlcCer) is required for liver tumor development.

To determine whether the observed increase in de novo SL synthesis is required for tumor development, 8 week-old L-dKO (n=5) and littermate control (n=5) mice were treated with the SPT inhibitor myriocin. Myriocin (0.03 mg/kg/bw) or drug vehicle alone was IP administered every second day.

At 20 weeks of age, mice were euthanized, livers were dissected and liver tumors were counted. Myriocin treatment significantly reduced the number of liver tumors in L-dKO mice (Figure 3E). This effect was further illustrated by principle component analysis (Figure S5E). Myriocin had no effect on the phosphorylation status of AKT-Ser473 and S6-Ser235/6, suggesting that the drug acted independently of mTOR signaling (Figure S5F). Liver and body weights of L-dKO and control mice treated with myriocin were unchanged (Figure S5G). Lipidomic analysis confirmed the in vivo action of myriocin (Figure 3D). Thus, de novo SL synthesis is required for tumor growth.

The above proteomic and lipidomic analyses indicated that L-dKO mice preferentially accumulate GlcCer. Furthermore, expression of the GlcCer synthesis enzyme GCS correlates with tumorigenicity (Liu, Han et al. 2000, Gupta, Bhinge et al. 2012, Kartal Yandim, Apohan et al. 2013, Liu, Hill et al. 2013, Tyler, Johansson et al. 2015), and a GCS inhibitor blocks proliferation of leukemic (Huang, Tsai et al. 2011), lung cancer (Suzuki, Cao et al. 2016) pancreatic tumor (Wang, Wei et al. 2015) and HCC cells (Stefanovic, Tutusaus et al. 2016). To determine whether accumulation specifically of GlcCer is important for tumor development in vivo, we knocked down GCS in hepatocytes in L-dKO mice. AAV-*shGCS* or the control virus AAV-*shScrmbl* was injected into tail vein of 6 to 8 week-old L-dKO (n=6) and control mice (n=4). Hepatic viral infection was confirmed by immunofluorescence (Figure S5H). At 20 weeks of age, mice were euthanized, livers were dissected and tumors were counted. Strikingly, chronic GCS inhibition reduced the number of liver tumors (Figure 2B). Thus, GlcCer accumulation is required for tumor development.

mTOR promotes glycerophospholipid synthesis: Cardiolipin.

The transcriptomic and proteomic analyses described above also suggested that mTOR promotes glycerophospholipid (PL) synthesis. PL synthesis begins with the acylation of glycerol 3-phosphate by GPAT (Glycerol 3-Phosphate Acyltransferase) to generate lysophosphatidic acid (LPA). LPA is then converted to phosphatidic acid (PA) by AGPAT (Acylglycerol-3-Acyltransferase). PA is converted to diacylglyceride (DAG), by the PAP (Phosphatidic Acid Phosphatase, also known as LIPIN) family of enzymes. In the so-called 'Kennedy pathway', DAG and choline or ethanolamine are condensed to yield phosphatidylcholine (PC) or phosphatidylethanolamine (PE), respectively (Gibellini and Smith 2010). Alternatively, DAG is conjugated to CDP by CDS (CDP-DAG synthase) to produce the liponucleotide CDP-DAG. CDP-DAG is used for the synthesis of phosphatidylinositol (PI), phosphatidylserine (PS), and cardiolipin (CL). CLs are synthesized exclusively in the mitochondria (Schlame and Haldar 1993, Schlame, Rua et al. 2000) by PGS1 (Phosphatidylglycerophosphate Synthase 1). PGS1 catalyzes the rate-limiting step in CL synthesis, condensing DAG and glycerol-3-phosphate to produce phosphatidylglycerol-phosphate (PGP). PGP is dephosphorylated by the PTEN-like mitochondrial phosphatase PTPMT1, generating a phosphatidylglycerol (PG) (Zhang, Guan et al. 2011). Cardiolipin synthase (CRLS1) attaches PG to DAG, producing immature CL that is then remodeled in a series of reactions. In the inner mitochondrial membrane (IMM) CLs stabilize the complexes of the electron

transport chain, thereby supporting oxidative phosphorylation (OxPhos) (Houtkooper and Vaz 2008, Duncan, Robinson et al. 2016).

The transcriptomic and proteomic analyses described above and immunoblotting revealed increased hepatic expression of the PL synthesis enzymes GPAT, AGPAT, LIPIN, CDS, PGS1, CRLS1 and PTPMT1 in L-dKO mice (Figures 1C and 5A), suggesting increased synthesis of PLs, cardiolipin in particular. Indeed, lipidomic analysis revealed elevated levels of the PLs phosphatidylinositol (PI), lysophosphatidylcholine (lysoPC) and cardiolipin (CL), with accumulation of CL being the most pronounced (Figure 4A). Importantly, the levels of PC and PE, both products of the Kennedy pathway, were reduced (Figure S6A, B). The above suggests that cardiolipin is preferentially synthesized in L-dKO mice. Thus, again consistent with the observed increase in fatty acid synthesis, L-dKO mice display increased hepatic synthesis of PLs, in particular via the biosynthetic pathway leading to cardiolipin (i.e., not the Kennedy pathway).

Increased cardiolipin accumulation is associated with enhanced respiration.

CLs stabilize complexes of the electron transport chain (ETC) thereby supporting oxidative phosphorylation (OxPhos) (Houtkooper and Vaz 2008, Duncan, Robinson et al. 2016). Expression of ETC complexes was unchanged in L-dKO mice, compared to control littermates, as determined by immunoblot analysis and electron microscopy (EM) (Figure S6C-E). However, hepatocytes from L-dKO mice exhibited hyper-tubular mitochondria and pronounced cristae, as determined EM analysis (Figures S6C and F). The

hyper-tubular mitochondrial morphology was confirmed by staining L-dKO primary hepatocytes with the mitochondria specific dye MitoTracker-Red (Figures 5B, S5B). To investigate mitochondrial function, OxPhos in particular, we measured the oxygen consumption rate (OCR) and mitochondrial reserve capacity of primary hepatocytes. Primary hepatocytes from L-dKO mice displayed enhanced OxPhos and increased mitochondrial reserve capacity, compared to wild-type hepatocytes (Figure 5C). Thus, increased cardiolipin accumulation correlates with enhanced mitochondrial function. The increase in cardiolipin may increase mitochondrial function to sustain the enhanced metabolic needs of tumor cells.

mTORC2 promotes FA, sphingolipid and cardiolipin accumulation.

The above suggests that hyperactive mTOR signaling promotes lipid synthesis and cancer. To confirm that tumor development is indeed mTOR dependent, 8 week-old L-dKO and control mice were chronically treated with the ATP competitive mTOR inhibitor INK128 (1 mg/kg/bw), or drug vehicle alone, for 12 weeks. Chronic INK128 administration reduced mTOR signaling (mTORC1 and mTORC2) (Figure S6G), and prevented both liver damage (Figure S6H) and tumor growth (Figure 6A), confirming that tumor development was mTOR dependent. We note that chronic INK128 administration also reduced hepatic TG content (Figure 6B) and hepatocyte size (Figure 6C).

Hepatic mTORC1 and mTORC2 are activated in L-dKO mice. To determine whether mTORC1 and/or mTORC2 signaling controls FA and lipid synthesis in L-dKO mice, we performed acute pharmacological inhibition

studies. 8 week-old L-dKO and control mice (n=4 per group) were treated acutely (24hrs) with rapamycin, INK128 or drug vehicle alone. Acute rapamycin treatment inhibited mTORC1, as assessed by reduced S6-Ser235/6, CAD-Ser1859 and ULK-Ser757 phosphorylation, and increased AKT-Ser473 phosphorylation, the latter due to inhibition of negative feedback from S6K (Figure S6I, mTORC2 panel). Acute INK128 administration inhibited both mTORC1 (assessed as above) and mTORC2, as assessed by reduced AKT-Ser473, GSK-Ser21/9, and NDRG1-Thr346 phosphorylation (Figure S6I). Acute INK128 treatment reduced both expression of ACC, FASN, and SCD1 (Figure 6D) and hepatic TG content in L-dKO mice, compared to INK128 treated control mice (Figure S7A). We note that acute INK128 administration increased overall hepatic TG content in L-dKO and control mice compared to mice treated with drug vehicle alone (Figure S7A), likely due to enhanced lipolysis in adipose tissue as suggested by increased serum FA levels (Figure S7B) (Cybulski, Polak et al. 2009, Kumar, Lawrence et al. 2010). Inhibition of mTORC1 alone (rapamycin) did not alter expression of hepatic FA synthesis enzymes or hepatic TG content (Figures S6I and S7A). Thus, hepatic FA synthesis is activated by mTORC2.

To confirm that mTORC2 promotes de novo FA and lipid synthesis, TG accumulation and liver cancer development, we deleted *Rictor*, an essential core component of mTORC2, in L-dKO mice. *Tsc1*$^{loxP/loxP}$*; Pten*$^{loxP/loxP}$ mice were crossed with *Rictor*$^{loxP/loxP}$ mice expressing *Alb-CRE*, to generate triple knockout (L-TriKO) mice lacking *Tsc1 Pten* and *Rictor* (Figure S7C, D). L-TriKO mice were born according to Mendelian ratios and gained weight normally (not shown). Immunoblot analysis of liver lysates revealed markedly

reduced mTORC2 activity in L-TriKO mice *(Tsc1$^{loxP/loxP}$; Pten$^{loxP/loxP}$; Rictor$^{loxP/loxP}$; Alb-CRE)* compared to littermate control mice *(Tsc1$^{loxP/loxP}$; Pten$^{loxP/loxP}$; Rictor$^{loxP/loxP}$)*, as assessed by AKT-Ser473, GSK-Ser21/9, NDRG1-Thr346, and PKC-Thr638/641 phosphorylation; mTORC1 activity was not change in L-TriKO mice, as assessed by S6-Ser235/6, CAD-Ser1859 and ULK-Ser757 phosphorylation (Figure S7E), thereby confirming the L-TriKO mouse model. Importantly, L-TriKO mice displayed reduced expression of ACC, FASN, SCD1 and their transcriptional activator SREBP1c (mature form), and reduced hepatic TG content (Figure 7A, B), compared to L-dKO mice. Expression of the SL synthesis genes *Spt* and *SMPD* was also reduced in L-TriKO mice, compared to L-dKO mice (Figure 7C). Similarly, immunoblotting of primary hepatocytes from knockout and control mice showed reduced CRLS1 expression in L-TriKO mice (Figure S7F). Lipidomic analysis was also performed on liver lysates from L-TriKO, L-dKO and control mice (n=4/group), revealing reduced sphingolipid and glycerophospholipid levels, including GlcCer and CL(18:≤1), respectively, specifically in L-TriKO mice (Figures 4 and S5C). Collectively, the above indicates that mTORC2 activates de novo SL and PL synthesis.

Importantly, in addition to reduced FA and lipid synthesis, L-TriKO mice also displayed reduced tumorigenicity (Figures 7D, E and S7G, H). We note that the few tumors that arose in L-TriKO mice exhibited increased mTORC2 activity, as assessed by immunohistochemical analysis of phosphorylated AKT473 (Figure S7I), suggesting that such tumors were due to 'escapers' in which *Rictor* was not deleted. Thus, it is mTORC2 that is lipogenic and oncogenic in L-dKO mice.

Discussion

Diverse mutations activate mTOR signaling to promote tumor development, but tumorigenic mechanisms downstream of mTOR signaling remain poorly defined, in particular for mTORC2. We examined tumor development in an mTOR-dependent HCC mouse model (L-dKO). We report that mTORC2 promotes hepatosteatosis and ultimately tumor development via fatty acid (FA) and lipid synthesis.

Similar to patients who develop NFALD that progresses to HCC (Postic and Girard 2008, Lambert, Ramos-Roman et al. 2014), L-dKO mice exhibit enhanced FA synthesis and thereby develop hepatosteatosis, liver damage and HCC (Figures 1A-E, S1A-G and S2A-H). Knockdown of fatty acid synthase (FASN) specifically in hepatocytes blocked tumor development (Figures 2A-D and S4A, H). Notably, FASN inhibition did not have a detrimental effect in wild-type hepatocytes, exposing a vulnerability specific to cancer cells. Non-cancerous cells, which have reduced metabolic requirements, obtain sufficient amounts of FAs from the diet. How do fatty acids promote tumor development? First, FAs are necessary for the synthesis of lipids, which may in turn be necessary for tumorigenicity. Indeed, we observed that lipid synthesis pathways, in particular de novo sphingolipid and glycerophospholipid synthesis, are also up-regulated in L-dKO mice (Figures 1C, 3A,B and 4A). We note that the expression of lipid biosynthetic enzymes (SPT in particular) is up-regulated in various human cancer types (not shown). Importantly, inhibition of the rate-limiting reactions in de novo SL synthesis or glucosylceramide synthesis prevented tumor development in

L-dKO mice, indicating that up-regulation of lipid synthesis is essential for tumorigenesis (Figures 2B, 3E, F and S5E). Second, enhanced FA synthesis causes hepatosteatosis, a pathological accumulation of fatty acids, which may in turn promote inflammation (NASH) and HCC (Park, Lee et al. 2010, Wolf, Adili et al. 2014, Ma, Kesarwala et al. 2016). Alternatively, FA could be used to produce the bioactive sphingolipid S1P leading to inflammation (Liang, Nagahashi et al. 2013, Taniguchi and Karin 2014). Consistent with the notion that FAs are promoting tumor development via inflammation, L-dKO mice exhibited up-regulated SPK1 (Sphingosine Kinase 1) and increased S1P levels which correlated with increased STAT3 phosphorylation (data not shown). The role of inflammation in mTOR driven tumor development, and in particular its promotion by FAs, will require further study.

How does up-regulation of sphingolipid (SL) and glycerophospholipid (PL) synthesis (in particularly of GlcCer and cardiolipin, respectively) promote cancer? First, SL and PL are structural components of membranes and may thereby support tumor growth simply as building blocks. Ceramide glycosylation by glucosylceramide synthease (GCS) yields the membrane component GlcCer, but also eliminates excess ceramide and its anti-proliferative effect (Ogretmen and Hannun 2004). Importantly, L-dKO mice preferentially accumulate GlcCer. Thus, the essential role of GlcCer synthesis in tumorgenicity may be two-fold, one is the production of a building block, the other is to eliminate ceramide. Second, CL in the inner mitochondrial membrane (IMM) stabilizes complexes of the ETC thereby enhancing energy production and satisfying the increased metabolic needs of tumor cells (Schlame and Haldar 1993, Schlame, Rua et al. 2000,

Houtkooper and Vaz 2008, van der Bliek, Shen et al. 2013, Yu-Wai-Man, Carelli et al. 2014, Duncan, Robinson et al. 2016, Peck, Schug et al. 2016). Importantly, we observed increased CL synthesis and mitochondrial energy production in liver of L-dKO mice (Figure 4A, 5A-C and S6D, F). Third, lipids provide second messengers in oncogenic signaling pathways (Hannun and Obeid 2008, Wymann and Schneiter 2008, Baenke, Peck et al. 2013). For example, the glycerophospholipid PI is phosphorylated to generate phosphatidylinositol-3,4,5-triphosphate that mediates growth factor signaling. It remains to be determined whether the increased lipid synthesis observed in L-dKO mice is affecting second messenger levels in oncogenic signaling pathways.

How does mTORC2 regulate FA synthesis? L-dKO mice display increased levels of mature SREBP1c and increased expression of SREBP1c target genes *Acc*, *Fasn*, *Scd1* and *Elovl*6 (Figures 1A, C and S2E). Pharmacological or genetic ablation of mTORC2 signaling in L-dKO mice (L-TriKO) prevented SREBP1c processing, decreased *Acc*, F*asn*, and *Scd1* expression, and thereby reduced de novo FA synthesis (Figures 6D and 7A, B). Thus, mTORC2 promotes de novo FA synthesis via SREBP1c, as shown previously (Hagiwara, Cornu et al. 2012, Kenerson, Subramanian et al. 2015). Alternatively, mTORC2 or its effectors may phosphorylate FA synthesis enzymes directly, as recently proposed for ACLY (Chen, Qian et al. 2016) (Figures 1A and 6D). Finally, mTORC2 increases expression of the fatty acid transporter CD36 (Figure 1A), an effect that was blocked in L-TriKO mice (Figure 7A), allowing up-take of FA from the bloodstream.

We note that mTORC1 has also been proposed to stimulates FA synthesis (reviewed in (Ricoult and Manning 2013)). For example, mTORC1 contributes to de novo FA synthesis in breast cancer cell lines (Ricoult, Yecies et al. 2015). However, mTORC1 alone is insufficient to promote de novo FA synthesis in vivo. First, liver specific *Tsc1* knockout mice (constitutively active mTORC1) are protected from age and diet induced hepatosteatosis (Kenerson, Yeh et al. 2011, Yecies, Zhang et al. 2011, Cornu, Oppliger et al. 2014, Kenerson, Subramanian et al. 2015). Second, liver specific *Raptor* knockout mice (abrogated mTORC1 activity) exhibit unaltered hepatic FA levels, even when fed a high fed diet (Umemura, Park et al. 2014). Third, activation of mTORC1 in the absence of mTORC2 signaling is insufficient to activate expression of FA synthesis genes (Titchenell, Quinn et al. 2016). Thus, mTORC2 may play a more important role than mTORC1 in hepatic FA synthesis.

How does mTORC2 activate lipid synthesis? We observed that mTORC2 controls expression of some lipid synthesis genes, suggesting that the mechanism is at the level of transcription (Figure 7A, C). However, mTORC2 is functionally at ER-mitochondria contact sites known as MAM (Mitochondria Associated Membrane) (Betz and Hall 2013, Betz, Stracka et al. 2013), where PL synthesis occurs. Thus, mTORC2 or its kinase effectors could also directly phosphosphorylate and activate PL synthesis enzymes. For example, pACLY-Ser455 activation in skeletal muscle was mediated by AKT and promoted CL synthesis (Das, Morvan et al. 2015). The mechanism by which mTORC2 activates lipid synthesis remains to be determined.

Does mTORC1 play a role in in lipid synthesis in L-dKO mice? mTORC1 stimulates pyrimidine biosynthesis via phosphorylation of CAD and transcriptional activation of the pentosphosphate pathway (Ben-Sahra, Howell et al. 2013, Robitaille, Christen et al. 2013). The pyrimidines uridine diphosphate (UDP) and cytidine diphosphate (CDP) are required for the rate-limiting reactions in GlcCer and PL synthesis, respectively. L-dKO mice display increased CAD phosphorylation (Figure S6I and S7E). Thus, our data favor a model in which mTORC1 and mTORC2 converge on lipid synthesis to drive tumor development.

Collectively, we provide mechanistic insights for oncogenic mTORC2 in promoting FA and lipid synthesis. Lipids are required for tumor growth, as macromolecules, but also to support mitochondrial function to match increased energy demand. Inhibition of FA or lipid synthesis pathways kills cancer cells, thus exposing a cancer-specific vulnerability that can be exploited for the rational design of targeted cancer drugs.

Experimental Procedures

Data analysis. Statistical analysis and data plotting was performed using Prism Graph Pad 6.0. Statistical significance was defined as <0.05. An unpaired Student's t-test was used to determine differences among two groups. Significance was judged when p-value is less than 0.05. Error bars in figures represent standard error of the mean (SEM). Kaplan-Meier method was used for survival analysis.

Animals. Liver-specific tuberous sclerosis complex 1 (*Tsc1*) and phosphatase and tensin homolog (*Pten*) double knockout mice were obtained by crossing $Tsc1^{lox/lox}$ mice (Kwiatkowski, Zhang et al. 2002) with $Pten^{lox/lox}$ mice (Horie, Suzuki et al. 2004, Stiles, Wang et al. 2004) to transgenic mice expressing Cre recombinase under the control of the hepatocyte-specific albumin promoter (*Alb-Cre*) (Postic and Magnuson 2000), to generate liver specific double knockout (L-dKO) mice. $Tsc1^{loxP/loxP}$; $Pten^{loxP/loxP}$ mice were crossed to $Rictor^{loxP/loxP}$; *Alb-Cre* (Cybulski, Polak et al. 2009) to obtain ($Tsc1^{loxP/loxP}$; $Pten^{loxP/loxP}$; $Rictor^{loxP/loxP}$; *Alb-Cre)* liver specific triple knockout (L-TriKO mice) mice. As controls, male littermate $Tsc1^{loxP/loxP}$; $Pten^{loxP/loxP}$ mice or $Tsc1^{loxP/loxP}$; $Pten^{loxP/loxP}$; $Rictor^{loxP/loxP}$ mice (which do not express the Cre-recombinase) were used. Mice were on mixed genetic background (C57BL/6J, 129/SvJae, BALB/cJ). Both L-dKO mice ($Tsc1^{loxP/loxP}$; $Pten^{loxP/loxP}$; *Alb-Cre)* and L-TriKO ($Tsc1^{loxP/loxP}$; $Pten^{loxP/loxP}$; $Rictor^{loxP/loxP}$; *Alb-Cre)* mice were born viable at the expected Mendelian ratio and displayed normal fertility. PCR genotyping for *Tsc1* (Kwiatkowski, Zhang et al. 2002)

Pten (Horie, Suzuki et al. 2004, Stiles, Wang et al. 2004) *and Rictor* (Cybulski, Polak et al. 2009) and Cre was performed as described. Mice were maintained under temperature and humidity-controlled conditions, lights on at 6:00 AM and off at 6:00 PM. In all experiments, mice were sacrificed at 6:00am and were ad-libitum fed, unless mentioned otherwise. All of the experiments were conducted on male mice. All experiments were performed in accordance with federal guidelines and were approved by the Kantonales Veterinaeramt of Kanton Basel-Stadt.

Whole-Body Metabolic Analysis. RER (Respiratory Exchange Rate), locomotor activity and food consumption were measured in 30 minute-intervals, for the indicated time using a comprehensive laboratory animal monitoring system (CLAMS, Linton Instrumentation and Columbus Instruments). Measurement was performed after 24 hrs of acclimatization. Mice had free access to food and water.

Virus Administration. To determine virus liver tropism, $5*10^{\wedge 11}$ viral genome of AAV8-U6-CMV-RFP, AAV-DJ-U6-CMV-eGFP and AAV-DJ-Albumin-eGFP was injected into tail veins of wild-type (control). For viral knockdown studies, AAV-DJ-albumin-*shFASN*-RFP, AAV-albumin-*shGCS*-RFP and AAV-albumin-*shScrmble*-RFP (purchased from Vector BioLabs) were used. Virus was administrated to mice by tail-vein injection ($5*10^{\wedge 11}$ vg, unless mentioned otherwise). To validate virus action mice were sacrificed one-month post injection (short-tem) livers were further used for biochemical analysis. To

assess the effect on liver tumors development mice were sacrificed about three months post infection.

OCR and ECAR measurements. Measurements were performed with an XF96 Extracellular Flux Analyzer (Seahorse Bioscience of Agilent) following manufacturer instructions. 2×10^5 hepatocytes were seeded into 96 culture plate (Seahorse Bioscience of Agilent) overnight or measured 1hr post-seeding. Media was exchanged prior to the measurement.

Author Contributions

Conceptualization, Y.G., H.R. and M.N.H.; Methodology, Y.G., S. M., P.J., I.R, H.R. and M.N.H.; Investigation, Y.G., M. C., H.S.K., I.R.; Writing – Original Draft, Y.G. and M.N.H.; Funding Acquisition, Y.G., M.N.H. and H.R.; Resources, H.R. and M.N.H.; Supervision, M.N.H. and H.R.

Conflict of Interest

The authors declare not conflict of interest.

Acknowledgements

We acknowledge support from the European Research Council, the Swiss National Science Foundation, SystemsX.ch, the Louis Jeantet Foundation, the Swiss cancer league, and the Canton of Basel.

Figures

Figure 1

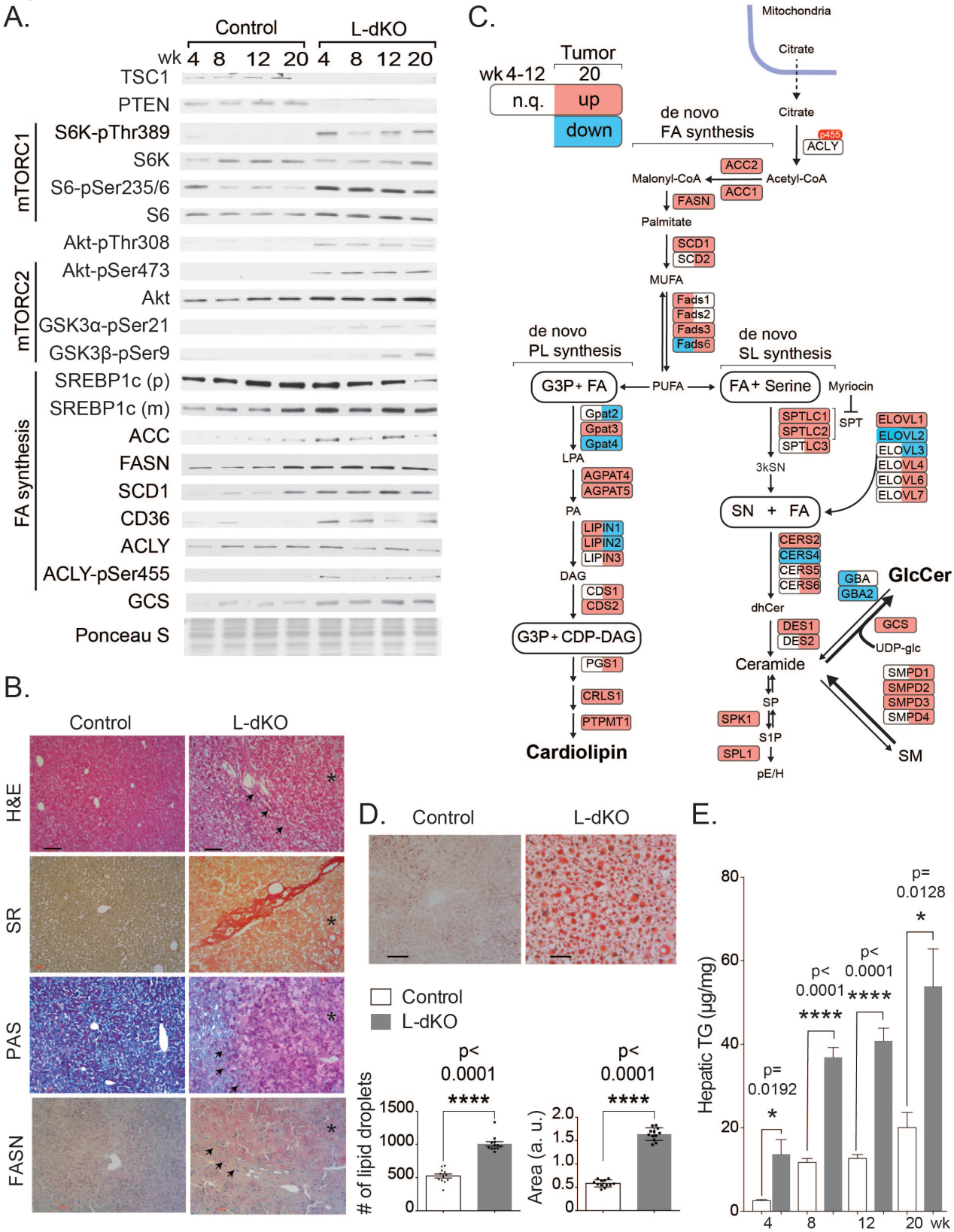
A.
Control
L-dKO
wk 4 8 12 20 4 8 12 20
TSC1
PTEN
mTORC1
S6K-pThr389
S6K
S6-pSer235/6
S6
mTORC2
Akt-pThr308
Akt-pSer473
Akt
GSK3α-pSer21
GSK3β-pSer9
FA synthesis
SREBP1c (p)
SREBP1c (m)
ACC
FASN
SCD1
CD36
ACLY
ACLY-pSer455
GCS
Ponceau S
B.
Control
L-dKO
H&E
SR
PAS
FASN
C.
Mitochondria
Citrate
Tumor
wk 4-12
20
n.q.
up
down
de novo
FA synthesis
Citrate
p455
ACLY
ACC2
Malonyl-CoA
Acetyl-CoA
ACC1
FASN
Palmitate
SCD1
SCD2
MUFA
Fads1
Fads2
Fads3
Fads6
de novo
PL synthesis
de novo
SL synthesis
G3P+ FA
PUFA
FA+ Serine
Myriocin
Gpat2
Gpat3
Gpat4
LPA
SPTLC1
SPTLC2
SPTLC3
SPT
ELOVL1
ELOVL2
ELOVL3
ELOVL4
ELOVL6
ELOVL7
3kSN
AGPAT4
AGPAT5
PA
SN + FA
LIPIN1
LIPIN2
LIPIN3
DAG
CERS2
CERS4
CERS5
CERS6
GBA
GBA2
GlcCer
CDS1
CDS2
dhCer
DES1
DES2
GCS
UDP-glc
G3P+ CDP-DAG
Ceramide
SMPD1
SMPD2
SMPD3
SMPD4
PGS1
SP
SPK1
S1P
CRLS1
SPL1
SM
PTPMT1
pE/H
Cardiolipin
D.
Control
L-dKO
Control
L-dKO
p< 0.0001
****
# of lipid droplets
1500
1000
500
0
p< 0.0001
****
Area (a. u.)
2.0
1.5
1.0
0.5
0
E.
Hepatic TG (μg/mg)
80
60
40
20
0
p= 0.0192
*
p< 0.0001
****
p< 0.0001
****
p= 0.0128
*
4
8
12
20
wk

Figure 1. *L-dKO mice develop HCC and exhibit enhanced de novo fatty acid and lipid synthesis* **(A)** Immunoblot analysis of liver extracts from ad-libitum fed 4, 8, 12, and 20 week-old L-dKO mice and littermate controls, for the indicated proteins. Each lane consists of a mixture of liver extracts obtained from six mice. **(B)** Representative staining of hepatic tumors from L-dKO mice and tumor-free control mice. Hematoxylin and Eosin (H&E), Sirius Red (SR), Periodic Acid Schiff (PAS), and FASN (Immunohistochemistry). Asterisks and arrows indicate HCCs and HCC margins, respectively. Scale bar 50µm **(C)** Relevant lipid biosynthetic enzymes are depicted. Up-or down-regulated enzymes in the proteome analyses of livers from young mice (4, 8 and 12 weeks of age, n=6 per time point) or proteome and transcriptome analyses of tumors (20 weeks of age, 12 dissected tumors from 3 mice) or immunoblotting are color coded: white, not quantified (n.q.) in transcriptome or proteome; blue, down-regulated in transcriptome or proteome; red, up-regulated in transcriptome or proteome. Phosphorylation site in a red box was up-regulated in phosphoproteomics **(D)** Representative images of frozen liver sections from 20 week-old L-dKO mice (tumors) and a tumor-free control, stained with Oil-Red-O (ORO) (n=3). Number and size (area) of hepatic lipid droplets were quantified using FIJI (a.u. arbitrary unit). **(E)** Hepatic triglyceride (TG) content from ad-libitum fed L-dKO and control mice (at least n=4 per group). pH/E, ethanolamine-1-phosphate and C_{16}-fatty aldehyde. To determine statistically significant differences unpaired Student's t-test was used. Error bars represent SEM.

Figure 2

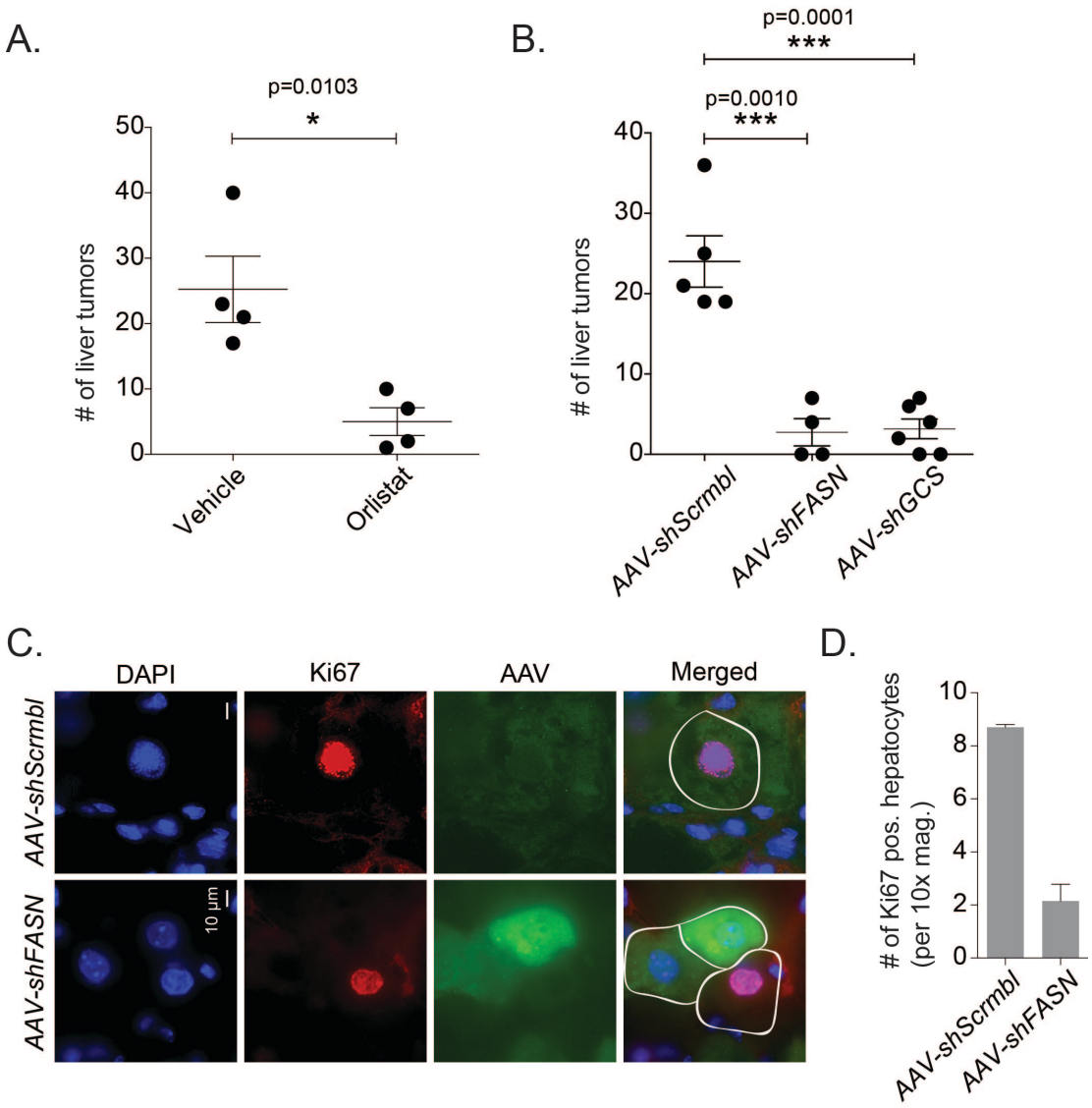

Figure 2. *FASN or GCS inhibition prevents tumor development in L-dKO mice*. **(A)** Number of liver tumors in L-dKO mice treated with orlistat or the drug vehicle alone. **(B)** Number of liver tumors in L-dKO mice treated with AAV-*shScrmbl*, AAV-*shFASN* or AAV-*shGCS*. **(C)** Representative immunofluorescence images from livers of L-dKO mice treated with AAV-*shFASN* or AAV-*shScrmbl* control. White circles designate hepatocytes successfully infected with the indicated virus. Nuclei, blue (DAPI); Ki67, red; AAV (virus), green. **(D)** Quantification of the number of Ki67 positive cells in livers from L-dKO mice infected with AAV-*shFASN* or AAV-*shScrmbl* control, per 10X magnification field (n=3). To determine statistically significant differences unpaired Student's t-test was used. Data represent mean ± SEM.

Figure 3

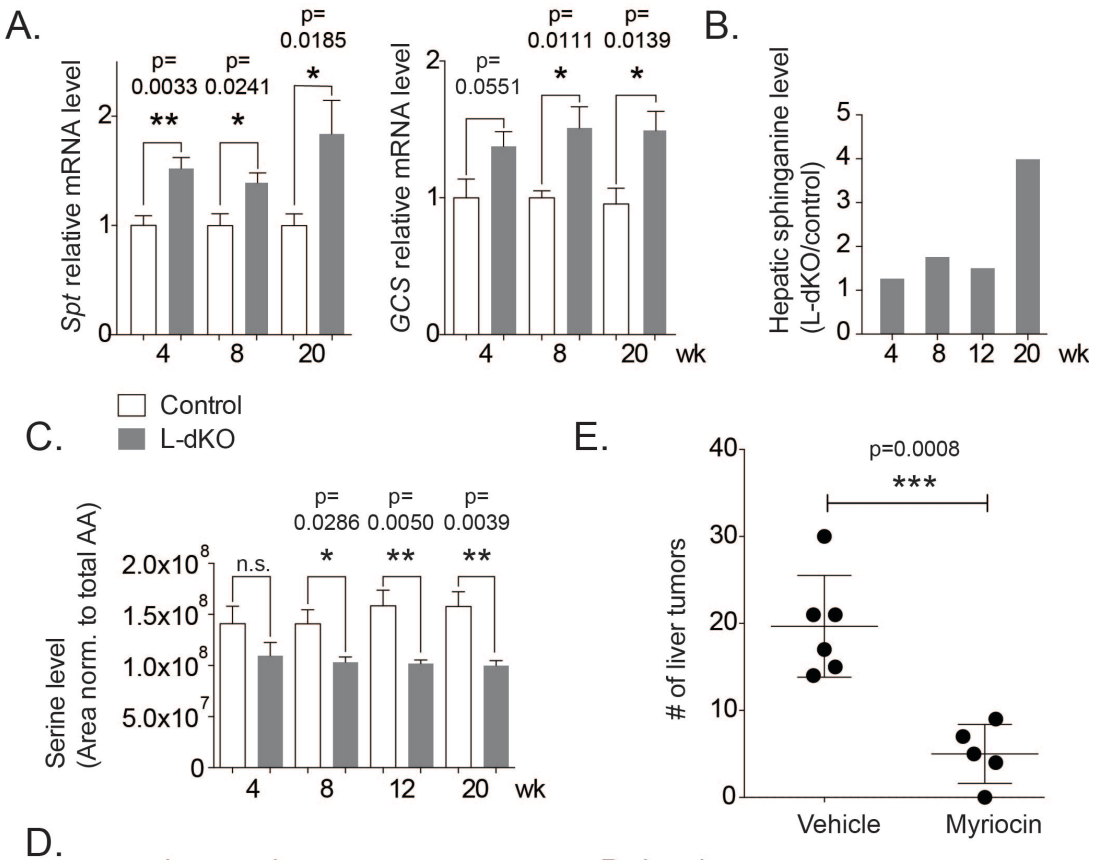
A.
Spt relative mRNA level
p= 0.0033
p= 0.0241
p= 0.0185
**
*
*
4 8 20
GCS relative mRNA level
p= 0.0551
p= 0.0111
p= 0.0139
*
*
4 8 20 wk
B.
Hepatic sphinganine level (L-dKO/control)
4 8 12 20 wk
Control
L-dKO
C.
Serine level (Area norm. to total AA)
p= 0.0286
p= 0.0050
p= 0.0039
n.s.
*
**
**
2.0x10^8
1.5x10^8
1.0x10^8
5.0x10^7
0
4 8 12 20 wk
E.
# of liver tumors
p=0.0008
***
Vehicle
Myriocin
D.
Increased
Reduced
-Log p
Difference
DHCer38:0-OH
DHCer38:1
DHCer36:0-OH
DHCer36:1
GlcCer42:1-OH
Cer36:1-OH
Cer36:2
GlcCer30:2-OH
GlcCer44:1
DHCer34:0-OH
DHCer36:1
DHCer36:0
GlcDHCer40:1
SM36:0
Cer44:2
GlcCer44:2-OH
GlcDHCer30:1
SM38:0
GlcCer36:1
GlcDHCer42:0
GlcDHCer44:0-OH
GlcDHCer34:1
DHCer30:0
DHCer38:0
GlcCer42:2
Cer28:1
GlcCer38:2
DHCer40:1
DHCer30:1
PI32:1
PC(O-)36:3
PI44:5
PC(O-)34:2
PC42:4
PC40:2
PC(O-)40:6
PE34:4
PC42:6
PC(O-)36:5
PC38:0
CE74:7
PE(O-)36:3
PE(O-)40:3
PC(O-)38:2
PS42:6
PC44:6

Figure 3. *mTOR promotes de novo sphingolipid synthesis and thereby tumor development.* **(A)** Relative hepatic mRNA level (normalized to cyclophilinD) in 4, 8 and 20 week-old L-dKO and control mice (n=6 per group), for the indicated genes. **(B)** Hepatic sphinganine levels in livers of 4, 8, 12 and 20 week-old mice (n=6 per group). Data represented as the ratio of L-dKO over age-matched control. **(C)** Hepatic serine levels in livers of 4, 8, 12 and 20 week-old mice (n=6 per group). Normalized (norm.) to total amino acids (AA). **(E)** Number of liver tumors in L-dKO mice after chronic myriocin treatment. **(F)** Scatter plot of the major lipid species significantly regulated in livers from myriocin treated mice (L-dKO vs. control), as compared to the drug vehicle. Glucosylceramide lipid species are indicated in red. Black line indicates the significant from the non-significant alterations, for threshold of 0.75 Log-Fold change. To determine statistically significant differences unpaired Student's t-test was used. Data represent mean ± SEM.

Figure 4

A.

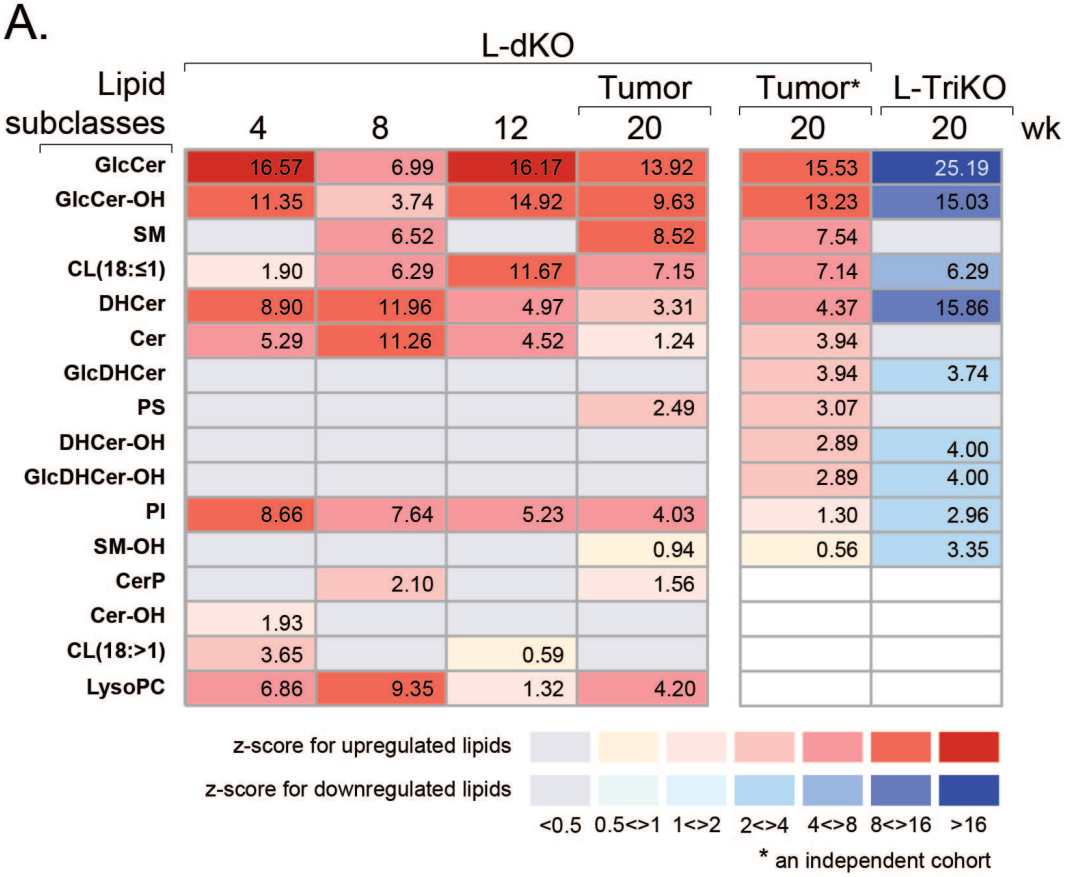

Figure 4. *L-dKO mice accumulate sphingolipids and glycerophospholipids in the liver.* **(A)** Enrichment of the indicated lipid subclasses (Z-Score, Binomial Proportions Test), for the indicated genotypes. Data expressed as the ratio of L-dKO over age-matched control (n=6 per time point); L-TriKO mice over L-dKO mice (20 week old) (n=4). Abbreviations: **GlcCer**, Glucosylceramide; **GlcCer-OH**, hydroxyglucosylceramide; **SM**, Sphingomyelin; **CL(18:≤1) or CL(18:>1)**, Cardiolipin with the indicate desaturation; **DHCer**, Dehydroceramide; **Cer**, Ceramide; **GlcDHCer**, glucosyldehydroceramide; **PS,** Glycerophosphoserine; **DHCer-OH**, hydro-deoxy-ceramide, **GlcDHCer-OH**, Gluc-hydro-deoxy-ceramide, **PI**, Glycerophosphoinositol, **SM-OH**, Hydro-sphingomyelin, **CerP**, Phospho-ceramide, **Cer-OH**, hydro-ceramide; **LysoPC,** Lysophosphatidylcholine.

Figure 5

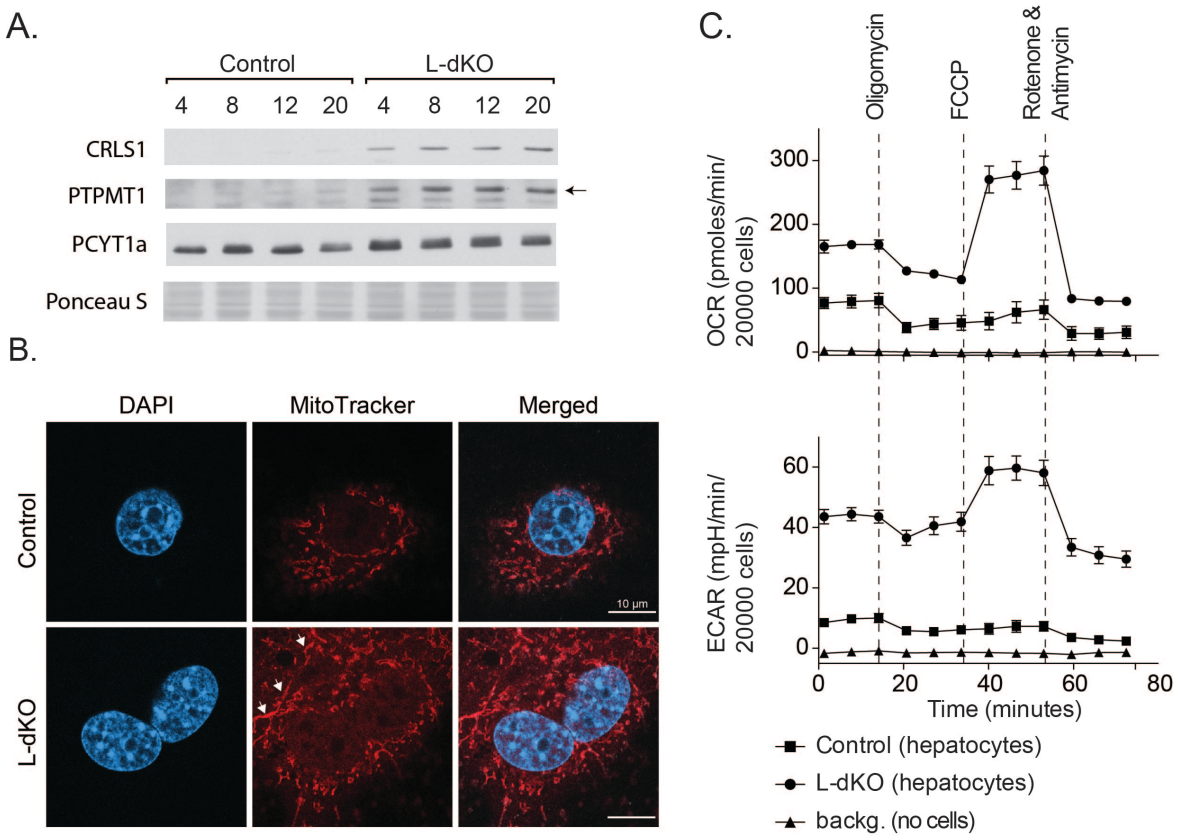

Figure 5. *mTOR promotes cardiolipin synthesis and oxidative phosphorylation in hepatocytes.* **(A)** Immunoblot analysis of liver extracts from 4, 8, 12, and 20 week-old L-dKO mice and control littermates, for the indicated proteins. Each lane consists of a mixture of liver extracts obtained from six mice. **(B)** Representative images of primary hepatocytes perfused from 8 week-old L-dKO and control mice. MitoTracker (red) indicates mitochondria.; white arrows indicate tubular mitochondrial networks. Nuclei, blue (DAPI); Scale bar 10µm. Acquired using LSM800 AriScan confocal microscope. **(C)** Oxygen consumption rate (OCR) and extracellular acidification rate (ECAR) analyses of primary hepatocytes perfused from 8 week-old L-dKO and control mice. Dashed lines indicate the time a given compound was added; Backg, background contains no cells; Pcyt1a, phosphate cytidylyltransferase 1, choline, alpha; data represent mean ± SEM.

Figure 6

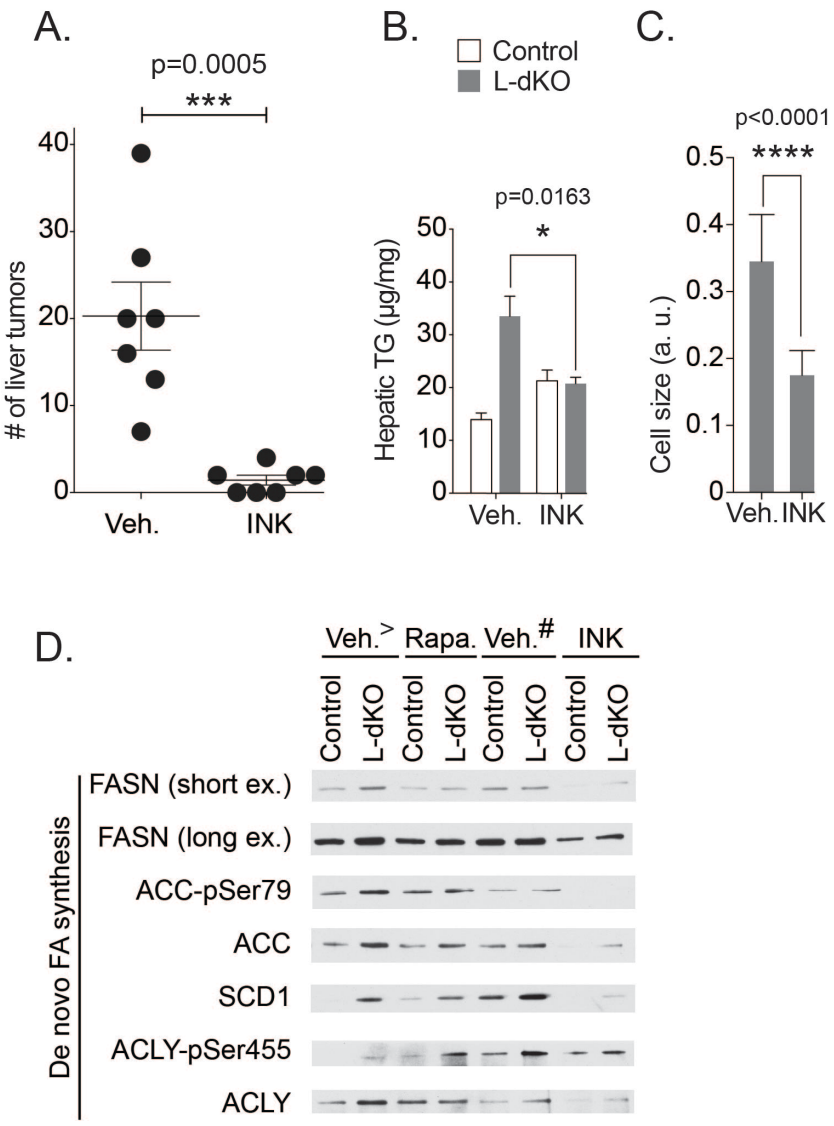

Figure 6. *mTOR promotes tumor development in L-dKO mice.* **(A)** Number of liver tumors in L-dKO mice treated with INK128 (INK) or the drug vehicle (Veh.). **(B)** Hepatic triglyceride (TG) content of L-dKO and control mice treated with INK128 or the drug vehicle (n=7 per group). **(C)** Cell-size expressed as area (a.u. arbitrary unit) calculated using FIJI from scanned histological samples stained for H&E. **(D)** Immunoblot analysis of liver extracts from 8 week-old L-dKO and control mice (n=4 per group) acutely (24hrs) treated with rapamycin (Rapa), INK128 or drug vehicle alone (Veh$^{>}$ and Veh$^{\#}$ treated with rapamycin or INK128 vehicle control, respectively), for the indicated proteins. Values are expressed as mean ± SEM.

Figure 7

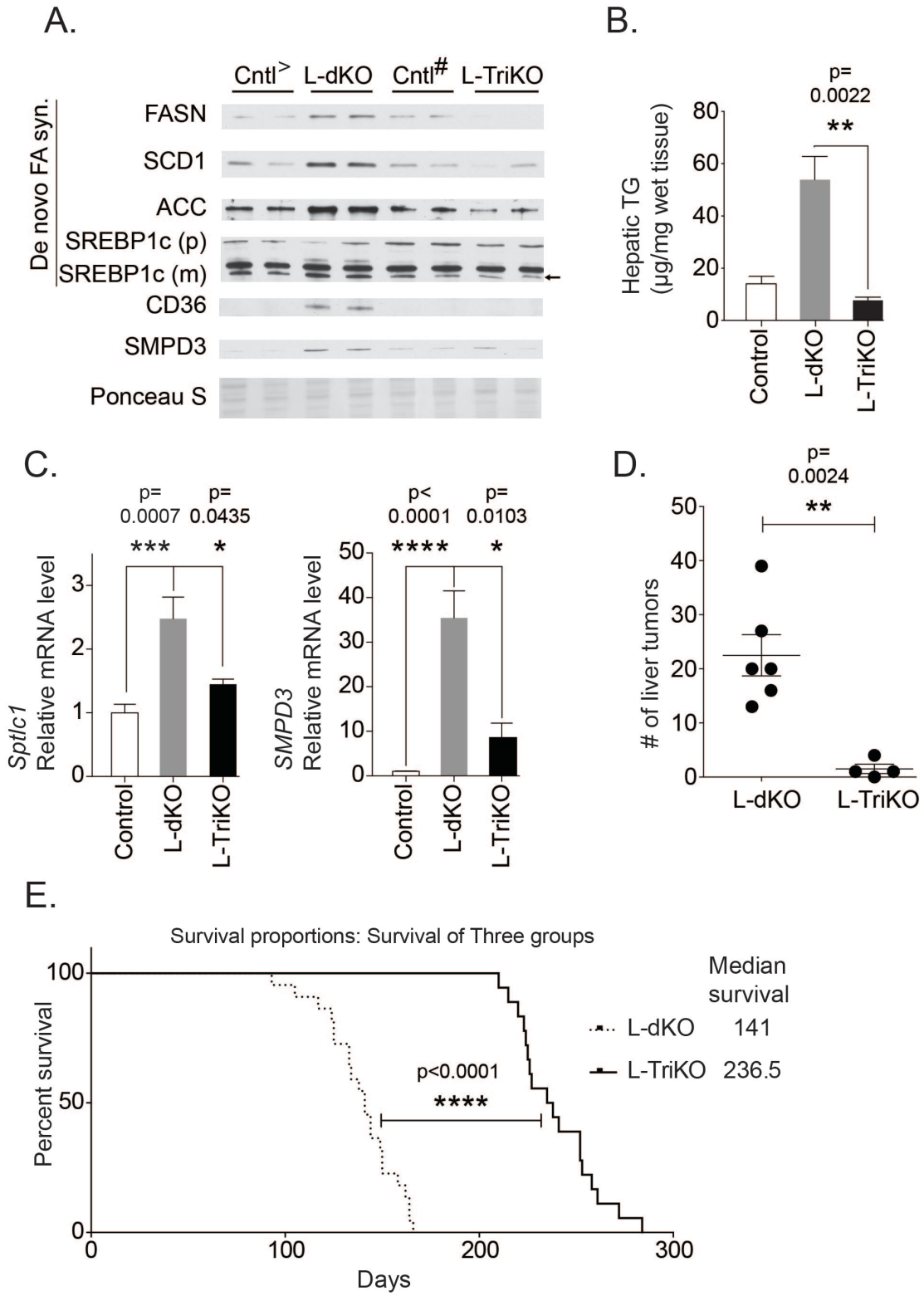
A.
Cntl>
L-dKO
Cntl#
L-TriKO
De novo FA syn.
FASN
SCD1
ACC
SREBP1c (p)
SREBP1c (m)
CD36
SMPD3
Ponceau S
B.
p= 0.0022
**
Hepatic TG (μg/mg wet tissue)
Control
L-dKO
L-TriKO
C.
p= 0.0007
p= 0.0435
***
*
Sptlc1 Relative mRNA level
p< 0.0001
p= 0.0103
****
*
SMPD3 Relative mRNA level
Control
L-dKO
L-TriKO
D.
p= 0.0024
**
# of liver tumors
L-dKO
L-TriKO
E.
Survival proportions: Survival of Three groups
Percent survival
Days
Median survival
L-dKO 141
L-TriKO 236.5
p<0.0001
****

Figure 7. *mTORC2 promotes fatty acid and lipid accumulation and carcinogenesis*. **(A)** Immunoblot analysis of liver extracts from 20 week-old L-dKO, L-TriKO and control mice (n=4 per group; Cntl$^{>}$ and Cntl$^{\#}$ are *Tsc1*$^{loxP/loxP}$*; Pten*$^{loxP/loxP}$*;* and *Tsc1*$^{loxP/loxP}$*; Pten*$^{loxP/loxP}$*; Rictor*$^{loxP/loxP}$, respectively), for the indicated proteins. **(B)** Hepatic triglyceride (TG) content of L-dKO, L-TriKO and pulled controls (n ≥ 4 per group). **(C)** Relative mRNA level (normalized to cyclophilinD) of the indicated genes in 20 week-old L-dKO (n=6), L-TriKO (n=4) and control (n=8) mice. **(D)** Number of macroscopic liver tumors detected in L-dKO and L-TriKO mice **(E)** Kaplan Meier survival curve of L-dKO and L-TriKO mice. (**** $p<0.0001$ for both Mantel-Cox and Gehan-Breslow-Wilcoxon tests, ## $p<0.0008$ Mantel-Cox and $p= 0.0021$ Gehan-Breslow-Wilcoxon tests). Error bars represent SEM.

Supplemental Figures

Figure S1, related to Figure 1

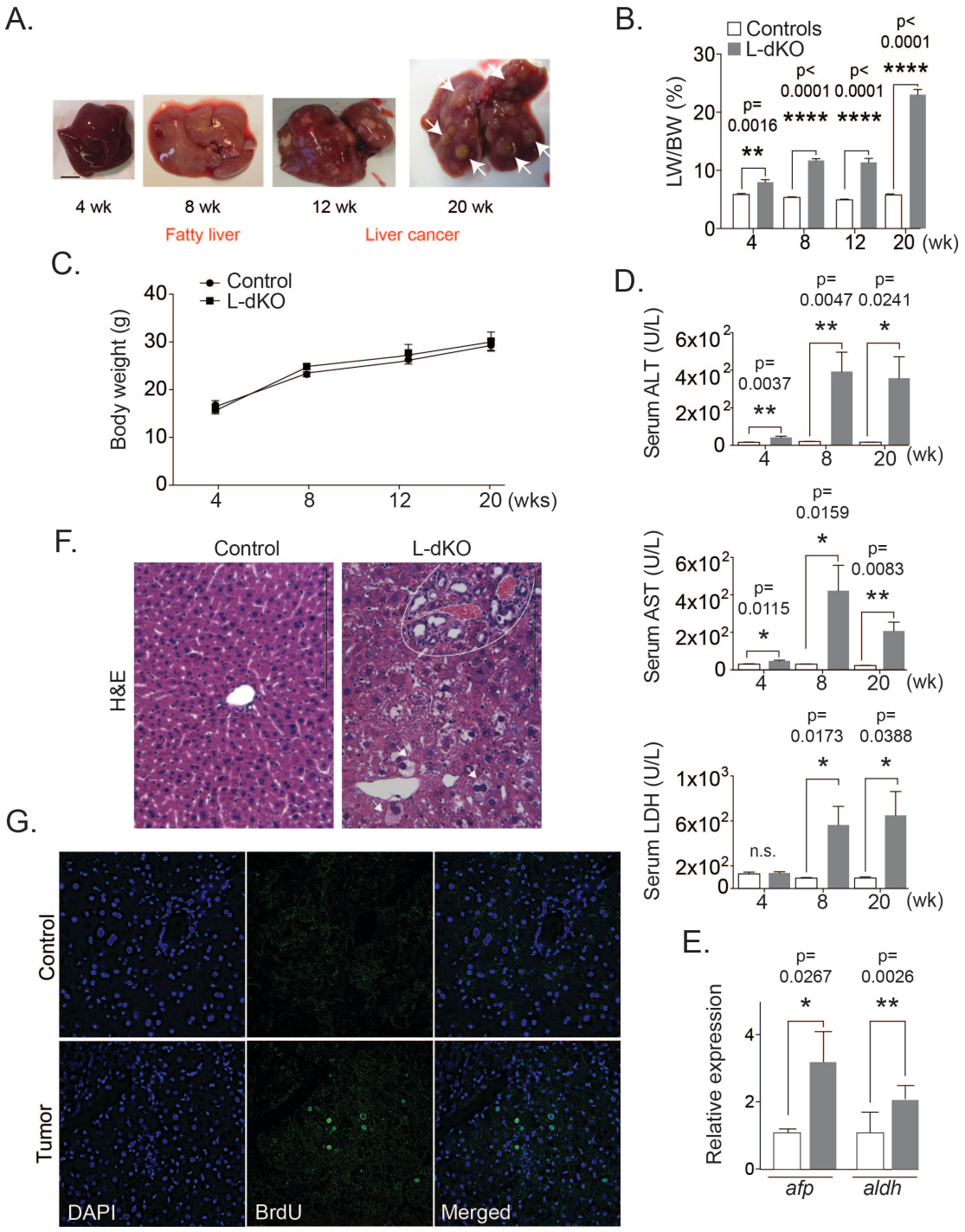

Figure S1, related to Figure 1. *Hepatic mTOR activation induces tumor development.* **(A)** Representative images of livers from 4, 8, 12 and 20 week-old L-dKO mice; white arrows indicates liver tumors. **(B)** Liver weight (LW) to body weight (BW) ratio (percentage) of L-dKO mice and age-matched control mice for the indicated time-points. **(C)** Total body weight of 4, 8, 12 and 20 week-old L-dKO and control mice ($n \geq 10$ per time point) **(D)** ALT (alanine aminotransferase), AST (aspartate aminotransferase) and LDH (lactate dehydrogenase) ($n \geq 4$) serum levels, in unit per liter (U/L) **(E)** Relative mRNA level (normalized to cyclophilinD) of *afp* and *aldh* in liver lysates from 8 week-old L-dKO and control mice ($n \geq 4$). **(F)** Representative hematoxylin and eosin (H&E) images from 8 week-old L-dKO and control mice; white arrows, hepatocytic-ballooning reminiscent of lipid accumulation (macrosteatosis); white circle, choleangiocytic proliferation **(G)** Representative immunofluorescence images of BrdU incorporation assessed in tumors from 16 week-old L-dKO and non-tumor control. To determine statistically significant differences unpaired Student's t-test was used. Data represent mean ± SEM.

Figure S2, related to Figure 1

A.

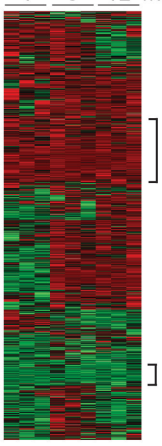

B.

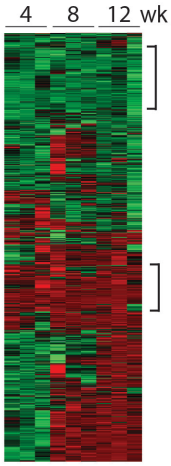

C.

Lipid Metabolism

Pathways enriched in proteome

	pValue -log	In data	Total
Immune response_Antigen presentation by MHC class I	6.99	9	28
Triacylglycerol metabolism	4.91	10	59
Translation_Regulation of translation initiation	4.89	7	27
Regulation of degradation of deltaF508 and wtCFTR	4.66	8	39
Fatty Acid Omega Oxidation	4.15	7	34
Biosynthesis of PA fatty acid	3.85	9	63
Translation_Regulation of EIF4F/insulin	3.67	11	56
Neurophysiological process_Axonal transport	3.61	8	54
Cytoskeleton remodeling	3.49	13	104
Regulation of lipid metabolism_Insulin signaling	3.24	7	47
CFTR folding and maturation	3.13	5	24
Activation of antioxidant_Sirtuin1 and PGC1-alpha/Arsenite	3.11	7	60
Apoptosis and survival_BAD_TNFα-induced Casp 8 sig.	2.75	10	46
Linoleic acid	2.60	5	31
Biosynthesis of unsaturated fatty acid	2.52	7	62

D.

Pathways enriched in phosphoproteome

	pValue -log	In data	Total
Cell adhesion_Tight junctions	5.26	6	36
Reg. of lipid metabolism_Insulin reg. of glycogen metabolism	4.13	6	56
Development_Activation of ESR1 and 2	3.60	7	47
Cell adhesion_Endothelial cell contacts	3.52	6	28
Reg. of lipid metabolism_Insulin signaling	3.51	7	49
Integrin-mediated cell adhesion and migration	3.46	5	48
Transport_The role of AVP in reg. of Aquaporin 2	3.38	5	50
Development_MAG-dependent inhibition of neurite outgrowth	2.92	4	37
Transcription_PPAR Pathway	2.91	5	63
Transport_Macropinocytosis regulation by growth factors	2.91	5	63
Cytoskeleton remodeling	2.72	6	102
Role of ZNF202 in reg. of genes involved in atherosclerosiss	2.64	3	21
Transcription_CREB pathway	2.46	4	49
Apoptosis and survival_HTR1A signaling	2.43	4	50
Signal transduction_PKA signaling	2.40	4	51

E.

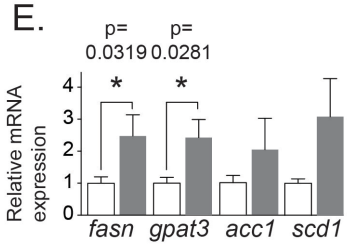

F.

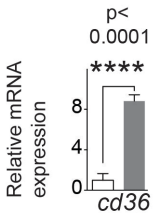

G.

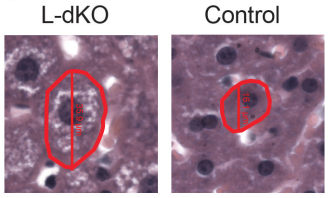

H.

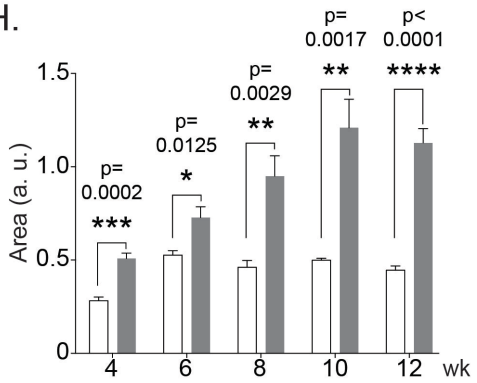

I.

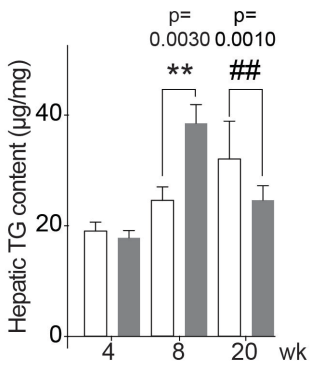

Figure S2, related to Figure 1. *(Phospho)proteomic analysis indicates enhanced fatty acid and lipid metabolism in L-dKO mice.* **(A)** Heat-maps of the unsupervised hierarchical clustering using Euclidian distance of proteome and **(B)** phosphoproteome performed on snap-frozen liver samples from 4, 8 and 12 week-old L-dKO and control mice. The corresponding pathway enrichment analysis was performed for proteins **(C)** and phosphosites **(D)** down- or up- regulated in all three time points (dark lines). Lipid metabolic pathways are marked in yellow. **(E), (F)** Relative hepatic mRNA level (normalized to cyclophilinD) of the indicated genes from 8 week-old L-dKO and control mice (n ≥ 4). **(G)** Representative H&E images from 8 week-old L-dKO and control mice. Red circle marks a hepatocyte with the diameter indicated. **(H)** Area calculated from H&E stained liver samples from 4, 6, 8, 10 and 12 L-dKO and control mice. Area is relative to the image magnification (a.u. arbitrary unit). **(I)** Hepatic triglyceride (TG) content from overnight fasted L-dKO and control mice (n ≥ 6 per group). To determine statistically significant differences unpaired Student's t-test was used. Data represent mean ± SEM.

Figure S3, related to Figure 1

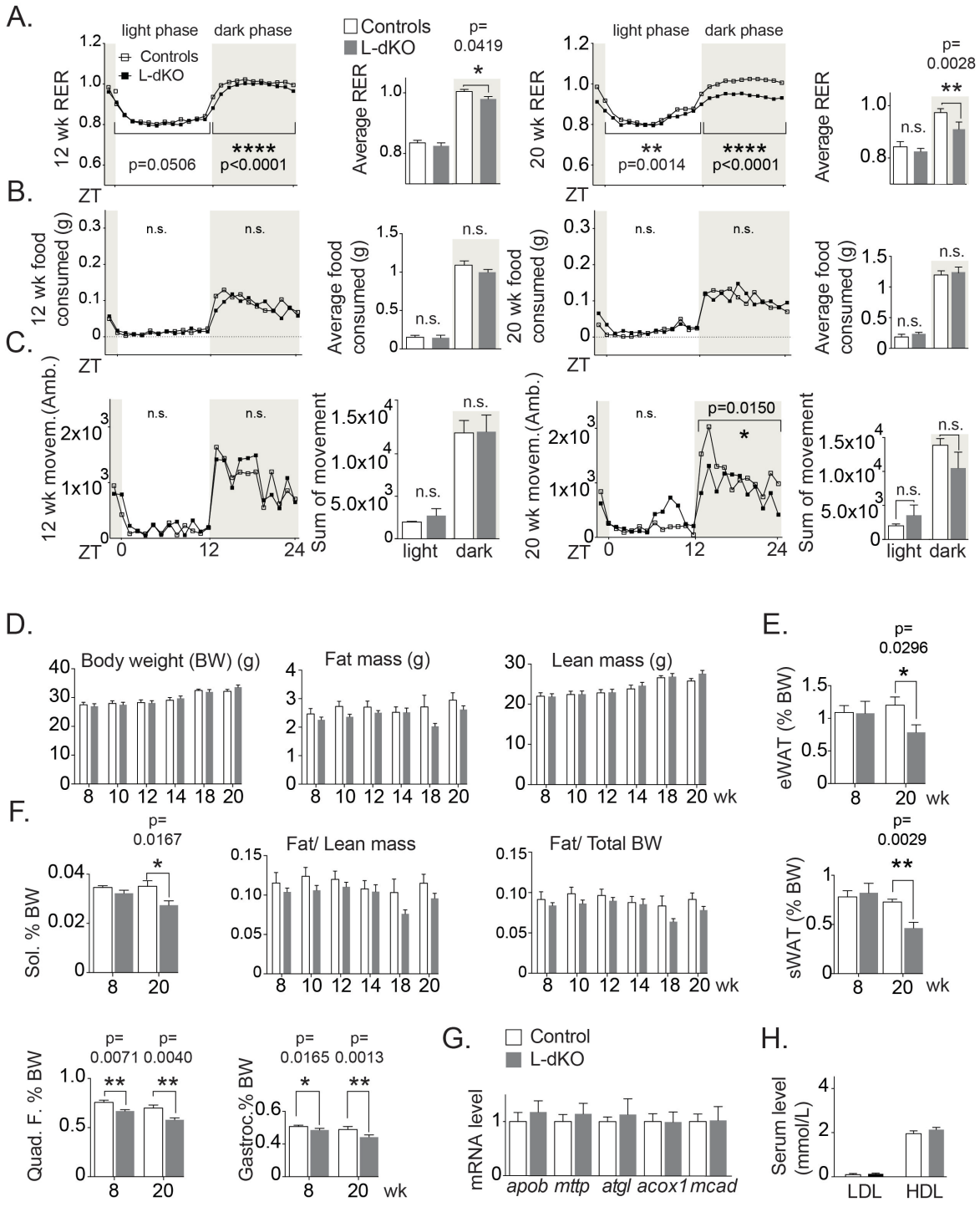

Figure S3, related to figure 1. *L-dKO mice exhibit whole body cachexia-like effects.* **(A)** RER (Respiratory Exchange Ratio, unit-less ratio of the rate of CO_2 production to the rate of O_2 consumption) **(B)** food consumption and **(C)** movement (ambulatory) of 12 and 20 week-old L-dKO and control mice measured over 72hrs (n=8 control, n=7 L-dKO). The last 48 hours of measurement were used for quantification. Sums of light or dark phases are also calculated. **(D)** Longitudinal whole-body fat composition analyses (EchoMRI) of live L-dKO and control mice (n=8 control, n=7 L-dKO). **(E)** Percent of epididymal white adipose tissue (eWAT) and subcutaneous WAT mass (normalized to the body weight (BW)) of 8 and 20 week-old L-dKO and control mice (n ≥ 6 per group). **(F)** Percent of skeletal muscle mass (normalized to the body weight) of 8 and 20 week-old L-dKO and control mice. Sol, Soleus muscle; Quad. f., Quadriceps Femoris muscle; Gastroc., Gastrocnemius muscle (n ≥ 6 per group); BW, body weight. **(F)** Relative mRNA level (normalized to cyclophilinD) from livers of 8 week-old L-dKO and control mice (n=6 per group), for the indicated genes. **(H)** LDL and HDL level in serum of 8 week-old L-dKO and control mice (n=4 per group). To determine statistically significant differences unpaired Student's t-test was used. Data represent mean ± SEM.

Figure S4, related to Figure 2

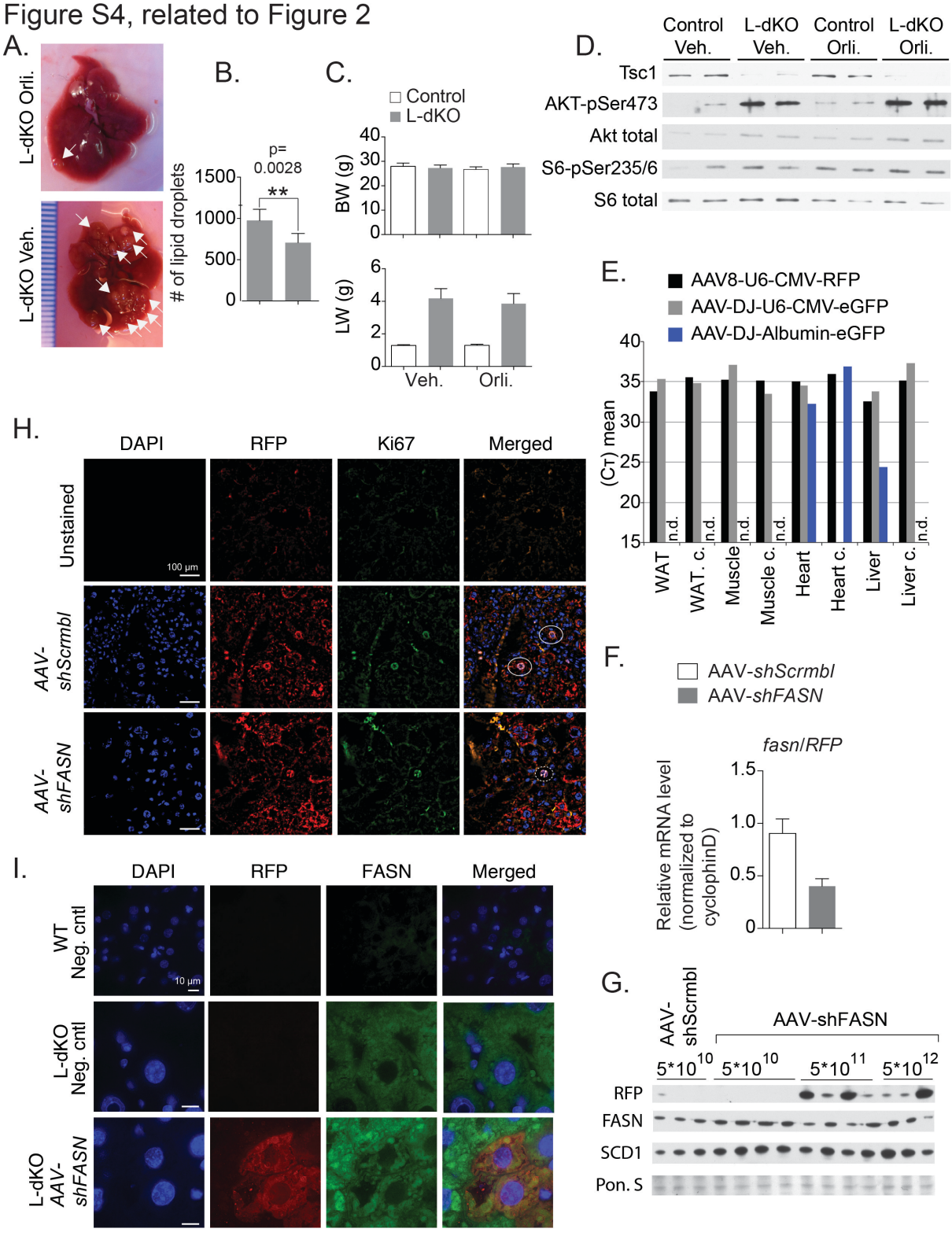

Figure S4, related to figure 2. *FA synthesis is required for tumor development.* **(A)** Representative images of livers from L-dKO mice treated with orlistat or the drug vehicle alone **(B)** and number of lipid droplets quantified from histological sections (not shown). White arrows indicated HCCs. **(C)** Body weights (BW) and liver weights (LW) **(D)** and immunoblot from liver lysates from L-dKO and control mice treated with orlistat (Orli.) or the drug vehicle (Veh.) alone. **(E)** The indicated adeno-associate viruses (AAV) were injected into tail veins of wild-type mice; control mice were injected with PBS. The expression of GFP or RFP was from a U6 or albumin promoter (as indicated). mRNA expression of GFP or RFP was assessed by quantitative PCR. The absolute (not normalized) Ct values are depicted, for the indicated tissue. n.d., not detected. **(F)** mRNA *fasn* expression relative to *RFP* expression of livers of mice infected with AAV-*shFASN* or AAV-*shScrmbl.* **(G)** Immunoblot analysis of liver extracts from mice (one per lane) infected with different viral genomes of AAV-*shFASN* and AAV-*shScrmbl* control, for the indicated proteins. Pon. S, Ponceau S. **(H)** Representative immunofluorescence images of livers from L-dKO mice infected (tail vein) with AAV-DJ-Albumin-*shFASN-RFP* (AAV-*shFASN*) or AAV-*shScrmbl*. shFASN or AAV-*shScrmbl* were expressed from the albumin promoter. White circles marks AAV-*shScrmbl* infected Ki67 positive hepatocytes. Dashed circle marks a non-infected hepatocyte that is Ki67 positive. Nuclei, blue (DAPI); Scale bar 100μm. **(I)** Representative immunofluorescence images of livers from L-dKO mice infected (tail vein) with AAV-*shFASN*. Neg. cntl, negative control was injected with PBS. Scale bar 10μm. Images obtained using 'DeltaVision Core' widefield microscope. Images were deconvoluted. Data represent mean ± SEM.

Figure S5, related to Figure 3

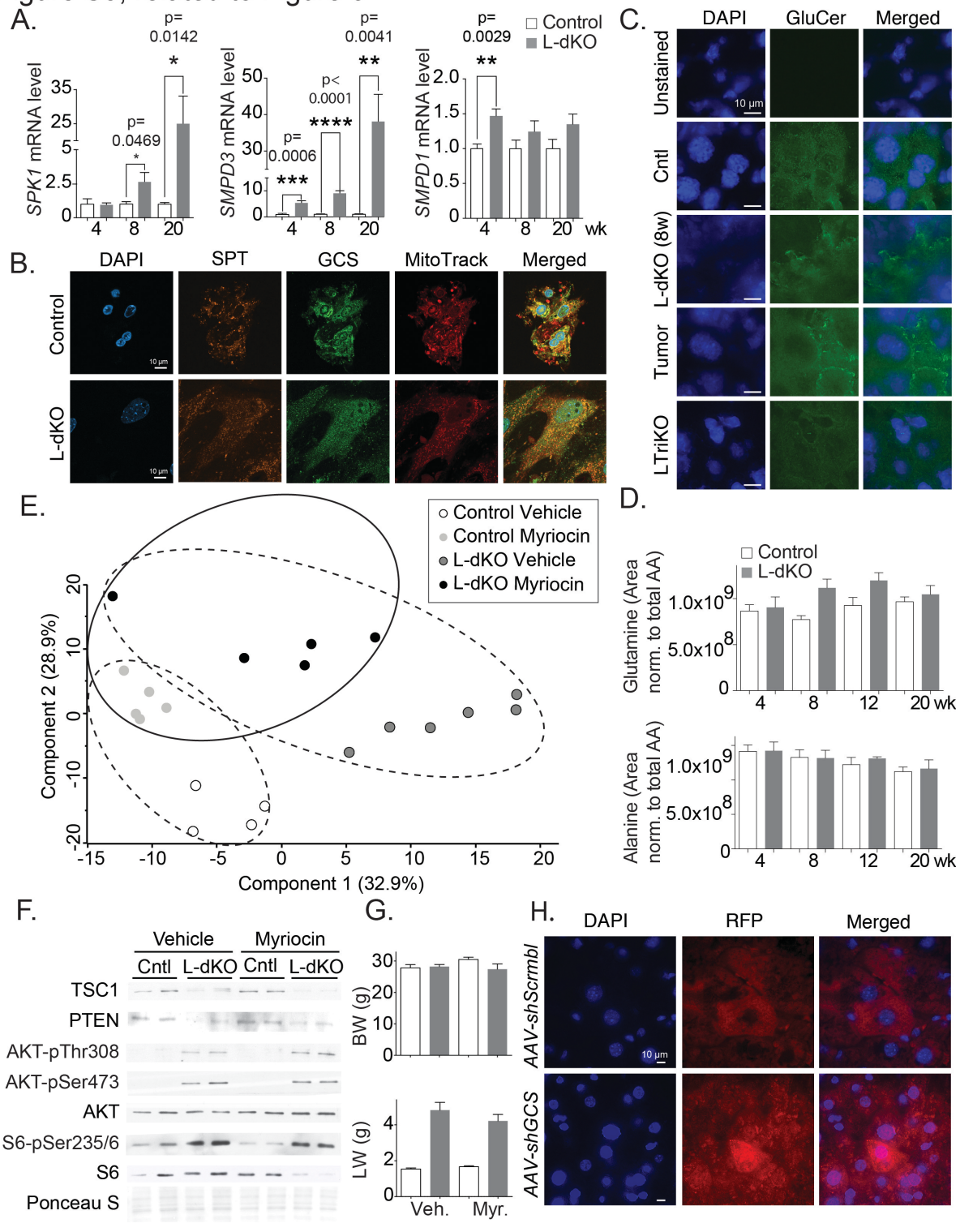

Figure S5, related to figure 3. *De novo sphingolipid synthesis is required for tumor development.* **(A)** mRNA expression levels in livers from 4, 8 and 20 week-old L-dKO and control mice (n=6 per genotype), for the indicated genes. SPK1, sphingosine kinase; SMPD3, neutral sphingomyelinase; SMPD1, acid sphingomyelinase. **(B)** Representative immunofluorescence images of primary hepatocytes from L-dKO or control mice. Nuclei, blue (DAPI); SPT, serine palmitoyltransferase; GCS, glucosylceramide synthase; MitoTrack, MitoTracker Red mitochondria. Scale bar 10μm. LSM800 AriScan confocal microscope. **(C)** Representative immunofluorescence images of livers from 8 week-old and 20 week-old (tumor) L-dKO, L-TriKO and control mice. GlcCer, glucosylceramide; nuclei, blue (DAPI); scale bar 10μm. **(D)** Hepatic glutamine and alanine levels from 4, 8, 12, and 20 week-old L-dKO and control mice normalized to total amino acids (AA). **(E)** Principal-component analysis (PCA) of lipidomics from L-dKO and control mice treated with myriocin or the drug vehicle alone. PCA analysis showed a clear discrimination between L-dKO and control mice, driven by principal component 1 (dashed circles). Principle component 2 drove the separation between myriocin and vehicle treated groups (closed circle). **(F)** Immunoblot analysis of liver extracts from L-dKO and control mice treated with myriocin or the drug vehicle only, for the indicated proteins. **(G)** Body weights (BW) and liver weights (LW) of L-dKO and control mice treated with myriocin (Myr.) or the drug vehicle (Veh.) alone. **(H)** Representative immunofluorescence images of livers from L-dKO mice infected (tail vein) with AAV-*shGCS.* Scale bar 10μm. 'DeltaVision Core' widefield microscope. Images were deconvoluted. Values are expressed as mean ± SEM.

Figure S6, related to Figures 4 to 6

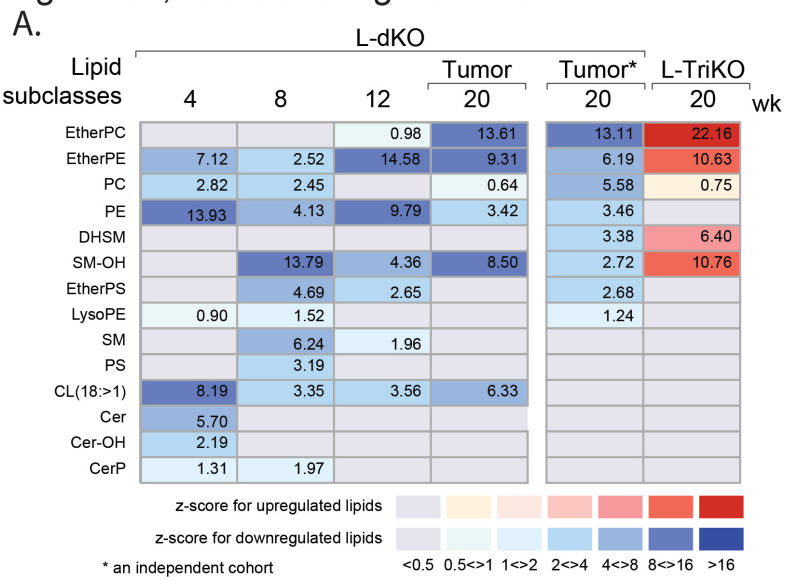

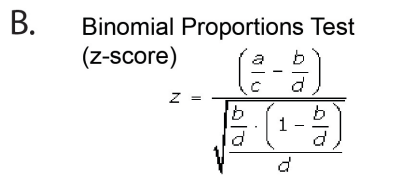

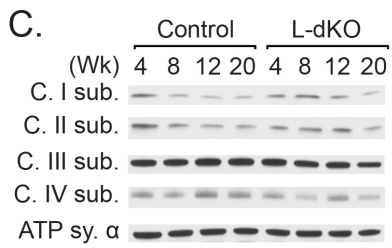

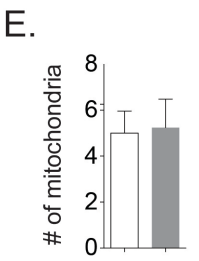

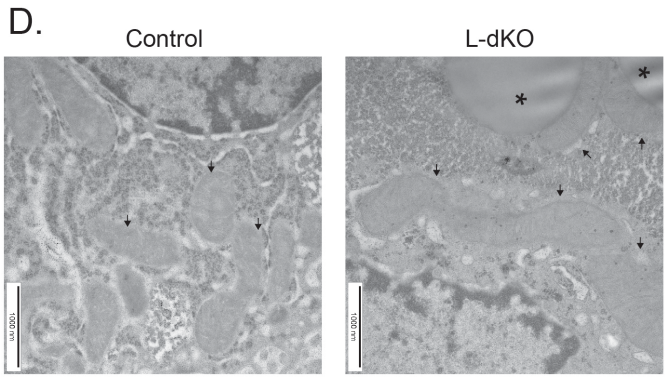

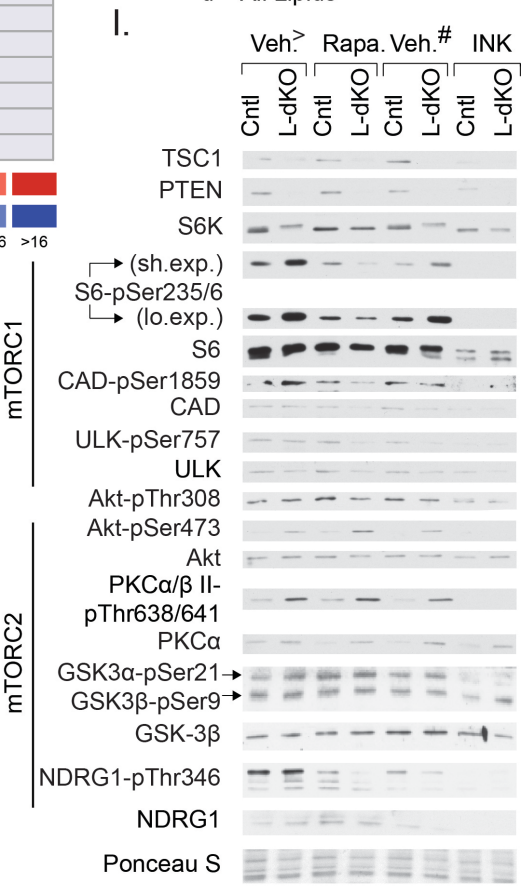

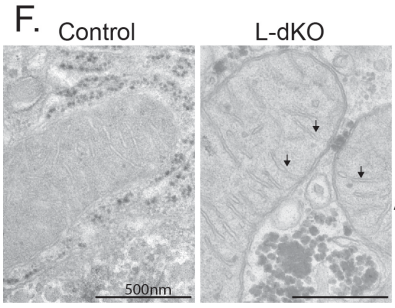

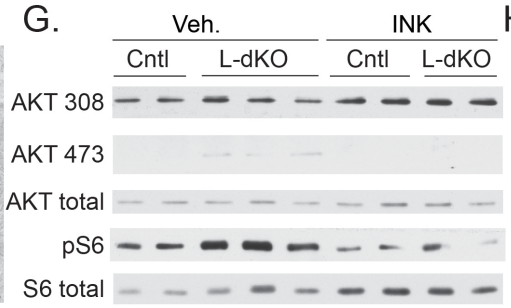

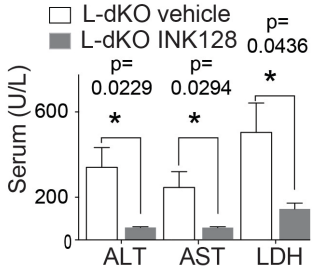

Figure S6, related to figures 4 to 6. *Enhanced cardiolipin accumulation and mitochondria function in mTOR-activated tumors* **(A)** Lipid subclasses depleted in livers of L-dKO mice or L-TriKO mice. Data expressed as the ratio of L-dKO over age-matched control (n=6 per time point); L-TriKO mice over L-dKO mice (20 week old) (n=4). **(B)** Binomial Proportion Test formula used for enrichment calculation. **(C)** Immunoblot analysis of liver extracts from 4, 8, 12 and 20 week-old L-dKO and control mice (6 mice per lane), for the electron transport chain components (c. complex; sub. subunit; ATP sy. α, ATP synthase α). Each lane consists of a mixture of liver extracts obtained from six mice. **(D)** Representative electronmicrographs of hepatocytes from 8 week-old L-dKO and control mice (n=3). Asterisks and arrows indicate lipid droplets and mitochondria, respectively. Scale bar 1000nm **(E)** Number of mitochondria in hepatocytes from L-dKO and control mice. Quantified from electron electronmicrographs (n=3). **(F)** Dark arrows indicates the prominent mitochondrial cristae observed in hepatocytes from L-dKO, compared to age-matched control. Scale bar 500nm. **(G)** Immunoblot analysis of liver lysates from L-dKO and control mice chronically treated with INK128 (INK) or the drug vehicle alone (veh.), for the indicated proteins. (n ≥ 2 per lane). **(H)** ALT, AST and LDH levels (U/L) in serum from L-dKO mice treated chronically with INK or the drug vehicle alone. **(I)** Immunoblot analysis of liver extracts from 8 week-old L-dKO and control mice (n=4 per group) acutely (24hrs) treated with rapamycin (Rapa), INK128 or drug vehicle alone ($Veh^{>}$ and $Veh^{\#}$ treated with rapamycin or INK128 vehicle control, respectively), for the indicated proteins. Error bars represent SEM. Abbreviations: **EtherPC**, Ether-phosphatidylcholine; **EtherPE**, Ether-phosphatidylethanolamine; **PC**, phosphatidylcholine; **PE**, phosphatidylethanolamine; **DHSM,** dihydrosphingomyelin; **SM-OH,** sphingomyelin-OH; **EtherPS**, Ether-phosphatidylserine; **LysoPE,** Lyso phosphatidylethanolamine; **SM**, sphingomyelin; **PS,** phosphatidylserine; **CL(18:>1)**, Highly desaturated Cardiolipin; **Cer,** Ceramide; **Cer-OH,** Ceramide-OH; **CerP,** ceramide phosphate.

Figure S7, related to Figure 7.

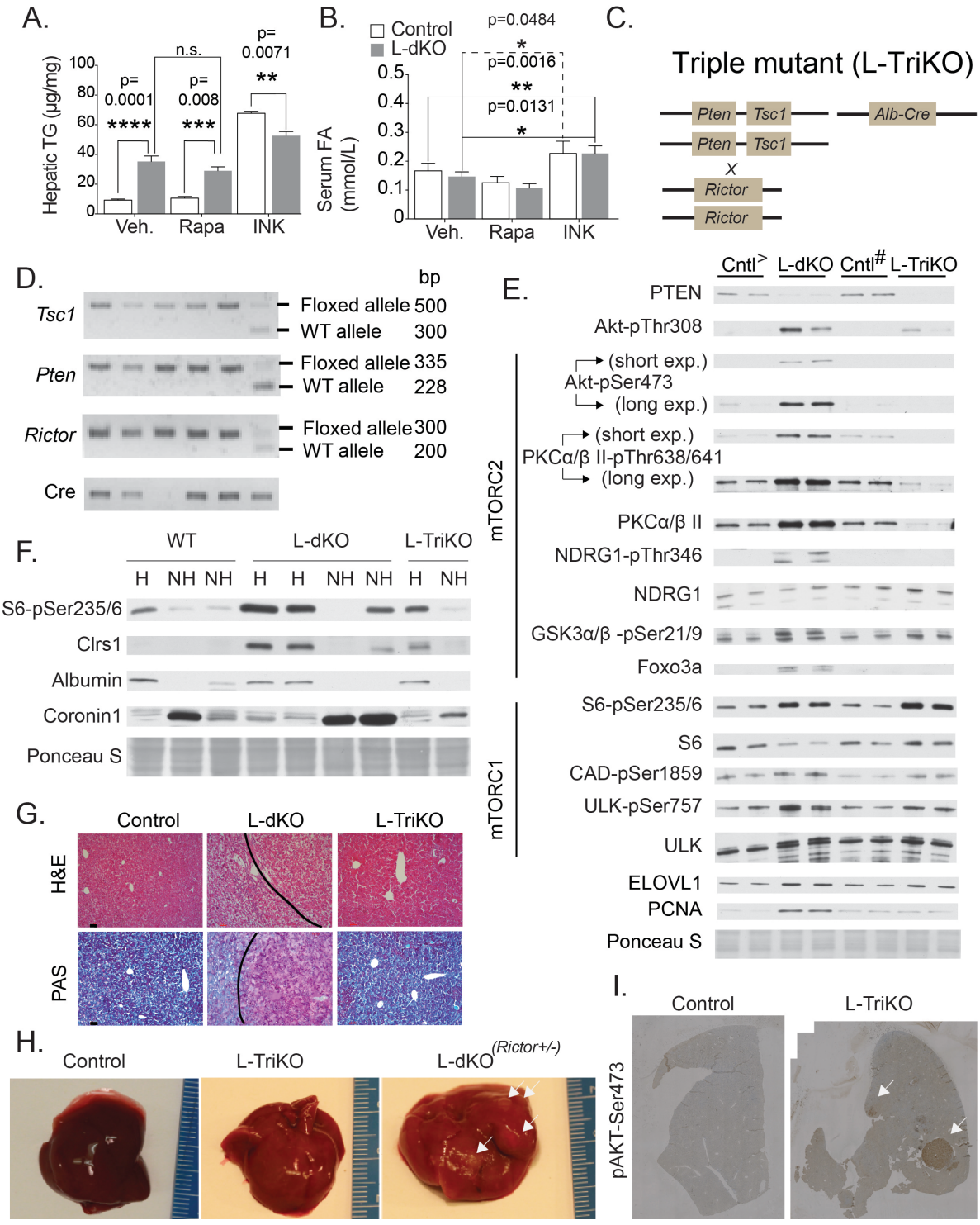

Figure S7, related to figure 7. *mTORC2 controls hepatic FA and lipid synthesis.* **(A)** Hepatic triglyceride (TG) content and **(B)** serum fatty acids (FA) from 8 week-old L-dKO and control mice (n=4 per group) acutely (24hrs) treated with rapamycin (Rapa), INK128 or drug vehicle alone (pulled n=8). **(C)** Generation of triple mutant mice (floxed genes annotated; Alb, albumin promoter) **(D)** Representative DNA gels from L-TriKO mice for the indicated genes and Cre (Asterisk marks a Cre negative sample). **(E)** Immunoblot analysis from liver extracts from 20 week-old L-dKO, L-TriKO and the respective control mice (n=4, 2 mice per lane) (cntl$^{>}$ is *Tsc1*$^{loxP/loxP}$*;Pten*$^{loxP/loxP}$*;* cntl$^{\#}$ is *Tsc1*$^{loxP/loxP}$*;Pten*$^{loxP/loxP}$*; Rictor*$^{loxP/loxP}$). **(F)** Immunoblot analysis of extracts from hepatocytes (H) and non-hepatocyte (NH) cell fractions from perfused livers from 8 week-old L-dKO, L-TriKO and control mice (WT), for the indicated proteins. Coronin 1 and albumin are immune cell marker and hepatocyte marker, respectively. **(G)** Representative Hematoxylin and Eosin (H&E) and Periodic Acid-Schiff histological analyses from L-dKO, L-TriKO and control mice. **(H)** Representative images of livers from L-TriKO, L-dKO$^{(Rictor-/+)}$ and control mice. **(I)** Immunohistochemistry analysis of livers from 30 week-old L-TriKO with tumors and an age-matched non-tumor control. Arrows indicates pAKT-Ser473 positive regions (tumors). Values are expressed as mean ± SEM.

Extended Experimental Procedures

Pharmacological treatments. INK128 (Intellikine, Inc) or the drug vehicle alone was given by orally route (1 mg/kg/bw). INK128 was dissolved in 5% 1-methyl-2-pyrrolidionone, 15% polyvinylpyrrolidone K30, and 80% water, as described (Hsieh, Liu et al. 2012). 8-week-old L-dKO mice and littermate controls (n=7 per group) were treated with INK128 or with the drug vehicle, every second day for 12 weeks. Rapamycin (LC Laboratories) was dissolved as published (Cornu, Oppliger et al. 2014) in 5% (vol/vol) PEG-400, 4% (vol/vol) ethanol, and 5% (vol/vol) Tween 80, and was injected intra-peritoneally (i.p.). For acute mTOR inhibition studies, rapamycin or INK128 or the drugs vehicles were administered to 8-10 weeks-old L-dKO and littermate controls (n=4 per group), twice (6 am and 6pm) over 24 hours at doses described above. Orlistat (Xenical) was orally given (120mg/kg) to 6-8 week-old L-dKO mice and littermates controls (n=4 per group) daily for 10 weeks, as described (Sounni, Cimino et al. 2014). Myriocin was formulated as described (He, Johnson et al. 2004). Myriocin or the drug vehicle was i.p. administered (0.03 mg/kg/bw) to 6-8 week-old L-dKO mice and littermate controls (n=5 myriocin, n=4 vehicle), every second day. For tumor burden assessment, mice were sacrificed (~ 20 weeks of age) and their livers removed. Subsequently, externally visible tumors (>0.2 mm) were counted by stereomicroscopy. To evaluate cell proliferation in tumors, 16 week-old L-dKO and littermate control mice were i.p. injected with 100 mg/kg BrdU (Roche) once a day, at 18:00pm for three days. At 6:00am of the forth day, mice were sacrificed and livers were removed. Liver lobes, containing both

tumor and non-tumor regions, were fixed in 4% paraffin and were then used for immunofluorescence imaging using the BrdU in situ detection kit (Roche).

Serum parameters. Prior to liver dissection, blood was collected from the inferior vena cava using a 23-gauge needle. Blood was placed immediately into a heparin-coated tube (BD microtainer) to obtain plasma. Subsequently, 50ul of plasma was diluted three times and loaded to a COBAS (Roche) analyzer. Serum parameters, including circulating transaminases (ALT, AST), LDH, albumin, as well as serum lipids levels (LDL, HDL) were measured.

Isolation of primary cells and cell culture. For isolation of primary mouse hepatocytes 8-12 week-old L-dKO and littermate controls were used. Primary hepatocytes were obtained by liver perfusion. Shortly, peritoneal cavity was opened and the inferior vena cava was cannulated using a 23-gauge needle catheter. Cannula was clamped using a surgical clip. The liver was then perfused with pre-warmed (37c) Ca2+ and Mg2+ free-HBSS containing EGTA (1 mM), at a rate ranging from <5 to 10ml/min prior to chest dissection. The aorta was ligated followed and the portal vein was transected. Liver was then perfused with pre-warmed (37c) HBSS with Ca2+ and Mg2+ containing collagenase digestion solution (collagenase type II (C6885 SIGMA) and DNase I (10 µg/mL)), at a rate of 7.5ml/min. Subsequently, the perfused and digested liver was carefully dissected and placed in a petri dish containing ice-cold HBSS. Glisson capsule was gently teased with forceps to get the cell suspension. Cell suspension was filtered through gauze to remove undigested tissue and connective tissue, followed by 5 min

centrifugation 650 × g. Thereafter, re-suspended with HBSS and followed by 3 min at 35 × g centrifugation to obtain parenchymal cells (hepatocytes, pellet) and non-parenchymal cells (non-hepatocytes, supernatant). Parenchymal cell suspensions, containing vital hepatocytes, were used for culture. Briefly, hepatocytes were resuspended in pre-warmed culture media (DMEM high glucose with 10% fetal bovine serum (FBS).

Quantitative PCR. Total RNA was isolated from ~50 mg of mouse livers. Liver samples were homogenized for 30 sec bead beating in lysing matrix D tubes (Q-Biogene) containing 1 mL of TRIzol reagent (Sigma). After the chloroform extraction and centrifugation, samples were mixed with 600 µL of 70% ethanol, and the extraction was continued with the RNeasy kit (Qiagen). DNase digestion was performed using RNase-Free DNase Set (Qiagen). cDNA synthesis was performed using SuperScript III reverse transcriptase (Invitrogen). Semi-quantitative real-time PCR was done using the fast SYBR green mix (Applied Biosystems) and quantitated using Applied Biosystems StepOnePlus Real-Time PCR Systems (Applied Biosystems). Duplicate (or triplicate) runs of each sample were normalized to cyclophilin D to determine relative expression levels. Values plotted represent averages from at least four different animals. The sequences for the primer pairs used in this study are listed in Table S7.

Immunoblot. Mouse livers were rapidly isolated, flash-frozen into liquid nitrogen, and stored at -80 °C. For protein extraction liver tissues were homogenized using a polytron, in ice-cold lysis buffer (100 mM Tris (pH 7.5),

2 mM EDTA, 2 mM EGTA, 0.5 M mannitol) supplemented with 1% Triton X-100, protease and phosphatase inhibitor mixture tablets (Roche). Lysates were centrifuged at 10,000 × g for 10 min at 4 °C, afterwards pelleted cell debris was removed. This was repeated three times. Total protein concentration was assessed (BCA Protein Assay; Thermo Scientific). Subsequently, 20 µg of proteins were loaded on SDS/PAGE and transferred to a nitrocellulose membrane. The following antibodies were used for immunoblotting: TSC1 (A300-316A), PTEN (CS #9188), p70 S6 Kinase (CS #2708), Phospho-p70 S6 Kinase (Thr389) (CS #9234), ULK1 (CS #6439), Phospho-ULK1 (Ser757) (CS #14202), CAD-pSer1859, GSK3α-pSer9/21 (CS #5676), SREBP1c (SC-8984), SCD1 (CS #2794), ACC (CS #3662), FASN (CS #3180), phospho-ACLY (Ser455), ACLY (CS #13390), Phospho-ACLY (Ser455) (CS #4331), CD36 (NB400-144), GCS (Bioss, bs-0701R or Abcam, ab197369), CAD (Bethyl, BP301-374), NDRG1 (CS#5196), phospho-NDRG1 (Thr346) (CS#3217). AKT (CS#9272), phospho-AKT (Thr308) (CS#4056), phospho-AKT (Ser473) (CS#9271), S6 ribosomal Protein (CS#2217), phospho-S6 ribosomal Protein (Ser235/236) (CS#4856), and α-actin (MAB1501) from Millipore. For detection, Supersignal west pico chemiluminescent substrate or Supersignal west femto maximum sensitivity substrate (Pierce) was used.

Histology and Immunostainings. Mice were euthanized, livers quickly dissected and fixed in 4% paraformaldehyde. After overnight dehydration through several steps of ethanol, tissues were then embedded into paraffin wax blocks. Afterwards, embedded-tissues were cut into 4-µm-thick sections

placed on SuperFrost slides (Thermo Scientific). Slides were then stained with: H&E (Merck), Periodic Acid Schiff (PAS) Stain Kit (Mucin Stain) (Abcam, ab150690) and Picro Sirius Red Stain Kit (Connective Tissue Stain) (Abcam, ab150681), according to the protocols provided by manufacturer.

Immunofluorescence (IF) and immunohistochemistry (IHC). 4mm paraffin sections were obtained as described above. Subsequently, For immunostainings the following antibody was used: RFP (ab62341, Abcam). For nuclei staining DAPI (Cell signaling) was used. FASN (CS #3180), GCS (bs-0701R) and CRLS1 (ab105782). Mitochondrial staining primary hepatocytes (perfused as described above), from the different mouse genotypes were placed on glass coverslips (thickness number 1,5 from VWR) in 12-well culture plate. After cells were attached and equally confluent, coverslips were used for immunocytostaining. Coverslips were placed in a homemade box-holder to keep humidity. After a quick washing step using pre-warmed PBS, cells were incubated for 45 min with MitoTracker red CMXRos (CS #9082) diluted in pre-warmed media and placed in 37°C. Subsequently, cells were washed, fixed, permeabilized and were immediately used for staining with Mitofusin-2 (CS #9482S). Coverslips were mounted on a glass slide and sealed using a nail polish. Slides were then visualized using a scanning confocal “LSM800 Inverted“ with AirScan.

Frozen Sections. Mouse livers were dissected into the different lobes and immediately immersed in OCT compound (Tissue Tek; Fisher Scientific; Hanover Park, IL) and frozen in 2-methyl butane precooled in liquid nitrogen.

Afterwards, tissues were cut into 10-µm-thick sections using a cryostat microtome, placed on glass slides on SuperFrost slides (Thermo Scientific), air dried, and stored at -80C. Subsequently, slides were warmed at RT and stained with ORO (Sigma) according to standard protocol, and quantified as described (Mehlem, Hagberg et al. 2013). Detection of glycosylceramide was performed as described (Sakai, Akiyama et al. 2007). Briefly, liver frozen sections from 20 week-old L-dKO, L-TriKO and control mice were warmed at RT and washed twice with PBS, subsequently incubated for 1 hr with 5% goat serum for blocking. Anti-GlcCer antibody (GlycoBiotech^{TM}) was diluted with PBS/1% BSA and left for overnight at 4°C. The same buffer was used to dilute an Alexa Fluor® 488 conjugate secondary antibody, followed by 2 hours incubation at RT. Stained sections were mounted with Vectashield H-1000 (Vector Laboratories, Burlingame, CA). Images were taken using a wide-filed DeltaVision microscope (Olympus IX71) and were de-convoluted.

Blood Analysis. Plasma free fatty acids was determined using a commercial kit (HR Series NEFA-HR(2) and Cayman). Plasma triglycerides (TG), LDL, HDL, and liver damage enzymes ALT, AST, LDH were measured using a biochemical analyzer (Cobas c 111 analyzer, Roche).

Hepatic TG Measurement. Hepatic triglycerides extraction was performed as described (Hagiwara, Cornu et al. 2012). Briefly, ~ 50 mg of mouse liver tissue was homogenized in a cold room, for 30 sec (x4, with a 3 min break on ice in between, to prevent heating) bead beating in lysing matrix D tubes (Q-Biogene) containing 1 mL chloroform:methanol (2:1). Tissue lysate was

transferred into a glass tube and 1 mL of distilled water was added. Subsequently, tubes were vigorously vortexed for 2 min and centrifuged at 800 × g for 10 min at 4 °C. Then, the upper aqueous phase was discarded and the lower solvent phase was dried under nitrogen gas at 50 °C, followed by re-suspension with 1 mL of chloroform. Triglycerides were then separated by Solid Phase Extraction (SPE) column (Interchim) and dissolved in chloroform/Triton X-100 (1%). Triglyceride levels determined using a commercial kit according to manufacturer instructions (TG PAP 150; Biomérieux).

Proteome and Phosphoproteome. For time-course proteome analysis 4, 8 and 12 week-old L-dKO and control mice were euthanized and livers dissected (n=6/group). For analysis of liver tumors, livers from 20 week-old L-dKO mice (n=4) were dissected and separated into individual lobes and tumors (3 tumors per mouse) were micro-dissected, and 20 week-old control mice were used (n=6). Tissues were immediately snap-frozen in liquid nitrogen. We performed a 'cryogenic grinding', in which a frozen liver biopsy was crushed into a fine powder, using an in-house-constructed metal mortar, pre-cooled on dry ice. Subsequently, crushed liver tissues were homogenized using a Heidolph homogenizer (RZR 2052 Control) at 300 rpm for 2 min. The lysates were transferred into a cooled 1.5-mL tube containing 150-400 µL lysis buffer (composed of: 50 mM Tris·HCl (pH 8.0), 8 M urea, 150 mM NaCl, 1 mM PMSF, Complete Mini Protease Inhibitors (Roche), 100 mM sodium pyrophosphate/β-glycerophosphate/NaF/NaN3/ para-Nitrophenylphosphate). The lysates were vortexed vigorously for 5 min, then

sonication in a VWR Ultrasonic cleaner bath (USC300T) for 1 min. This was repeated three times with 2 min rest in between. Samples were then centrifuged at 2500 × g for 10 min at 15°C to remove cell debris. The protein concentration in the supernatants was determined by the Bradford assay. Proteins of the supernatants were reduced with 2.5 mM DTT for 1 h at 37°C, and alkylated with 50 mM iodoacetamide for 30 min at room temperature in the dark. The urea concentration was reduced to 4 M with 25 mM Tris_HCl, pH 8.0. Protein digestion was performed with two rounds of endoproteinase LysC (1:100w/w, Wako) at 37 °C for 2 h. The urea concentration of the LysC digest was reduced to approximately 1.2 M with 100 mM Tris-HCl, pH 8.0. Subsequently, trypsin digestion (1:100 w/w) was done for 2 hr at 37°C, followed by a second round of trypsin digestion (1:100 w/w) overnight at 37°C. Digestion was stopped by adding TFA to 0.4% (vol/vol) final concentration that lowered the pH of the solution to below pH 2.0. Afterwards, the digest was centrifuged at 12,000 rpm for 10 min at RT and the pellet was discarded. For strong cation exchange chromatography (SCX), the peptides were desalted on a C18 reverse-phase SepPak cartridge (Waters). The peptide load was kept to about 5% (w/w) of the weight of the column packing. The cartridges were primed with 5 ml 100% acetonitrile, followed by 5 ml 50% AcCN containing 0.5% AcOH and equilibrated with 10 ml 0.1% TFA. Sample was then loaded in 0.4% TFA and the cartridge was washed with 20 ml of 0.1% TFA. Finally, TFA was removed with 1 ml of 0.5% AcOH and the peptides were eluted with 4 ml of 80% AcCN/0.5% AcOH. The peptide peptide concentration was estimated as described (Wisniewski, Zougman et al. 2009) and dried in a SpeedVac.

SCX (Strong Cation Exchange) Chromatography. SCX fractionation was modified from (Dephoure and Gygi 2011). Storage buffer was removed from a HiTrap SP cartridge (GE Healthcare) and washed twice with 1 mL of SCX buffer A {5 mM KH2PO4 (pH 2.65), 30% AcCN}. Then, the cartridge was equilibrated twice with 1 mL of SCX buffer B {5 mM KH2PO4 (pH 2.65), 30% AcCN containing 500 mM KCl}, followed by re-eqilibration with 2 mL of SCX buffer A. The dried peptides were resuspended in 2 mL of SCX buffer A, centrifuged at 12,000 rpm for 2 min. The pellet was discarded and peptides were loaded with a syringe onto the HiTrap SP cartridge. The flow-through was collected. The bound peptides were then desorbed in a stepwise manner: with 1 mL of SCX buffer A containing 50 mM, 100 mM, 150 mM, 250 mM, 350 mM, and 500 mM KCl. Each fraction was collected individually and the peptide concentration was estimated at 280 nm. The fractions were dried in a SpeedVac and peptides were then desalted on SepPak cartridges (the size of the cartridge was adjusted to the peptide load) as described above. The peptide concentration was measured at 280 nm. 20% of each fraction was removed for subsequent proteome analysis by LC/MS/MS (see below).

Phosphopeptide Enrichment. Desalted peptides were dissolved in TiO_2-binding buffer to obtain a peptide concentration of ~ 1ug/uL (Kettenbach and Gerber 2011). TiO_2 beads (GL Sciences Inc.) equilibrated in binding buffer were then added to the peptide solution. Adsorption of the peptides to the TiO_2 beads was done at RT for 1 hr with vigorous shaking. The beads were pelleted at 3000 rpm for 2 min and washed three times with 50%AcCN/0.1%

TFA. Bound peptides (enriched for phosphopeptides) were eluted with 50 mM K_2HPO_4, pH 10. The eluted peptides were immediately acidified with 50%AcCN/ 5% formic acid. The enriched phosphopeptide pool was desalted on Stage Tips (Thermo Scientific, Reinach, Switzerland), and dried in a SpeedVac.

LC/MS/MS Analysis. The dried phosphopeptides were dissolved in 20 µL of 0.1% AcOH, 0.005% TFA. Peptides from the proteomes and phosphoproteomes were analyzed by capillary LC/MS/MS using a homemade separating column (0.075 mm × 18 cm) packed with Reprosil C18 reverse-phase material (2.4 µm particle size, Dr. Maisch, Ammerbuch-Entringen, Germany). The column was connected on line to an Orbitrap FT hybrid instrument (Thermo Scientific, Reinach, Switzerland). The solvents used for peptide separation were 0.1% acetic acid in water/0.005% TFA (solvent A) and 0.1% acetic acid/0.005% TFA and 80% acetonitrile in water (solvent B). 2 µl of peptide digest were injected with a Proxeon Easy-LC capillary pump (Thermo Scientific) set to 0.3 µl/min. A linear gradient from 0 to 40% solvent B in solvent A in 190 min was delivered with the nano pump at a flow rate of 300 nl/min for the proteome, while a shorter linear gradient of 95 min under identical conditions for the phosphoproteome was used. At the end of the linear gradient, the percentage of solvent B was increased to 75% in ten minutes. The eluting peptides were ionized at 2.5 kV. The mass spectrometer was operated in data-dependent mode. The precursor scan was done in the Orbitrap set to a 60,000 resolution, while the fragment ions were mass analyzed in the LTQ instrument. A top ten method for the

phosphoproteome, and a top twenty method for the proteome were run so that the ten or twenty most intense precursors were selected for fragmentation. The MS/MS spectra were then searched against a mouse databank extracted from the SwissProt databank.

Protein Identification and Data Processing. The LC/MS/MS data were searched with Proteome Discoverer 1.4 (Thermo Scientific) using Mascot and Sequest HT search engines set to 10 ppm precursor ion tolerance, while the fragment ions were set to 0.6 Da tolerance. The following modifications were used during the search: carbamidomethyl-cysteine was set as a fixed modification, protein N-terminal acetylation, oxidized methionine, and phosphorylation for serine, threonine, and tyrosine were set to variable modifications. The peptide search matches were set to 'medium confidence', which corresponds to 5% false discovery rate. For the searches, the Swiss-Prot KB database set to *M. musculus* was used for Mascot, while for Sequest HT, a local databank was constructed by extracting all *M. musculus* entries from UniProtKB. Two missed cleavages were allowed during the searches. The peptide false-discovery rate was set to 2%.

Label-free quantification. The RAW files from the LC/MS/MS were imported into the Progenesis software (Non-linear Dynamics, Waters) and the matched SCX fractions were aligned. Alignment was only accepted when the histogram of the corresponding feature areas was above 80%. After alignment, the search results of Proteome Discoverer were imported into Progenesis for matching the identified peptides with the aligned features.

The intensities of all identified features were exported via Excel into a FileMaker database. Class I (≥75% localization probability) was kept for further analysis.

Statistical Analysis

Proteome: The data was analyzed with the Perseus software, version 1.4.0.2. For the volcano plots, an ANOVA two-sample t test was performed, adjusting S0 to 0.5, number of randomizations to 250, and FDR to 5%. For the heat maps, only proteins that showed at least at one time point a significant deregulation were included. Z-scoring was performed with grouping within same time points. Finally, for unsupervised hierarchical clustering, the distance was set to Euclidian, the linkage to average, and the maximal numbers of clusters to 300 (Tyanova, Temu et al. 2016).

Lipidome: The data was analyzed with the Perseus software, version 1.4.0.2. For the volcano plots, an ANOVA two-sample t test was performed, adjusting S0 to 0.1, number of randomizations to 250, and FDR to 5%. For the heat maps, only proteins that showed at least at one time point a significant deregulation were included. Z-scoring was performed with grouping within same time points. Finally, for unsupervised hierarchical clustering, the distance was set to Euclidian, the linkage to average, and the maximal numbers of clusters to 300 (Tyanova, Temu et al. 2016).

Lipid Extraction Protocols. Lipid extraction was performed using a modified MTBE protocol (Matyash, Liebisch et al. 2008). Briefly, for time-course lipidome analysis fresh liver samples from 4, 8 12 and 20 (cancer

tumors were obtained) week-old L-dKO and control mice (n=6/time point) were used. For assessment of mTORC2-regulated lipids, 20 week-old L-TriKO, L-dKO and control mice were used (n=4/group). For assessment of myriocin lipidome ~20 week-old L-dKO (n=5 myriocin, n=6 vehicle) and control (n=5 myriocin, n=4 vehicle) mice were used. As described above, in all cases, tissues were immediately snap-frozen in liquid nitrogen. Subsequently, tissues were pulverized into a fine powder in an in-house-constructed metal mortar, pre-cooled on dry ice ('cryogenic grinding'). Of that, 30-35 mg ground liver tissue was resuspended in 100 ml H_2O and transferred into a 2 ml Eppendorf tube. Then, 360 ul methanol was added and vortexed. A mixture of lipid standards (Table S4) plus 50 ml 1.4 mm Zirconium glass beads (Bertin Technologies, France) were added and the pulverized tissue was homogenized using a Cryolysis System (Bertin Technologies, France) (program: 6200-3x45-045) cooled to 4°C. MTBE (1.2 ml) was then added and the sample was incubated for one hour at room temperature with a shaking (750 rpm). Phase separation was induced by adding 200 ml H_2O. After 10 minutes incubation at RT, sample was centrifuged at 1000x*g* for 10 minutes (RT). The upper (organic) phase was transferred in a 13 mm screw cap glass tube and the lower phase was extracted with 400 ml artificial upper phase (MTBE/methanol/water (10:3:1.5, v/v)). The two upper phases were combined and the total lipid extract was divided in 3 equal aliquots (one for phospholipids (TL), one for sterols (S) in 2 ml amber vials and one for sphingolipid (SL) detection in a 13 mm glass tube) and dried in a Centrivap at 50°C or under a nitrogen flow. The TL and S aliquots were ready to be analyzed by mass spectrometry and were kept at –80°C. The SL aliquot was

deacylated to eliminate phospholipids by treatment (Clarke method, as described (Clarke and Dawson 1981) and (Cheng, Park et al. 2001)) with 0.5 ml monomethylamine reagent, which was added to the dried lipid, followed by sonication (5 min), mixing, incubation for one hour at 53°C and drying, as above. The monomethylamine treated lipids were desalted by n-butanol extraction. 300 ml H_2O saturated n-butanol was added to the dried lipids. The sample was vortexed, sonicated for 5 minutes and 150 ml MS grade water was added. The mixture was vortexed thoroughly and centrifuged at 3200x*g* for 10 minutes. The upper phase was transferred in a 2 ml amber vial. The lower phase was extracted twice more with 300 ml H_2O saturated n-butanol and the upper phases were combined and dried (as above).

Phospholipid and Sphingolipid Detection on a Triple Quadrupole LC-MS, TSQ Vantage (ThermoFischer Scientific). LC-MS grade solvents were used and the samples were pipetted in a 96 well plate (final volume = 100 ml). Positive mode solvent: Chloroform/Methanol/Water (2:7:1, v/v) + 5mM Ammonium Acetate. Negative mode solvent: Chloroform/Methanol (1:2, v/v) + 5mM Ammonium Acetate. The TL and SL aliquots were resuspended in 250 ml Chloroform/methanol (1:1 v/v, LC-MS) and sonicated for 5 minutes. The TL were diluted 1:10 in negative and positive mode solvents and the SL were diluted 1:20 in positive mode solvent and infused onto the mass spectrometer using a Nanomate (Advion). The detection conditions for each lipid class are listed in Table S5. Ceramide species were also quantified with a loss of water in the first quadrupole. Each biological replicate was read in 2 technical replicates (TR). Each TR measured 3 times the series of transitions.

The phosphate content was also quantified and normalized for each sample. Tandem mass spectrometry for the identification and quantification of phospho- and sphingolipid molecular species was performed using multiple reaction monitoring (MRM) with a TSQ Vantage Triple Stage Quadrupole Mass Spectrometer (Thermo Fisher Scientific) equipped with a robotic nanoflow ion source, Nanomate HD (Advion Biosciences, Ithaca, NY). Each individual ion dissociation pathway was optimized with regard to collision energy. Lipid concentrations were calculated relative to the relevant internal standards and then normalized to the total phosphate content of each total lipid extract (Ding, Loizides-Mangold et al. 2013).

Determination of Total Phosphorus. The dried total lipid extract was resuspended in 250 ml chloroform/methanol (1:1) and 50 ml were placed into a 13 mm disposable pyrex tube. The solvent was completely evaporated and 0, 2, 5, 10, 20 ml of a 3 mM KH2PO4 standard solution were placed into separate pyrex tubes. To each tube 20 ml of water and 140 ml of 70% perchloric acid were added. Samples were heated at 180C for 1 hour in a hood. Tubes were then removed from the block and kept at RT for 5 min. Then 800 ml of freshly prepared H2O / 1.25% NH4- Molybdate (100 mg / 8 ml H2O) / 10% ascorbic acid (100 mg / 6 ml H2O) in the ratio of 5:2:1 were added. Tubes were heated at 100C for 5 min with a marble on each tube to prevent evaporation. Tubes were cooled at RT for 5 min. 100 ml of each sample was then transferred into a 96-well microplate and the absorbance at 820 nm was measured.

Chemicals for Lipidome Analysis. Methylmalonic acid (MMA), hydrogen chloride (3 M in 1-butanol) and LC MS grade ammonium formate were purchased from Sigma-Aldrich. Phosphoric acid (85 wt % solution in water) was from Acros Organics (Thermo Scientific)**.** MTBE was from Fluka (Buchs, Switzerland). Methylamine (33% in absolute ethanol) was from Sigma-Aldrich. HPLC grade chloroform was purchased from Acros Organics. LC-MS grade methanol and LC-MS grade ammonium acetate were from Fluka. LC- MS grade water was purchased from Biosolve (Valkenswaard, Netherlands).

Metabolite Extraction Protocol. Pulverized liver tissue were obtained as described above (30-35mg) and re-suspended in 200 μl extraction solvent (ethanol/water/diethylether/pyridine/ammonium hydroxide 4.2N (15:15:5:1:0.018)). To that, a mixture of lipid standards (Table S6) and 50 ml 1.4 mm Zirconium glass beads (Bertin Technologies, France) were added. The pulverized tissue was broken in a Cryolysis System (Bertin Technologies, France) (program: 6200-3x45-045) cooled at 4°C. The sample was incubated for 20 minutes on ice, centrifuged at 21000xg for 2 min and the supernatant was transferred to an Eppendorf tube. The pellet was extracted a second time with 200 μl of extraction solvent, and the combined supernatants were centrifuged at 21000x*g* for 5 min to remove remaining cell debris and split into two equal aliquots in 300 μl glass inserts. The metabolite extract was dried in a Centrivap at 50°C for 30 min and then 60°C for 2 hrs.

Derivatization of Amino Groups. Was performed as described (Boughton, Callahan et al. 2011) with modifications. Dried lipid extract was re-

suspended in 10 μl 0.1% formic acid, 70 μl borate buffer (200mM boric acid pH 8.8 (with NaOH), 10mM TCEP, 1mM ascorbic acid, 35.7 μM $^{13}C^{15}N$ – Valine (internal standard)). The mixture was sonicated for 5 minutes and 20 µl of 10mM AQC (2.85mg/ml in acetonitrile) was added. The sample was incubated for 15 min at 55°C with shaking (750 rpm) followed by overnight incubation at 24°C.

LC-MS. After incubation the sample was centrifuged as above and loaded onto a NUCLEOSHELL RP 18 (Particle size: 2.7 µm , length: 100 mm, Diameter: 2 mm) and the following gradient was applied: solvent A : milliQ water + 0.1% formic acid, solvent B: isopropanol + 0.1 % formic acid, at a flow of 300 ml/min.

Supplemental Tables

Table S1 - Supplementary table of RNA sequencing data of lipid related genes that are up-or down-regulated in L-dKO/ control mice. Available as a separate file.

Table S2 - Supplementary table for enrichment heat map L-dKO/ control ad-libitum fed mice (increased). Available as a separate file.

Table S3 - Supplementary table for enrichment heat map L-dKO/control ad-libitum fed mice (decreased). Available as a separate file.

Table S4 (related to lipidome analysis): Mammalian standard mix for one sample

Standard	nmole	Provider	Product Nr
DLPC Phosphatidylcholine (PC)12:0-12:0	0.4	Avanti	850335
PE31:1 Phosphatidylethanolamine (PE)17:0-14:1	1	Avanti	LM-1104
PI31:1 Phosphatidylinositol (PI)17:0-14:1	1	Avanti	LM-1504
PS31:1 Phosphatidylserine (PS)17:0-14:1	3.3	Avanti	LM-1304
CL56:0 Cardiolipin (CL)14:0-14:0-14:0-14:0	0.7	Avanti	710332
C17Cer Ceramide (Cer)d18:1-17:0	2.5	Avanti	860517
C8GC Glucosylceramide (GlcCer)d18:1-8:0	0.5	Avanti	860540
C12SM Sphingomyelin (SM) d18:1-12:0	0.1	Avanti	860583
Ergosterol	8	Fluka	45480

Table S5 (related to lipidome analysis): Detection of Lipids by MS/MS

Lipid class	standard	Polarity	Mode	m/z ion	CE
Phosphatidylcholine $[M+H]^+$	**PC31:1**	+	Product ion	184.07	30
Phosphatidylethanolamine $[M+H]^+$	**PE31:1**	+	Neutral ion loss	141.02	20
Phosphatidylinositol $[M-H]^-$	**PI31:1**	-	Product ion	241.01	44
Phosphatidylserine $[M-H]^-$	**PS31:1**	-	Neutral ion loss	87.03	23
Cardiolipin $[M-2H]^{2-}$	**CL56:0**	-	Product ion	acyl chain	32

Ceramide $[M+H]^+$	**C17Cer**	+	Product ion	264.30	25
Dihydroceramide [M+H]+	**C17Cer**	+	Product ion	266.40	25
Hexacylceramide $[M+H]^+$	**C8GC**	+	Product ion	264.30	30
Hexacyldihydroceramide [M+H]+	**C8GC**	+	Product ion	266.40	30
Sphingomyelin [M+H]+	**C12SM**	+	Product ion	184.07	26

Table S6 (related to metabolome analysis): Standard mice for one sample

Standard	**nmole**	**Provider**	**Product Nr**
C17So D-erythro-sphingosine (C17 base)	0.04	Avanti	860640
C17Sa D-erythro-sphinganine (C17 base)	0.04	Avanti	860654
C17So-1P D-erythro-sphingosine-1-phosphate (C17 base)	1	Avanti	860641
C17Sa-1P D-erythro-sphinganine-1-phosphate (C17 base)	1	Avanti	860655

Table S7. Primer sequences used for qRT-PCR

Gene name	Forward (5'- 3')	Reverse (5' - 3')
acc1	AAGGCTATGTGAAGGATG	CTGTCTGAAGAGGTTAGG
fasn	GCTGCGGAAACTTCAGGAAAT	AGAGACGTGTCACTCCTGGACTT
scd1	GTCAGGAGGGCAGGTTTC	GAGCGTGGACTTCGGTTC
acox	CTTCAGGCCCAAGTGAGTCA	GCGAACAAGGTCGACAGAAGT
mcad	GATGCCATCACCCTCGTGTAAC	AAGCCCTTTTCCCCTGAAG
cd36	TGGCCTTACTTGGGATTGG	CCAGTGTATATGTAGGCTCATCCA
mttp	TGGTGAAAGGGCTTATTCTGTT	TTGCAGCTGAATATCCTGAGAA
cyclophilin	TGGAAGAGCACCAAGACAGACA	TGCCGGAGTCGACAATGAT
apob	AAACATGCAGAGCTACTTTGGAG	TTTAGGATCACTTCCTGGTCAAA
RFP	GCGGCCACTACACCTGCGAC	TCGGCGTGCTCGTACTGCTC
spk1	GATGCATGAGGTGGTGAATG	GCTACACAGGGGTTTCTGGA
gcs	AGCTGGAGAACTGGTCGCTA	CACACTGTGCGCCATCAG
spt(sptlc1)	TCGAGTTAAGGCCACAGCTT	CATAGAACCCTCGAGGACCA
smpd acid	GGCGAGTACAGCAAGTGTGA	CTCCCGTCCAGTACACCATT
smpd neutral	AGTACGAGGACCGGGTTTCT	GAGACAACATTGGCAGCAGA
gpat	CAACACCATCCCCGACATC	GTGACCTTCGATTATGCGATCA

Supplementary findings

Relevant findings that could not be included in the manuscript are discussed below.

Inflammation in L-dKO mice.

As mentioned above, inflammation may further amplify liver damage induced by lipids (so called NASH). L-dKO mice exhibited increased inflammatory cytokines, such as *tnfa*, *il6* and probably expansion of resident macrophages (kupffer cells), as assessed by the surrogate marker *cd68* (Figure 1, below). This was confirmed by isolation of inflammatory cells using FACS analysis (8 week-old L-dKO and littermates control mice). Specifically, we observed elevated levels of $Gr1^+$ inflammatory cells in livers of L-dKO mice. $Gr1^+$ are myeloid infiltrating suppressor cells that promote cancer (Di Mitri, Toso et al. 2014, Atala 2015). Immunofluorescence analysis on frozen liver sections confirmed the presence of $Gr1^+$ cells. $Gr1^+$ cells also localized to regions in which the sphingolipid GlcCer was present, suggesting a relationship between GlcCer accumulation, $Gr1^+$ cells and perhaps cancer. Furthermore, L-dKO exhibited increased spleen mass from 8 weeks of age, suggesting that L-dKO mice suffer from systemic inflammatory response (Figure 1, below). Indeed, we also identified that elevated Gr1 levels in peripheral blood and spleen (not shown). Together, these data indicates that L-dKO mice display hepatic and systemic inflammatory response, whether that is functionally related to lipids and/or to tumor development remains to be investigated.

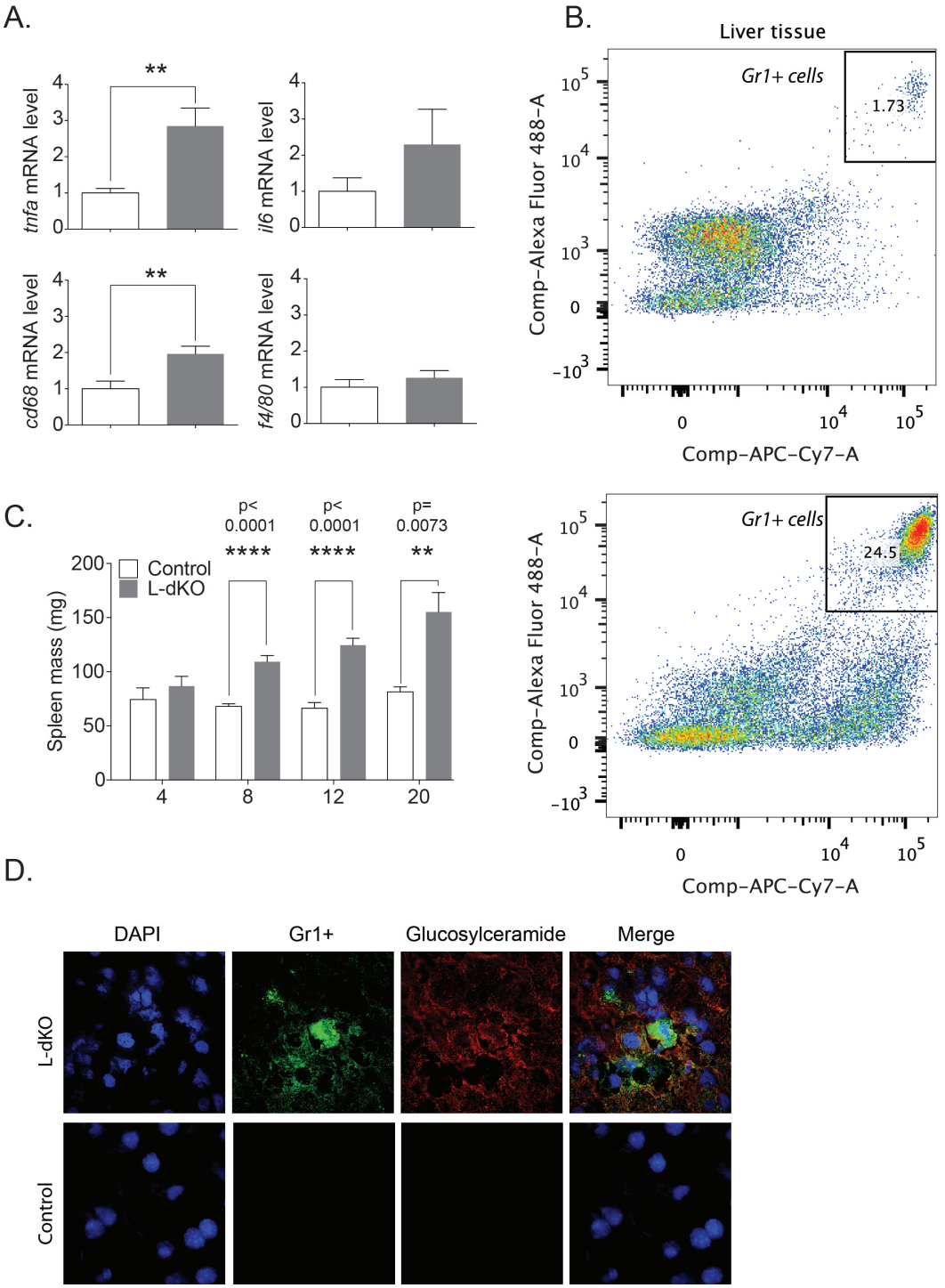

Figure 1. *L-dKO mice exhibit hepatic and systemic inflammation.* **(A)** Relative mRNA in livers from 8 week-old L-dKO and control mice, for the indicated genes. **(B)** Representative plot of FACS analysis performed on livers from 8 week-old L-dKO and control mice. **(C)** Spleen mass from 4, 8, 12 and 200 week-old L-dKO and control mice (n=6). **(D)** Representative immunofluorescence images of frozen liver sections from tumors of L-dKO mice (control here is non-stained L-dKO).

L-dKO mice display enhanced de-novo serine synthesis.

Serine is required for de novo SL and protein synthesis, as well as a one-carbon unit source essential for de novo purine synthesis. In proliferating cells, the glycolytic intermediate 3-phosphoglycerate is converted to serine, via the de novo serine biosynthesis pathway (SSP) (Locasale 2013, Amelio, Cutruzzola et al. 2014). PHGDH (phosphoglycerate dehydrogenase) generates 3-phosphohydroxypurvate, which is subsequently transaminated (PSAT1) and dephosphorylated (PSPH) to generate serine. Cancer cells that exhibit genomic amplifications (copy number gain) of PHGDH are dependent on serine synthesis (Possemato, Marks et al. 2011, Labuschagne, van den Broek et al. 2014, Pacold, Brimacombe et al. 2016). As depicted in the figure below (Figure 2), L-dKO mice exhibit increase de novo serine biosynthetic enzymes. These data suggests that mTOR-driven tumors require serine synthesis, probably also for lipid synthesis.

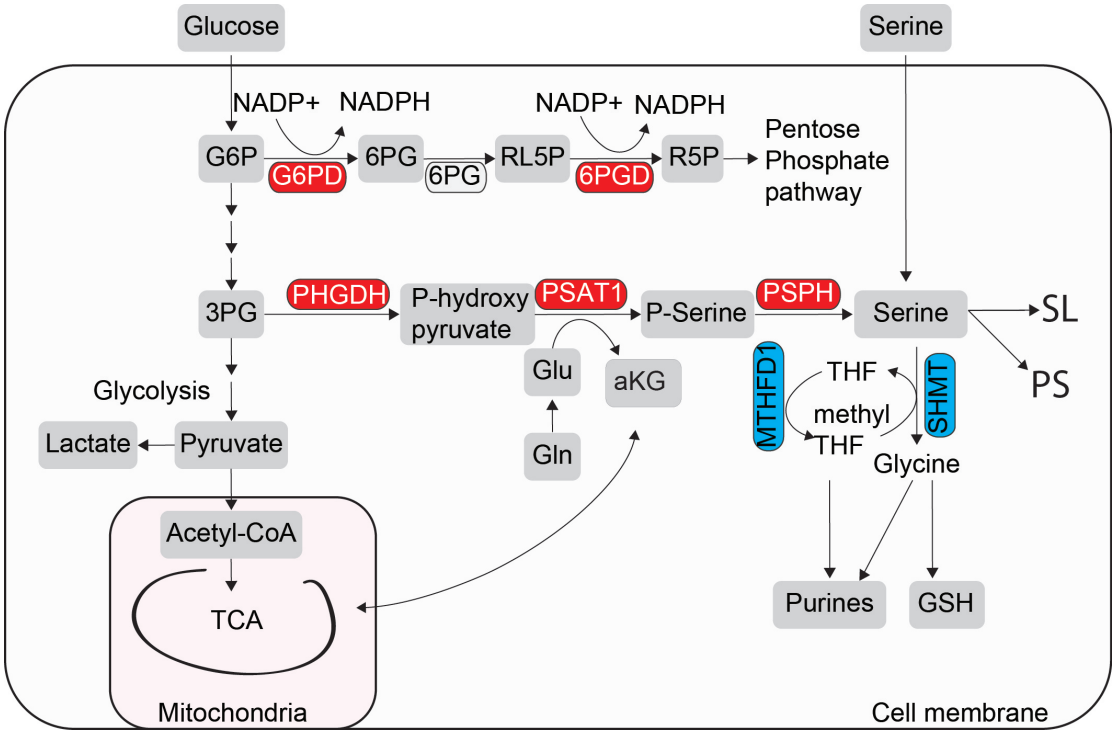

Figure 2. *Increased expression of enzymes in the de novo serine pathway in L-dKO mice.* Proteins that are up-regulated in livers of L-dKO mice (from 4 to 20 weeks) are depicted in red. Down-regulated enzymes are in blue. Abbreviation: 6PG, 6-phosphogluconate RL5P, Ribulose 5-phosphate; R5P, Ribose 5-phosphate; 6PGD, 6-phosphogluconate dehydrogenase; 6PG, 6-phosphogluconolactonase

6.0. Acknowledgements

First of foremost, my deepest gratitude to my family for endless love and joy, I am truly sorry for every missed moment beside you. To my parents, brothers and sister for their support and wisdom over the years.

I would like to express my gratefulness to Mike. Thank you for opening the door to the fascinating life of TOR, and for being an excellent mentor and a great inspiration for me.

Many thanks to my colleagues for pushing me to the best and better. In particular, to Marco Colombi for his great help in handling the high-throughput studies. To Dr. Asier S. G. for teaching me the art of figure making. To Dr. Mitsugu S., Dr. Verena A., Dr. Sravanth H.K., Dr. Eva D. K. for scientific discussions. To Wolfgang O. for his prudence.

I would like to acknowledge my co-mentor Prof. Howard Riezman for his absolutely essential guidance into the (complex) life of lipids. To Isabelle Riezman for performing the lipidomic analysis and for scientific instructions.

7.0. Bibliography

Aguilera-Romero, A., C. Gehin and H. Riezman (2014). "Sphingolipid homeostasis in the web of metabolic routes." Biochim Biophys Acta **1841**(5): 647-656.

Albert, V. and M. N. Hall (2015). "mTOR signaling in cellular and organismal energetics." Curr Opin Cell Biol **33**: 55-66.

Alessi, D. R., S. R. James, C. P. Downes, A. B. Holmes, P. R. Gaffney, C. B. Reese and P. Cohen (1997). "Characterization of a 3-phosphoinositide-dependent protein kinase which phosphorylates and activates protein kinase Balpha." Curr Biol **7**(4): 261-269.

Allen, E., P. Mieville, C. M. Warren, S. Saghafinia, L. Li, M. W. Peng and D. Hanahan (2016). "Metabolic Symbiosis Enables Adaptive Resistance to Anti-angiogenic Therapy that Is Dependent on mTOR Signaling." Cell Rep **15**(6): 1144-1160.

Amelio, I., F. Cutruzzola, A. Antonov, M. Agostini and G. Melino (2014). "Serine and glycine metabolism in cancer." Trends Biochem Sci **39**(4): 191-198.

Argiles, J. M., S. Busquets, B. Stemmler and F. J. Lopez-Soriano (2014). "Cancer cachexia: understanding the molecular basis." Nat Rev Cancer **14**(11): 754-762.

Atala, A. (2015). "Re: Tumour-infiltrating Gr-1+ myeloid cells antagonize senescence in cancer." J Urol **193**(6): 2146.

Bae, J. S., A. R. Oh, H. J. Lee, Y. H. Ahn and J. Y. Cha (2016). "Hepatic Elovl6 gene expression is regulated by the synergistic action of ChREBP and SREBP-1c." Biochem Biophys Res Commun.

Baenke, F., B. Peck, H. Miess and A. Schulze (2013). "Hooked on fat: the role of lipid synthesis in cancer metabolism and tumour development." Dis Model Mech **6**(6): 1353-1363.

Baffy, G. (2013). "Hepatocellular Carcinoma in Non-alcoholic Fatty Liver Disease: Epidemiology, Pathogenesis, and Prevention." J Clin Transl Hepatol **1**(2): 131-137.

Bellentani, S., F. Scaglioni, M. Marino and G. Bedogni (2010). "Epidemiology of non-alcoholic fatty liver disease." Dig Dis **28**(1): 155-161.

Beloribi-Djefaflia, S., S. Vasseur and F. Guillaumond (2016). "Lipid metabolic reprogramming in cancer cells." Oncogenesis **5**: e189.

Ben-Sahra, I., J. J. Howell, J. M. Asara and B. D. Manning (2013). "Stimulation of de Novo Pyrimidine Synthesis by Growth Signaling Through mTOR and S6K1." Science **339**(6125): 1323-1328.

Ben-Sahra, I., G. Hoxhaj, S. J. Ricoult, J. M. Asara and B. D. Manning (2016). "mTORC1 induces purine synthesis through control of the mitochondrial tetrahydrofolate cycle." Science **351**(6274): 728-733.

Benjamin, D., M. Colombi, C. Moroni and M. N. Hall (2011). "Rapamycin passes the torch: a new generation of mTOR inhibitors." Nat Rev Drug Discov **10**(11): 868-880.

Betz, C. and M. N. Hall (2013). "Where is mTOR and what is it doing there?" J Cell Biol **203**(4): 563-574.

Betz, C., D. Stracka, C. Prescianotto-Baschong, M. Frieden, N. Demaurex and M. N. Hall (2013). "Feature Article: mTOR complex 2-Akt signaling at

mitochondria-associated endoplasmic reticulum membranes (MAM) regulates mitochondrial physiology." Proc Natl Acad Sci U S A **110**(31): 12526-12534.
Bhat, M., N. Sonenberg and G. J. Gores (2013). "The mTOR pathway in hepatic malignancies." Hepatology **58**(2): 810-818.
Bononi, A., S. Missiroli, F. Poletti, J. M. Suski, C. Agnoletto, M. Bonora, E. De Marchi, C. Giorgi, S. Marchi, S. Patergnani, A. Rimessi, M. R. Wieckowski and P. Pinton (2012). "Mitochondria-associated membranes (MAMs) as hotspot Ca(2+) signaling units." Adv Exp Med Biol **740**: 411-437.
Boughton, B. A., D. L. Callahan, C. Silva, J. Bowne, A. Nahid, T. Rupasinghe, D. L. Tull, M. J. McConville, A. Bacic and U. Roessner (2011). "Comprehensive profiling and quantitation of amine group containing metabolites." Anal Chem **83**(19): 7523-7530.
Breslow, D. K. (2013). "Sphingolipid homeostasis in the endoplasmic reticulum and beyond." Cold Spring Harb Perspect Biol **5**(4): a013326.
Burri, L., N. Hoem, S. Banni and K. Berge (2012). "Marine omega-3 phospholipids: metabolism and biological activities." Int J Mol Sci **13**(11): 15401-15419.
Caron, A., D. Richard and M. Laplante (2015). "The Roles of mTOR Complexes in Lipid Metabolism." Annu Rev Nutr **35**: 321-348.
Chandarlapaty, S., A. Sawai, M. Scaltriti, V. Rodrik-Outmezguine, O. Grbovic-Huezo, V. Serra, P. K. Majumder, J. Baselga and N. Rosen (2011). "AKT Inhibition Relieves Feedback Suppression of Receptor Tyrosine Kinase Expression and Activity." Cancer Cell **19**(1): 58-71.
Chauvin, C., V. Koka, A. Nouschi, V. Mieulet, C. Hoareau-Aveilla, A. Dreazen, N. Cagnard, W. Carpentier, T. Kiss, O. Meyuhas and M. Pende (2014). "Ribosomal protein S6 kinase activity controls the ribosome biogenesis transcriptional program." Oncogene **33**(4): 474-483.
Chen, Y., J. Qian, Q. He, H. Zhao, L. Toral-Barza, C. Shi, X. Zhang, J. Wu and K. Yu (2016). "mTOR complex-2 stimulates acetyl-CoA and de novo lipogenesis through ATP citrate lyase in HER2/PIK3CA-hyperactive breast cancer." Oncotarget **7**(18): 25224-25240.
Cheng, J., T. S. Park, A. S. Fischl and X. S. Ye (2001). "Cell cycle progression and cell polarity require sphingolipid biosynthesis in Aspergillus nidulans." Mol Cell Biol **21**(18): 6198-6209.
Christie, W. (2013). AOCS Lipid Library.
Clarke, N. G. and R. M. Dawson (1981). "Alkaline O leads to N-transacylation. A new method for the quantitative deacylation of phospholipids." Biochem J **195**(1): 301-306.
Colombi, M., K. D. Molle, D. Benjamin, K. Rattenbacher-Kiser, C. Schaefer, C. Betz, A. Thiemeyer, U. Regenass, M. N. Hall and C. Moroni (2011). "Genome-wide shRNA screen reveals increased mitochondrial dependence upon mTORC2 addiction." Oncogene **30**(13): 1551-1565.
Cornu, M., V. Albert and M. N. Hall (2013). "mTOR in aging, metabolism, and cancer." Curr Opin Genet Dev **23**(1): 53-62.
Cornu, M., W. Oppliger, V. Albert, A. M. Robitaille, F. Trapani, L. Quagliata, T. Fuhrer, U. Sauer, L. Terracciano and M. N. Hall (2014). "Hepatic mTORC1 controls locomotor activity, body temperature, and lipid metabolism through FGF21." Proceedings of the National Academy of Sciences of the United States of America **111**(32): 11592-11599.

Corradetti, M. N., K. Inoki, N. Bardeesy, R. A. DePinho and K. L. Guan (2004). "Regulation of the TSC pathway by LKB1: evidence of a molecular link between tuberous sclerosis complex and Peutz-Jeghers syndrome." Genes Dev **18**(13): 1533-1538.
Cowart, L. A. and Y. A. Hannun (2007). "Selective substrate supply in the regulation of yeast de novo sphingolipid synthesis." J Biol Chem **282**(16): 12330-12340.
Csibi, A., G. Lee, S. O. Yoon, H. Tong, D. Ilter, I. Elia, S. M. Fendt, T. M. Roberts and J. Blenis (2014). "The mTORC1/S6K1 pathway regulates glutamine metabolism through the eIF4B-dependent control of c-Myc translation." Curr Biol **24**(19): 2274-2280.
Cybulski, N. and M. N. Hall (2009). "TOR complex 2: a signaling pathway of its own." Trends Biochem Sci **34**(12): 620-627.
Cybulski, N., P. Polak, J. Auwerx, M. A. Ruegg and M. N. Hall (2009). "mTOR complex 2 in adipose tissue negatively controls whole-body growth." Proc Natl Acad Sci U S A **106**(24): 9902-9907.
Das, S., F. Morvan, B. Jourde, V. Meier, P. Kahle, P. Brebbia, G. Toussaint, D. J. Glass and M. Fornaro (2015). "ATP citrate lyase improves mitochondrial function in skeletal muscle." Cell Metab **21**(6): 868-876.
Dazert, E. and M. N. Hall (2011). "mTOR signaling in disease." Curr Opin Cell Biol **23**(6): 744-755.
DeBerardinis, R. J., J. J. Lum, G. Hatzivassiliou and C. B. Thompson (2008). "The biology of cancer: metabolic reprogramming fuels cell growth and proliferation." Cell Metab **7**(1): 11-20.
Dennis, E. A. and E. P. Kennedy (1972). "Intracellular sites of lipid synthesis and the biogenesis of mitochondria." J Lipid Res **13**(2): 263-267.
Dephoure, N. and S. P. Gygi (2011). "A solid phase extraction-based platform for rapid phosphoproteomic analysis." Methods **54**(4): 379-386.
Di Mitri, D., A. Toso, J. J. Chen, M. Sarti, S. Pinton, T. R. Jost, R. D'Antuono, E. Montani, R. Garcia-Escudero, I. Guccini, S. Da Silva-Alvarez, M. Collado, M. Eisenberger, Z. Zhang, C. Catapano, F. Grassi and A. Alimonti (2014). "Tumour-infiltrating Gr-1+ myeloid cells antagonize senescence in cancer." Nature **515**(7525): 134-137.
Dibble, C. C. and L. C. Cantley (2015). "Regulation of mTORC1 by PI3K signaling." Trends Cell Biol **25**(9): 545-555.
Dibble, C. C., W. Elis, S. Menon, W. Qin, J. Klekota, J. M. Asara, P. M. Finan, D. J. Kwiatkowski, L. O. Murphy and B. D. Manning (2012). "TBC1D7 Is a Third Subunit of the TSC1-TSC2 Complex Upstream of mTORC1." Molecular Cell **47**(4): 535-546.
Dibble, C. C. and B. D. Manning (2013). "Signal integration by mTORC1 coordinates nutrient input with biosynthetic output." Nature Cell Biology **15**(6): 555-564.
Dibble, C. C. and B. D. Manning (2013). "Signal integration by mTORC1 coordinates nutrient input with biosynthetic output." Nat Cell Biol **15**(6): 555-564.
Ding, J., U. Loizides-Mangold, G. Rando, V. Zoete, O. Michielin, J. K. Reddy, W. Wahli, H. Riezman and B. Thorens (2013). "The peroxisomal enzyme L-PBE is required to prevent the dietary toxicity of medium-chain fatty acids." Cell Rep **5**(1): 248-258.

Dowling, R. J., I. Topisirovic, T. Alain, M. Bidinosti, B. D. Fonseca, E. Petroulakis, X. Wang, O. Larsson, A. Selvaraj, Y. Liu, S. C. Kozma, G. Thomas and N. Sonenberg (2010). "mTORC1-mediated cell proliferation, but not cell growth, controlled by the 4E-BPs." Science **328**(5982): 1172-1176.
Duncan, A. L., A. J. Robinson and J. E. Walker (2016). "Cardiolipin binds selectively but transiently to conserved lysine residues in the rotor of metazoan ATP synthases." Proc Natl Acad Sci U S A **113**(31): 8687-8692.
Duran, R. V. and M. N. Hall (2012). "Glutaminolysis feeds mTORC1." Cell Cycle **11**(22): 4107-4108.
Duran, R. V., W. Oppliger, A. M. Robitaille, L. Heiserich, R. Skendaj, E. Gottlieb and M. N. Hall (2012). "Glutaminolysis activates Rag-mTORC1 signaling." Mol Cell **47**(3): 349-358.
Duvel, K., J. L. Yecies, S. Menon, P. Raman, A. I. Lipovsky, A. L. Souza, E. Triantafellow, Q. Ma, R. Gorski, S. Cleaver, M. G. Vander Heiden, J. P. MacKeigan, P. M. Finan, C. B. Clish, L. O. Murphy and B. D. Manning (2010). "Activation of a metabolic gene regulatory network downstream of mTOR complex 1." Mol Cell **39**(2): 171-183.
Efeyan, A. and D. M. Sabatini (2010). "mTOR and cancer: many loops in one pathway." Current Opinion in Cell Biology **22**(2): 169-176.
Eltschinger, S. and R. Loewith (2016). "TOR Complexes and the Maintenance of Cellular Homeostasis." Trends Cell Biol **26**(2): 148-159.
Eltschinger, S. and R. Loewith (2016). "TOR Complexes and the Maintenance of Cellular Homeostasis." Trends in Cell Biology **26**(2): 148-159.
Faller, W. J., T. J. Jackson, J. R. Knight, R. A. Ridgway, T. Jamieson, S. A. Karim, C. Jones, S. Radulescu, D. J. Huels, K. B. Myant, K. M. Dudek, H. A. Casey, A. Scopelliti, J. B. Cordero, M. Vidal, M. Pende, A. G. Ryazanov, N. Sonenberg, O. Meyuhas, M. N. Hall, M. Bushell, A. E. Willis and O. J. Sansom (2015). "mTORC1-mediated translational elongation limits intestinal tumour initiation and growth." Nature **517**(7535): 497-500.
Fazel, Y., A. B. Koenig, M. Sayiner, Z. D. Goodman and Z. M. Younossi (2016). "Epidemiology and natural history of non-alcoholic fatty liver disease." Metabolism **65**(8): 1017-1025.
Feng, Y. H., W. Y. Chen, Y. H. Kuo, C. L. Tung, C. J. Tsao, A. L. Shiau and C. L. Wu (2016). "Elovl6 is a poor prognostic predictor in breast cancer." Oncol Lett **12**(1): 207-212.
Flavin, R., S. Peluso, P. L. Nguyen and M. Loda (2010). "Fatty acid synthase as a potential therapeutic target in cancer." Future Oncol **6**(4): 551-562.
Frias, M. A., C. C. Thoreen, J. D. Jaffe, W. Schroder, T. Sculley, S. A. Carr and D. M. Sabatini (2006). "mSin1 is necessary for Akt/PKB phosphorylation, and its isoforms define three distinct mTORC2s." Curr Biol **16**(18): 1865-1870.
Garcia-Barros, M., N. Coant, J. P. Truman, A. J. Snider and Y. A. Hannun (2014). "Sphingolipids in colon cancer." Biochim Biophys Acta **1841**(5): 773-782.
Gibellini, F. and T. K. Smith (2010). "The Kennedy pathway--De novo synthesis of phosphatidylethanolamine and phosphatidylcholine." IUBMB Life **62**(6): 414-428.
Guenther, S., L. J. Muirhead, A. V. Speller, O. Golf, N. Strittmatter, R. Ramakrishnan, R. D. Goldin, E. Jones, K. Veselkov, J. Nicholson, A. Darzi and Z. Takats (2015). "Spatially resolved metabolic phenotyping of breast

cancer by desorption electrospray ionization mass spectrometry." Cancer Res **75**(9): 1828-1837.
Guertin, D. A., D. M. Stevens, M. Saitoh, S. Kinkel, K. Crosby, J. H. Sheen, D. J. Mullholland, M. A. Magnuson, H. Wu and D. M. Sabatini (2009). "mTOR complex 2 is required for the development of prostate cancer induced by Pten loss in mice." Cancer Cell **15**(2): 148-159.
Guillaumond, F., G. Bidaut, M. Ouaissi, S. Servais, V. Gouirand, O. Olivares, S. Lac, L. Borge, J. Roques, O. Gayet, M. Pinault, C. Guimaraes, J. Nigri, C. Loncle, M. N. Lavaut, S. Garcia, A. Tailleux, B. Staels, E. Calvo, R. Tomasini, J. L. Iovanna and S. Vasseur (2015). "Cholesterol uptake disruption, in association with chemotherapy, is a promising combined metabolic therapy for pancreatic adenocarcinoma." Proc Natl Acad Sci U S A **112**(8): 2473-2478.
Guillou, H., D. Zadravec, P. G. Martin and A. Jacobsson (2010). "The key roles of elongases and desaturases in mammalian fatty acid metabolism: Insights from transgenic mice." Prog Lipid Res **49**(2): 186-199.
Gupta, V., K. N. Bhinge, S. B. Hosain, K. Xiong, X. Gu, R. Shi, M. Y. Ho, K. H. Khoo, S. C. Li, Y. T. Li, S. V. Ambudkar, S. M. Jazwinski and Y. Y. Liu (2012). "Ceramide glycosylation by glucosylceramide synthase selectively maintains the properties of breast cancer stem cells." J Biol Chem **287**(44): 37195-37205.
Gupta, V., G. A. Patwardhan, Q. J. Zhang, M. C. Cabot, S. M. Jazwinski and Y. Y. Liu (2010). "Direct quantitative determination of ceramide glycosylation in vivo: a new approach to evaluate cellular enzyme activity of glucosylceramide synthase." J Lipid Res **51**(4): 866-874.
Hagiwara, A., M. Cornu, N. Cybulski, P. Polak, C. Betz, F. Trapani, L. Terracciano, M. H. Heim, M. A. Ruegg and M. N. Hall (2012). "Hepatic mTORC2 activates glycolysis and lipogenesis through Akt, glucokinase, and SREBP1c." Cell Metab **15**(5): 725-738.
Hannun, Y. A. and L. M. Obeid (2008). "Principles of bioactive lipid signalling: lessons from sphingolipids." Nat Rev Mol Cell Biol **9**(2): 139-150.
He, Q., V. J. Johnson, M. F. Osuchowski and R. P. Sharma (2004). "Inhibition of serine palmitoyltransferase by myriocin, a natural mycotoxin, causes induction of c-myc in mouse liver." Mycopathologia **157**(3): 339-347.
Hilvo, M., C. Denkert, L. Lehtinen, B. Muller, S. Brockmoller, T. Seppanen-Laakso, J. Budczies, E. Bucher, L. Yetukuri, S. Castillo, E. Berg, H. Nygren, M. Sysi-Aho, J. L. Griffin, O. Fiehn, S. Loibl, C. Richter-Ehrenstein, C. Radke, T. Hyotylainen, O. Kallioniemi, K. Iljin and M. Oresic (2011). "Novel theranostic opportunities offered by characterization of altered membrane lipid metabolism in breast cancer progression." Cancer Res **71**(9): 3236-3245.
Hitosugi, T., J. Fan, T. W. Chung, K. Lythgoe, X. Wang, J. Xie, Q. Ge, T. L. Gu, R. D. Polakiewicz, J. L. Roesel, G. Z. Chen, T. J. Boggon, S. Lonial, H. Fu, F. R. Khuri, S. Kang and J. Chen (2011). "Tyrosine phosphorylation of mitochondrial pyruvate dehydrogenase kinase 1 is important for cancer metabolism." Mol Cell **44**(6): 864-877.
Horie, Y., A. Suzuki, E. Kataoka, T. Sasaki, K. Hamada, J. Sasaki, K. Mizuno, G. Hasegawa, H. Kishimoto, M. Iizuka, M. Naito, K. Enomoto, S. Watanabe, T. W. Mak and T. Nakano (2004). "Hepatocyte-specific Pten deficiency results in steatohepatitis and hepatocellular carcinomas." J Clin Invest **113**(12): 1774-1783.

Horie, Y., A. Suzuki, E. Kataoka, T. Sasaki, K. Hamada, J. Sasaki, K. Mizuno, G. Hasegawa, H. Kishimoto, M. Iizuka, M. Naito, K. Enomoto, S. Watanabe, T. W. Mak and T. Nakano (2004). "Hepatocyte-specific Pten deficiency results in steatohepatitis and hepatocellular carcinomas." Journal of Clinical Investigation **113**(12): 1774-1783.
Horton, J. D., J. L. Goldstein and M. S. Brown (2002). "SREBPs: activators of the complete program of cholesterol and fatty acid synthesis in the liver." J Clin Invest **109**(9): 1125-1131.
Houtkooper, R. H. and F. M. Vaz (2008). "Cardiolipin, the heart of mitochondrial metabolism." Cell Mol Life Sci **65**(16): 2493-2506.
Hsieh, A. C., Y. Liu, M. P. Edlind, N. T. Ingolia, M. R. Janes, A. Sher, E. Y. Shi, C. R. Stumpf, C. Christensen, M. J. Bonham, S. Wang, P. Ren, M. Martin, K. Jessen, M. E. Feldman, J. S. Weissman, K. M. Shokat, C. Rommel and D. Ruggero (2012). "The translational landscape of mTOR signalling steers cancer initiation and metastasis." Nature **485**(7396): 55-61.
Hsieh, A. C. and D. Ruggero (2010). "Targeting eukaryotic translation initiation factor 4E (eIF4E) in cancer." Clin Cancer Res **16**(20): 4914-4920.
Huang, W. C., C. C. Tsai, C. L. Chen, T. Y. Chen, Y. P. Chen, Y. S. Lin, P. J. Lu, C. M. Lin, S. H. Wang, C. W. Tsao, C. Y. Wang, Y. L. Cheng, C. Y. Hsieh, P. C. Tseng and C. F. Lin (2011). "Glucosylceramide synthase inhibitor PDMP sensitizes chronic myeloid leukemia T315I mutant to Bcr-Abl inhibitor and cooperatively induces glycogen synthase kinase-3-regulated apoptosis." FASEB J **25**(10): 3661-3673.
Inoki, K. and K. L. Guan (2009). "Tuberous sclerosis complex, implication from a rare genetic disease to common cancer treatment." Hum Mol Genet **18**(R1): R94-100.
Inoki, K., Y. Li, T. Zhu, J. Wu and K. L. Guan (2002). "TSC2 is phosphorylated and inhibited by Akt and suppresses mTOR signalling." Nat Cell Biol **4**(9): 648-657.
Inoki, K., Y. Li, T. Q. Zhu, J. Wu and K. L. Guan (2002). "TSC2 is phosphorylated and inhibited by Akt and suppresses mTOR signalling." Nature Cell Biology **4**(9): 648-657.
Inoki, K., H. Ouyang, T. Zhu, C. Lindvall, Y. Wang, X. Zhang, Q. Yang, C. Bennett, Y. Harada, K. Stankunas, C. Y. Wang, X. He, O. A. MacDougald, M. You, B. O. Williams and K. L. Guan (2006). "TSC2 integrates Wnt and energy signals via a coordinated phosphorylation by AMPK and GSK3 to regulate cell growth." Cell **126**(5): 955-968.
Jacinto, E., R. Loewith, A. Schmidt, S. Lin, M. A. Ruegg, A. Hall and M. N. Hall (2004). "Mammalian TOR complex 2 controls the actin cytoskeleton and is rapamycin insensitive." Nature Cell Biology **6**(11): 1122-U1130.
Jeon, T. I. and T. F. Osborne (2012). "SREBPs: metabolic integrators in physiology and metabolism." Trends Endocrinol Metab **23**(2): 65-72.
Jimenez-Valerio, G., M. Martinez-Lozano, N. Bassani, A. Vidal, M. Ochoa-de-Olza, C. Suarez, X. Garcia-Del-Muro, J. Carles, F. Vinals, M. Graupera, S. Indraccolo and O. Casanovas (2016). "Resistance to Antiangiogenic Therapies by Metabolic Symbiosis in Renal Cell Carcinoma PDX Models and Patients." Cell Rep **15**(6): 1134-1143.
Joshi, A. S., M. N. Thompson, N. Fei, M. Huttemann and M. L. Greenberg (2012). "Cardiolipin and mitochondrial phosphatidylethanolamine have

overlapping functions in mitochondrial fusion in Saccharomyces cerevisiae." J Biol Chem **287**(21): 17589-17597.
Kartal Yandim, M., E. Apohan and Y. Baran (2013). "Therapeutic potential of targeting ceramide/glucosylceramide pathway in cancer." Cancer Chemother Pharmacol **71**(1): 13-20.
Kawashima, M., N. Iwamoto, N. Kawaguchi-Sakita, M. Sugimoto, T. Ueno, Y. Mikami, K. Terasawa, T. A. Sato, K. Tanaka, K. Shimizu and M. Toi (2013). "High-resolution imaging mass spectrometry reveals detailed spatial distribution of phosphatidylinositols in human breast cancer." Cancer Sci **104**(10): 1372-1379.
Kenerson, H. L., L. D. Aicher, L. D. True and R. S. Yeung (2002). "Activated mammalian target of rapamycin pathway in the pathogenesis of tuberous sclerosis complex renal tumors." Cancer Research **62**(20): 5645-5650.
Kenerson, H. L., S. Subramanian, R. McIntyre, M. Kazami and R. S. Yeung (2015). "Livers with constitutive mTORC1 activity resist steatosis independent of feedback suppression of Akt." PLoS One **10**(2): e0117000.
Kenerson, H. L., M. M. Yeh, M. Kazami, X. Y. Jiang, K. J. Riehle, R. L. Mcintyre, J. O. Park, S. Kwon, J. S. Campbell and R. S. Yeung (2013). "Akt and mTORC1 Have Different Roles During Liver Tumorigenesis in Mice." Gastroenterology **144**(5): 1055-1065.
Kenerson, H. L., M. M. Yeh and R. S. Yeung (2011). "Tuberous Sclerosis Complex-1 Deficiency Attenuates Diet-Induced Hepatic Lipid Accumulation." Plos One **6**(3).
Kettenbach, A. N. and S. A. Gerber (2011). "Rapid and Reproducible Single-Stage Phosphopeptide Enrichment of Complex Peptide Mixtures: Application to General and Phosphotyrosine-Specific Phosphoproteomics Experiments." Analytical Chemistry **83**(20): 7635-7644.
Kiebish, M. A., X. Han, H. Cheng, J. H. Chuang and T. N. Seyfried (2008). "Cardiolipin and electron transport chain abnormalities in mouse brain tumor mitochondria: lipidomic evidence supporting the Warburg theory of cancer." J Lipid Res **49**(12): 2545-2556.
Kim, E., P. Goraksha-Hicks, L. Li, T. P. Neufeld and K. L. Guan (2008). "Regulation of TORC1 by Rag GTPases in nutrient response." Nat Cell Biol **10**(8): 935-945.
Kim, J., M. Kundu, B. Viollet and K. L. Guan (2011). "AMPK and mTOR regulate autophagy through direct phosphorylation of Ulk1." Nature Cell Biology **13**(2): 132-U171.
Kim, J. W., I. Tchernyshyov, G. L. Semenza and C. V. Dang (2006). "HIF-1-mediated expression of pyruvate dehydrogenase kinase: a metabolic switch required for cellular adaptation to hypoxia." Cell Metab **3**(3): 177-185.
Kridel, S. J., F. Axelrod, N. Rozenkrantz and J. W. Smith (2004). "Orlistat is a novel inhibitor of fatty acid synthase with antitumor activity." Cancer Research **64**(6): 2070-2075.
Kuhajda, F. P., K. Jenner, F. D. Wood, R. A. Hennigar, L. B. Jacobs, J. D. Dick and G. R. Pasternack (1994). "Fatty-Acid Synthesis - a Potential Selective Target for Antineoplastic Therapy." Proceedings of the National Academy of Sciences of the United States of America **91**(14): 6379-6383.
Kumar, A., J. C. Lawrence, Jr., D. Y. Jung, H. J. Ko, S. R. Keller, J. K. Kim, M. A. Magnuson and T. E. Harris (2010). "Fat cell-specific ablation of rictor in

mice impairs insulin-regulated fat cell and whole-body glucose and lipid metabolism." Diabetes **59**(6): 1397-1406.
Kwiatkowski, D. J., H. Zhang, J. L. Bandura, K. M. Heiberger, M. Glogauer, N. el-Hashemite and H. Onda (2002). "A mouse model of TSC1 reveals sex-dependent lethality from liver hemangiomas, and up-regulation of p70S6 kinase activity in Tsc1 null cells." Hum Mol Genet **11**(5): 525-534.
Kwiatkowski, D. J., H. B. Zhang, J. L. Bandura, K. M. Heiberger, M. Glogauer, N. el-Hashemite and H. Onda (2002). "A mouse model of TSC1 reveals sex-dependent lethality from liver hemangiomas, and up-regulation of p70S6 kinase activity in Tsc1 null cells." Human Molecular Genetics **11**(5): 525-534.
Labuschagne, C. F., N. J. van den Broek, G. M. Mackay, K. H. Vousden and O. D. Maddocks (2014). "Serine, but not glycine, supports one-carbon metabolism and proliferation of cancer cells." Cell Rep **7**(4): 1248-1258.
Lambert, J. E., M. A. Ramos-Roman, J. D. Browning and E. J. Parks (2014). "Increased de novo lipogenesis is a distinct characteristic of individuals with nonalcoholic fatty liver disease." Gastroenterology **146**(3): 726-735.
Laplante, M. and D. M. Sabatini (2012). "mTOR signaling in growth control and disease." Cell **149**(2): 274-293.
Lee, J. M., H. Lee, S. Kang and W. J. Park (2016). "Fatty Acid Desaturases, Polyunsaturated Fatty Acid Regulation, and Biotechnological Advances." Nutrients **8**(1).
Levy, M. and A. H. Futerman (2010). "Mammalian ceramide synthases." IUBMB Life **62**(5): 347-356.
Li, J., S. F. Ding, N. A. Habib, B. F. Fermor, C. B. Wood and R. S. Gilmour (1994). "Partial characterization of a cDNA for human stearoyl-CoA desaturase and changes in its mRNA expression in some normal and malignant tissues." Int J Cancer **57**(3): 348-352.
Li, L., G. M. Pilo, X. Li, A. Cigliano, G. Latte, L. Che, C. Joseph, M. Mela, C. Wang, L. Jiang, S. Ribback, M. M. Simile, R. M. Pascale, F. Dombrowski, M. Evert, C. F. Semenkovich, X. Chen and D. F. Calvisi (2016). "Inactivation of fatty acid synthase impairs hepatocarcinogenesis driven by AKT in mice and humans." J Hepatol **64**(2): 333-341.
Li, S., M. S. Brown and J. L. Goldstein (2010). "Bifurcation of insulin signaling pathway in rat liver: mTORC1 required for stimulation of lipogenesis, but not inhibition of gluconeogenesis." Proc Natl Acad Sci U S A **107**(8): 3441-3446.
Liang, J., M. Nagahashi, E. Y. Kim, K. B. Harikumar, A. Yamada, W. C. Huang, N. C. Hait, J. C. Allegood, M. M. Price, D. Avni, K. Takabe, T. Kordula, S. Milstien and S. Spiegel (2013). "Sphingosine-1-phosphate links persistent STAT3 activation, chronic intestinal inflammation, and development of colitis-associated cancer." Cancer Cell **23**(1): 107-120.
Liu, P., W. Gan, Y. R. Chin, K. Ogura, J. Guo, J. Zhang, B. Wang, J. Blenis, L. C. Cantley, A. Toker, B. Su and W. Wei (2015). "PtdIns(3,4,5)P3-Dependent Activation of the mTORC2 Kinase Complex." Cancer Discov **5**(11): 1194-1209.
Liu, P., W. Gan, H. Inuzuka, A. S. Lazorchak, D. Gao, O. Arojo, D. Liu, L. Wan, B. Zhai, Y. Yu, M. Yuan, B. M. Kim, S. Shaik, S. Menon, S. P. Gygi, T. H. Lee, J. M. Asara, B. D. Manning, J. Blenis, B. Su and W. Wei (2013). "Sin1 phosphorylation impairs mTORC2 complex integrity and inhibits downstream Akt signalling to suppress tumorigenesis." Nat Cell Biol **15**(11): 1340-1350.

Liu, Y. Y., T. Y. Han, A. E. Giuliano, N. Hansen and M. C. Cabot (2000). "Uncoupling ceramide glycosylation by transfection of glucosylceramide synthase antisense reverses adriamycin resistance." J Biol Chem **275**(10): 7138-7143.
Liu, Y. Y., R. A. Hill and Y. T. Li (2013). "Ceramide glycosylation catalyzed by glucosylceramide synthase and cancer drug resistance." Adv Cancer Res **117**: 59-89.
Llovet, J. M., J. Zucman-Rossi, E. Pikarsky, B. Sangro, M. Schwartz, M. Sherman and G. Gores (2016). "Hepatocellular carcinoma." Nat Rev Dis Primers **2**: 16018.
Locasale, J. W. (2013). "Serine, glycine and one-carbon units: cancer metabolism in full circle." Nat Rev Cancer **13**(8): 572-583.
Loewith, R., E. Jacinto, S. Wullschleger, A. Lorberg, J. L. Crespo, D. Bonenfant, W. Oppliger, P. Jenoe and M. N. Hall (2002). "Two TOR complexes, only one of which is rapamycin sensitive, have distinct roles in cell growth control." Mol Cell **10**(3): 457-468.
Lonardo, A., C. D. Byrne, S. H. Caldwell, H. Cortez-Pinto and G. Targher (2016). "Global epidemiology of non-alcoholic fatty liver disease. Meta-analytic assessment of prevalence, incidence and outcomes." Hepatology.
Long, X., Y. Lin, S. Ortiz-Vega, K. Yonezawa and J. Avruch (2005). "Rheb binds and regulates the mTOR kinase." Curr Biol **15**(8): 702-713.
Ma, C., A. H. Kesarwala, T. Eggert, J. Medina-Echeverz, D. E. Kleiner, P. Jin, D. F. Stroncek, M. Terabe, V. Kapoor, M. ElGindi, M. Han, A. M. Thornton, H. Zhang, M. Egger, J. Luo, D. W. Felsher, D. W. McVicar, A. Weber, M. Heikenwalder and T. F. Greten (2016). "NAFLD causes selective CD4(+) T lymphocyte loss and promotes hepatocarcinogenesis." Nature **531**(7593): 253-257.
Ma, X. M. and J. Blenis (2009). "Molecular mechanisms of mTOR-mediated translational control." Nat Rev Mol Cell Biol **10**(5): 307-318.
Mamane, Y., E. Petroulakis, O. LeBacquer and N. Sonenberg (2006). "mTOR, translation initiation and cancer." Oncogene **25**(48): 6416-6422.
Manning, B. D., A. R. Tee, M. N. Logsdon, J. Blenis and L. C. Cantley (2002). "Identification of the tuberous sclerosis complex-2 tumor suppressor gene product tuberin as a target of the phosphoinositide 3-kinase/akt pathway." Mol Cell **10**(1): 151-162.
Manning, B. D., A. R. Tee, M. N. Logsdon, J. Blenis and L. C. Cantley (2002). "Identification of the tuberous sclerosis complex-2 tumor suppressor gene product tuberin as a target of the phosphoinositide 3-Kinase/Akt pathway." Molecular Cell **10**(1): 151-162.
Masui, K., W. K. Cavenee and P. S. Mischel (2014). "mTORC2 in the center of cancer metabolic reprogramming." Trends in Endocrinology and Metabolism **25**(7): 364-373.
Masui, K., K. Tanaka, D. Akhavan, I. Babic, B. Gini, T. Matsutani, A. Iwanami, F. Liu, G. R. Villa, Y. C. Gu, C. Campos, S. J. Zhu, H. J. Yang, W. H. Yong, T. F. Cloughesy, I. K. Mellinghoff, W. K. Cavenee, R. J. Shaw and P. S. Mischel (2013). "mTOR Complex 2 Controls Glycolytic Metabolism in Glioblastoma through FoxO Acetylation and Upregulation of c-Myc." Cell Metabolism **18**(5): 726-739.
Masui, K., K. Tanaka, S. Ikegami, G. R. Villa, H. Yang, W. H. Yong, T. F. Cloughesy, K. Yamagata, N. Arai, W. K. Cavenee and P. S. Mischel (2015).

"Glucose-dependent acetylation of Rictor promotes targeted cancer therapy resistance." Proc Natl Acad Sci U S A **112**(30): 9406-9411.
Matyash, V., G. Liebisch, T. V. Kurzchalia, A. Shevchenko and D. Schwudke (2008). "Lipid extraction by methyl-tert-butyl ether for high-throughput lipidomics." J Lipid Res **49**(5): 1137-1146.
Medes, G., A. Thomas and S. Weinhouse (1953). "Metabolism of neoplastic tissue. IV. A study of lipid synthesis in neoplastic tissue slices in vitro." Cancer Res **13**(1): 27-29.
Mehlem, A., C. E. Hagberg, L. Muhl, U. Eriksson and A. Falkevall (2013). "Imaging of neutral lipids by oil red O for analyzing the metabolic status in health and disease." Nat Protoc **8**(6): 1149-1154.
Mendoza, M. C., E. E. Er and J. Blenis (2011). "The Ras-ERK and PI3K-mTOR pathways: cross-talk and compensation." Trends Biochem Sci **36**(6): 320-328.
Menendez, J. A. and R. Lupu (2007). "Fatty acid synthase and the lipogenic phenotype in cancer pathogenesis." Nat Rev Cancer **7**(10): 763-777.
Menon, S., C. C. Dibble, G. Talbott, G. Hoxhaj, A. J. Valvezan, H. Takahashi, L. C. Cantley and B. D. Manning (2014). "Spatial control of the TSC complex integrates insulin and nutrient regulation of mTORC1 at the lysosome." Cell **156**(4): 771-785.
Menon, S., J. L. Yecies, H. H. Zhang, J. J. Howell, J. Nicholatos, E. Harputlugil, R. T. Bronson, D. J. Kwiatkowski and B. D. Manning (2012). "Chronic Activation of mTOR Complex 1 Is Sufficient to Cause Hepatocellular Carcinoma in Mice." Science Signaling **5**(217).
Mester, J. and E. Charis (2015). "PTEN hamartoma tumor syndrome." Handb Clin Neurol **132**: 129-137.
Mischel, P. (2015). "Targeting PI3K-mTOR signaling in glioblastoma: A central role for mTORC2 in drug resistance and metabolic reprogramming." Molecular Cancer Therapeutics **14**(7).
Mittal, S., Y. H. Sada, H. B. El-Serag, F. Kanwal, Z. Duan, S. Temple, S. B. May, J. R. Kramer, P. A. Richardson and J. A. Davila (2015). "Temporal trends of nonalcoholic fatty liver disease-related hepatocellular carcinoma in the veteran affairs population." Clin Gastroenterol Hepatol **13**(3): 594-601 e591.
Ngeow, J. and C. Eng (2016). "Germline PTEN Mutation Analysis for PTEN Hamartoma Tumor Syndrome." Methods Mol Biol **1388**: 63-73.
Ogretmen, B. and Y. A. Hannun (2004). "Biologically active sphingolipids in cancer pathogenesis and treatment." Nat Rev Cancer **4**(8): 604-616.
Olson, K. A., J. C. Schell and J. Rutter (2016). "Pyruvate and Metabolic Flexibility: Illuminating a Path Toward Selective Cancer Therapies." Trends Biochem Sci **41**(3): 219-230.
Pacold, M. E., K. R. Brimacombe, S. H. Chan, J. M. Rohde, C. A. Lewis, L. J. Swier, R. Possemato, W. W. Chen, L. B. Sullivan, B. P. Fiske, S. Cho, E. Freinkman, K. Birsoy, M. Abu-Remaileh, Y. D. Shaul, C. M. Liu, M. Zhou, M. J. Koh, H. Chung, S. M. Davidson, A. Luengo, A. Q. Wang, X. Xu, A. Yasgar, L. Liu, G. Rai, K. D. Westover, M. G. Vander Heiden, M. Shen, N. S. Gray, M. B. Boxer and D. M. Sabatini (2016). "A PHGDH inhibitor reveals coordination of serine synthesis and one-carbon unit fate." Nat Chem Biol **12**(6): 452-458.

Pagadala, M., T. Kasumov, A. J. McCullough, N. N. Zein and J. P. Kirwan (2012). "Role of ceramides in nonalcoholic fatty liver disease." Trends Endocrinol Metab **23**(8): 365-371.
Papandreou, I., R. A. Cairns, L. Fontana, A. L. Lim and N. C. Denko (2006). "HIF-1 mediates adaptation to hypoxia by actively downregulating mitochondrial oxygen consumption." Cell Metab **3**(3): 187-197.
Park, E. J., J. H. Lee, G. Y. Yu, G. He, S. R. Ali, R. G. Holzer, C. H. Osterreicher, H. Takahashi and M. Karin (2010). "Dietary and genetic obesity promote liver inflammation and tumorigenesis by enhancing IL-6 and TNF expression." Cell **140**(2): 197-208.
Pavlova, N. N. and C. B. Thompson (2016). "The Emerging Hallmarks of Cancer Metabolism." Cell Metab **23**(1): 27-47.
Pearce, L. R., D. Komander and D. R. Alessi (2010). "The nuts and bolts of AGC protein kinases." Nat Rev Mol Cell Biol **11**(1): 9-22.
Peck, B., Z. T. Schug, Q. Zhang, B. Dankworth, D. T. Jones, E. Smethurst, R. Patel, S. Mason, M. Jiang, R. Saunders, M. Howell, R. Mitter, B. Spencer-Dene, G. Stamp, L. McGarry, D. James, E. Shanks, E. O. Aboagye, S. E. Critchlow, H. Y. Leung, A. L. Harris, M. J. Wakelam, E. Gottlieb and A. Schulze (2016). "Inhibition of fatty acid desaturation is detrimental to cancer cell survival in metabolically compromised environments." Cancer Metab **4**: 6.
Peck, B. and A. Schulze (2016). "Lipid desaturation - the next step in targeting lipogenesis in cancer?" FEBS J **283**(15): 2767-2778.
Pelletier, J., J. Graff, D. Ruggero and N. Sonenberg (2015). "Targeting the eIF4F translation initiation complex: a critical nexus for cancer development." Cancer Res **75**(2): 250-263.
Peterson, T. R., S. S. Sengupta, T. E. Harris, A. E. Carmack, S. A. Kang, E. Balderas, D. A. Guertin, K. L. Madden, A. E. Carpenter, B. N. Finck and D. M. Sabatini (2011). "mTOR Complex 1 Regulates Lipin 1 Localization to Control the SREBP Pathway." Cell **146**(3): 408-420.
Pietrocola, F., L. Galluzzi, J. M. Bravo-San Pedro, F. Madeo and G. Kroemer (2015). "Acetyl coenzyme A: a central metabolite and second messenger." Cell Metab **21**(6): 805-821.
Pisarsky, L., R. Bill, E. Fagiani, S. Dimeloe, R. W. Goosen, J. Hagmann, C. Hess and G. Christofori (2016). "Targeting Metabolic Symbiosis to Overcome Resistance to Anti-angiogenic Therapy." Cell Rep **15**(6): 1161-1174.
Porstmann, T., B. Griffiths, Y. L. Chung, O. Delpuech, J. R. Griffiths, J. Downward and A. Schulze (2005). "PKB/Akt induces transcription of enzymes involved in cholesterol and fatty acid biosynthesis via activation of SREBP." Oncogene **24**(43): 6465-6481.
Porstmann, T., C. R. Santos, B. Griffiths, M. Cully, M. Wu, S. Leevers, J. R. Griffiths, Y. L. Chung and A. Schulze (2008). "SREBP activity is regulated by mTORC1 and contributes to Akt-dependent cell growth." Cell Metab **8**(3): 224-236.
Possemato, R., K. M. Marks, Y. D. Shaul, M. E. Pacold, D. Kim, K. Birsoy, S. Sethumadhavan, H. K. Woo, H. G. Jang, A. K. Jha, W. W. Chen, F. G. Barrett, N. Stransky, Z. Y. Tsun, G. S. Cowley, J. Barretina, N. Y. Kalaany, P. P. Hsu, K. Ottina, A. M. Chan, B. Yuan, L. A. Garraway, D. E. Root, M. Mino-Kenudson, E. F. Brachtel, E. M. Driggers and D. M. Sabatini (2011). "Functional genomics reveal that the serine synthesis pathway is essential in breast cancer." Nature **476**(7360): 346-350.

Postic, C. and J. Girard (2008). "Contribution of de novo fatty acid synthesis to hepatic steatosis and insulin resistance: lessons from genetically engineered mice." J Clin Invest **118**(3): 829-838.
Postic, C. and J. Girard (2008). "The role of the lipogenic pathway in the development of hepatic steatosis." Diabetes & Metabolism **34**(6): 643-648.
Postic, C. and M. A. Magnuson (2000). "DNA excision in liver by an albumin-Cre transgene occurs progressively with age." Genesis **26**(2): 149-150.
Pusapati, R. V., A. Daemen, C. Wilson, W. Sandoval, M. Gao, B. Haley, A. R. Baudy, G. Hatzivassiliou, M. Evangelista and J. Settleman (2016). "mTORC1-Dependent Metabolic Reprogramming Underlies Escape from Glycolysis Addiction in Cancer Cells." Cancer Cell **29**(4): 548-562.
Raturi, A. and T. Simmen (2013). "Where the endoplasmic reticulum and the mitochondrion tie the knot: the mitochondria-associated membrane (MAM)." Biochim Biophys Acta **1833**(1): 213-224.
Ricoult, S. J. and B. D. Manning (2013). "The multifaceted role of mTORC1 in the control of lipid metabolism." EMBO Rep **14**(3): 242-251.
Ricoult, S. J., J. L. Yecies, I. Ben-Sahra and B. D. Manning (2015). "Oncogenic PI3K and K-Ras stimulate de novo lipid synthesis through mTORC1 and SREBP." Oncogene.
Robitaille, A. M., S. Christen, M. Shimobayashi, M. Cornu, L. L. Fava, S. Moes, C. Prescianotto-Baschong, U. Sauer, P. Jenoe and M. N. Hall (2013). "Quantitative Phosphoproteomics Reveal mTORC1 Activates de Novo Pyrimidine Synthesis." Science **339**(6125): 1320-1323.
Sakai, K., M. Akiyama, Y. Sugiyama-Nakagiri, J. R. McMillan, D. Sawamura and H. Shimizu (2007). "Localization of ABCA12 from Golgi apparatus to lamellar granules in human upper epidermal keratinocytes." Exp Dermatol **16**(11): 920-926.
Sancak, Y., T. R. Peterson, Y. D. Shaul, R. A. Lindquist, C. C. Thoreen, L. Bar-Peled and D. M. Sabatini (2008). "The Rag GTPases bind raptor and mediate amino acid signaling to mTORC1." Science **320**(5882): 1496-1501.
Sanders, F. W. and J. L. Griffin (2016). "De novo lipogenesis in the liver in health and disease: more than just a shunting yard for glucose." Biol Rev Camb Philos Soc **91**(2): 452-468.
Santos, C. R. and A. Schulze (2012). "Lipid metabolism in cancer." FEBS J **279**(15): 2610-2623.
Sarbassov, D. D., S. M. Ali, D. H. Kim, D. A. Guertin, R. R. Latek, H. Erdjument-Bromage, P. Tempst and D. M. Sabatini (2004). "Rictor, a novel binding partner of mTOR, defines a rapamycin-insensitive and raptor-independent pathway that regulates the cytoskeleton." Curr Biol **14**(14): 1296-1302.
Scherer, A. and J. F. Dufour (2016). "Treatment of Non-Alcoholic Fatty Liver Disease." Dig Dis **34 Suppl 1**: 27-31.
Schlame, M. and D. Haldar (1993). "Cardiolipin is synthesized on the matrix side of the inner membrane in rat liver mitochondria." J Biol Chem **268**(1): 74-79.
Schlame, M., D. Rua and M. L. Greenberg (2000). "The biosynthesis and functional role of cardiolipin." Prog Lipid Res **39**(3): 257-288.
Schulze, A. and J. Downward (2011). "Flicking the Warburg switch-tyrosine phosphorylation of pyruvate dehydrogenase kinase regulates mitochondrial activity in cancer cells." Mol Cell **44**(6): 846-848.

Schulze, A. and A. L. Harris (2012). "How cancer metabolism is tuned for proliferation and vulnerable to disruption." Nature **491**(7424): 364-373.
Seguin, F., M. A. Carvalho, D. C. Bastos, M. Agostini, K. G. Zecchin, M. P. Alvarez-Flores, A. M. Chudzinski-Tavassi, R. D. Coletta and E. Graner (2012). "The fatty acid synthase inhibitor orlistat reduces experimental metastases and angiogenesis in B16-F10 melanomas." Br J Cancer **107**(6): 977-987.
Shimobayashi, M. and M. N. Hall (2014). "Making new contacts: the mTOR network in metabolism and signalling crosstalk." Nat Rev Mol Cell Biol **15**(3): 155-162.
Shimobayashi, M. and M. N. Hall (2016). "Multiple amino acid sensing inputs to mTORC1." Cell Research **26**(1): 7-20.
Siow, D., M. Sunkara, T. M. Dunn, A. J. Morris and B. Wattenberg (2015). "ORMDL/serine palmitoyltransferase stoichiometry determines effects of ORMDL3 expression on sphingolipid biosynthesis." J Lipid Res **56**(4): 898-908.
Siow, D., M. Sunkara, A. Morris and B. Wattenberg (2015). "Regulation of de novo sphingolipid biosynthesis by the ORMDL proteins and sphingosine kinase-1." Adv Biol Regul **57**: 42-54.
Sounni, N. E., J. Cimino, S. Blacher, I. Primac, A. Truong, G. Mazzucchelli, A. Paye, D. Calligaris, D. Debois, P. De Tullio, B. Mari, E. De Pauw and A. Noel (2014). "Blocking lipid synthesis overcomes tumor regrowth and metastasis after antiangiogenic therapy withdrawal." Cell Metab **20**(2): 280-294.
Sparks, C. A. and D. A. Guertin (2010). "Targeting mTOR: prospects for mTOR complex 2 inhibitors in cancer therapy." Oncogene **29**(26): 3733-3744.
Sparks, C. A. and D. A. Guertin (2010). "Targeting mTOR: prospects for mTOR complex 2 inhibitors in cancer therapy." Oncogene **29**(26): 3733-3744.
Spirtes, M. A., G. Medes and S. Weinhouse (1953). "A study of acetate metabolism and fatty acid synthesis in liver slices of hyperthyroid rats." J Biol Chem **204**(2): 705-713.
Stefanovic, M., A. Tutusaus, G. A. Martinez-Nieto, C. Barcena, E. de Gregorio, C. Moutinho, E. Barbero-Camps, A. Villanueva, A. Colell, M. Mari, C. Garcia-Ruiz, J. C. Fernandez-Checa and A. Morales (2016). "Targeting glucosylceramide synthase upregulation reverts sorafenib resistance in experimental hepatocellular carcinoma." Oncotarget **7**(7): 8253-8267.
Steneberg, P., A. G. Sykaras, F. Backlund, J. Straseviciene, I. Soderstrom and H. Edlund (2015). "Hyperinsulinemia Enhances Hepatic Expression of the Fatty Acid Transporter Cd36 and Provokes Hepatosteatosis and Hepatic Insulin Resistance." J Biol Chem **290**(31): 19034-19043.
Stiles, B., Y. Wang, A. Stahl, S. Bassilian, W. P. Lee, Y. J. Kim, R. Sherwin, S. Devaskar, R. Lesche, M. A. Magnuson and H. Wu (2004). "Live-specific deletion of negative regulator Pten results in fatty liver and insulin hypersensitivity." Proceedings of the National Academy of Sciences of the United States of America **101**(7): 2082-2087.
Stiles, B., Y. Wang, A. Stahl, S. Bassilian, W. P. Lee, Y. J. Kim, R. Sherwin, S. Devaskar, R. Lesche, M. A. Magnuson and H. Wu (2004). "Liver-specific deletion of negative regulator Pten results in fatty liver and insulin hypersensitivity [corrected]." Proc Natl Acad Sci U S A **101**(7): 2082-2087.
Suzuki, M., K. Cao, S. Kato, Y. Komizu, N. Mizutani, K. Tanaka, C. Arima, M. C. Tai, K. Yanagisawa, N. Togawa, T. Shiraishi, N. Usami, T. Taniguchi, T. Fukui, K. Yokoi, K. Wakahara, Y. Hasegawa, Y. Mizutani, Y. Igarashi, J.

Inokuchi, S. Iwaki, S. Fujii, A. Satou, Y. Matsumoto, R. Ueoka, K. Tamiya-Koizumi, T. Murate, M. Nakamura, M. Kyogashima and T. Takahashi (2016). "Targeting ceramide synthase 6-dependent metastasis-prone phenotype in lung cancer cells." J Clin Invest **126**(1): 254-265.
Takano, T., I. Usui, T. Haruta, J. Kawahara, T. Uno, M. Iwata and M. Kobayashi (2001). "Mammalian target of rapamycin pathway regulates insulin signaling via subcellular redistribution of insulin receptor substrate 1 and integrates nutritional signals and metabolic signals of insulin." Molecular and Cellular Biology **21**(15): 5050-5062.
Tanaka, K., I. Babic, D. Nathanson, D. Akhavan, D. Guo, B. Gini, J. Dang, S. Zhu, H. Yang, J. De Jesus, A. N. Amzajerdi, Y. Zhang, C. C. Dibble, H. Dan, A. Rinkenbaugh, W. H. Yong, H. V. Vinters, J. F. Gera, W. K. Cavenee, T. F. Cloughesy, B. D. Manning, A. S. Baldwin and P. S. Mischel (2011). "Oncogenic EGFR signaling activates an mTORC2-NF-kappaB pathway that promotes chemotherapy resistance." Cancer Discov **1**(6): 524-538.
Taniguchi, K. and M. Karin (2014). "IL-6 and related cytokines as the critical lynchpins between inflammation and cancer." Semin Immunol **26**(1): 54-74.
Tee, A. R., D. C. Fingar, B. D. Manning, D. J. Kwiatkowski, L. C. Cantley and J. Blenis (2002). "Tuberous sclerosis complex-1 and -2 gene products function together to inhibit mammalian target of rapamycin (mTOR)-mediated downstream signaling." Proceedings of the National Academy of Sciences of the United States of America **99**(21): 13571-13576.
Tee, A. R., B. D. Manning, P. P. Roux, L. C. Cantley and J. Blenis (2003). "Tuberous sclerosis complex gene products, Tuberin and Hamartin, control mTOR signaling by acting as a GTPase-activating protein complex toward Rheb." Curr Biol **13**(15): 1259-1268.
Titchenell, P. M., W. J. Quinn, M. Lu, Q. Chu, W. Lu, C. Li, H. Chen, B. R. Monks, J. Chen, J. D. Rabinowitz and M. J. Birnbaum (2016). "Direct Hepatocyte Insulin Signaling Is Required for Lipogenesis but Is Dispensable for the Suppression of Glucose Production." Cell Metab **23**(6): 1154-1166.
Tyanova, S., T. Temu, P. Sinitcyn, A. Carlson, M. Y. Hein, T. Geiger, M. Mann and J. Cox (2016). "The Perseus computational platform for comprehensive analysis of (prote)omics data." Nat Methods **13**(9): 731-740.
Tyler, A., A. Johansson, T. Karlsson, S. K. Gudey, T. Brannstrom, K. Grankvist and P. Behnam-Motlagh (2015). "Targeting glucosylceramide synthase induction of cell surface globotriaosylceramide (Gb3) in acquired cisplatin-resistance of lung cancer and malignant pleural mesothelioma cells." Exp Cell Res **336**(1): 23-32.
Um, S. H., F. Frigerio, M. Watanabe, F. Picard, M. Joaquin, M. Sticker, S. Fumagalli, P. R. Allegrini, S. C. Kozma, J. Auwerx and G. Thomas (2004). "Absence of S6K1 protects against age- and diet-induced obesity while enhancing insulin sensitivity." Nature **431**(7005): 200-205.
Umemura, A., E. J. Park, K. Taniguchi, J. H. Lee, S. Shalapour, M. A. Valasek, M. Aghajan, H. Nakagawa, E. Seki, M. N. Hall and M. Karin (2014). "Liver damage, inflammation, and enhanced tumorigenesis after persistent mTORC1 inhibition." Cell Metab **20**(1): 133-144.
van der Bliek, A. M., Q. Shen and S. Kawajiri (2013). "Mechanisms of mitochondrial fission and fusion." Cold Spring Harb Perspect Biol **5**(6).
Vance, J. E. (1990). "Phospholipid synthesis in a membrane fraction associated with mitochondria." J Biol Chem **265**(13): 7248-7256.

Wang, T., J. Wei, N. Wang, J. L. Ma and P. P. Hui (2015). "The glucosylceramide synthase inhibitor PDMP sensitizes pancreatic cancer cells to MEK/ERK inhibitor AZD-6244." Biochem Biophys Res Commun **456**(3): 821-826.
Wang, X., R. Sato, M. S. Brown, X. Hua and J. L. Goldstein (1994). "SREBP-1, a membrane-bound transcription factor released by sterol-regulated proteolysis." Cell **77**(1): 53-62.
Warburg, O. (1956). "On the origin of cancer cells." Science **123**(3191): 309-314.
Wisniewski, J. R., A. Zougman, N. Nagaraj and M. Mann (2009). "Universal sample preparation method for proteome analysis." Nat Methods **6**(5): 359-362.
Wolf, M. J., A. Adili, K. Piotrowitz, Z. Abdullah, Y. Boege, K. Stemmer, M. Ringelhan, N. Simonavicius, M. Egger, D. Wohlleber, A. Lorentzen, C. Einer, S. Schulz, T. Clavel, U. Protzer, C. Thiele, H. Zischka, H. Moch, M. Tschop, A. V. Tumanov, D. Haller, K. Unger, M. Karin, M. Kopf, P. Knolle, A. Weber and M. Heikenwalder (2014). "Metabolic activation of intrahepatic CD8+ T cells and NKT cells causes nonalcoholic steatohepatitis and liver cancer via cross-talk with hepatocytes." Cancer Cell **26**(4): 549-564.
Wullschleger, S., R. Loewith and M. N. Hall (2006). "TOR signaling in growth and metabolism." Cell **124**(3): 471-484.
Wymann, M. P. and R. Schneiter (2008). "Lipid signalling in disease." Nat Rev Mol Cell Biol **9**(2): 162-176.
Yakir Guri, M. N. H. (2016). "mTOR Signaling Confers Resistance to Targeted Cancer Drugs." Trends in Cancer.
Yang, G., D. S. Murashige, S. J. Humphrey and D. E. James (2015). "A Positive Feedback Loop between Akt and mTORC2 via SIN1 Phosphorylation." Cell Rep **12**(6): 937-943.
Yang, Q., K. Inoki, T. Ikenoue and K. L. Guan (2006). "Identification of Sin1 as an essential TORC2 component required for complex formation and kinase activity." Genes Dev **20**(20): 2820-2832.
Yecies, J. L. and B. D. Manning (2011). "mTOR links oncogenic signaling to tumor cell metabolism." Journal of Molecular Medicine-Jmm **89**(3): 221-228.
Yecies, J. L., H. H. Zhang, S. Menon, S. H. Liu, D. Yecies, A. I. Lipovsky, C. Gorgun, D. J. Kwiatkowski, G. S. Hotamisligil, C. H. Lee and B. D. Manning (2011). "Akt Stimulates Hepatic SREBP1c and Lipogenesis through Parallel mTORC1-Dependent and Independent Pathways (vol 14, pg 21, 2011)." Cell Metabolism **14**(2): 280-280.
Yu-Wai-Man, P., V. Carelli and P. F. Chinnery (2014). "197th ENMC international workshop: Neuromuscular disorders of mitochondrial fusion and fission - OPA1 and MFN2 molecular mechanisms and therapeutic strategies: 26-28 April 2013, Naarden, The Netherlands." Neuromuscul Disord **24**(8): 736-742.
Yue, S., J. Li, S. Y. Lee, H. J. Lee, T. Shao, B. Song, L. Cheng, T. A. Masterson, X. Liu, T. L. Ratliff and J. X. Cheng (2014). "Cholesteryl ester accumulation induced by PTEN loss and PI3K/AKT activation underlies human prostate cancer aggressiveness." Cell Metab **19**(3): 393-406.
Zhang, J., Z. Guan, A. N. Murphy, S. E. Wiley, G. A. Perkins, C. A. Worby, J. L. Engel, P. Heacock, O. K. Nguyen, J. H. Wang, C. R. Raetz, W. Dowhan

and J. E. Dixon (2011). "Mitochondrial phosphatase PTPMT1 is essential for cardiolipin biosynthesis." Cell Metab **13**(6): 690-700.
Zhou, J., M. Febbraio, T. Wada, Y. Zhai, R. Kuruba, J. He, J. H. Lee, S. Khadem, S. Ren, S. Li, R. L. Silverstein and W. Xie (2008). "Hepatic fatty acid transporter Cd36 is a common target of LXR, PXR, and PPARgamma in promoting steatosis." Gastroenterology **134**(2): 556-567.
Zinzalla, V., D. Stracka, W. Oppliger and M. N. Hall (2011). "Activation of mTORC2 by association with the ribosome." Cell **144**(5): 757-768.
Zoncu, R., A. Efeyan and D. M. Sabatini (2011). "mTOR: from growth signal integration to cancer, diabetes and ageing." Nat Rev Mol Cell Biol **12**(1): 21-35.

8.0. Appendix

8.1. mTOR signaling confers resistance to targeted cancer drugs

CellPress

Review

mTOR Signaling Confers Resistance to Targeted Cancer Drugs

Yakir Guri[1] and Michael N. Hall[1,*]

Cancer is a complex disease and a leading cause of death worldwide. Extensive research over decades has led to the development of therapies that target cancer-specific signaling pathways. However, the clinical benefits of such drugs are at best transient due to tumors displaying intrinsic or adaptive resistance. The underlying compensatory pathways that allow cancer cells to circumvent a drug blockade are poorly understood. We review here recent studies suggesting that mammalian TOR (mTOR) signaling is a major compensatory pathway conferring resistance to many cancer drugs. mTOR-mediated resistance can be cell-autonomous or non-cell-autonomous. These findings suggest that mTOR signaling should be monitored routinely in tumors and that an mTOR inhibitor should be considered as a co-therapy.

Resistance Mechanisms Limit the Success of Cancer Therapeutics

Over recent decades many small molecules have been developed to specifically target oncogenic pathways. However, with few exceptions, these drugs as a single agent have not led to a cure. The limited success of targeted drugs is due to tumors displaying resistance. Two modes of cancer drug resistance exist, intrinsic and adaptive (also referred to as evasive or acquired). Intrinsic resistance is non-responsiveness to a therapy, whereas adaptive resistance is defined as responsiveness followed by relapse. Intrinsic resistance is generally the result of a tumor widely containing a pre-existing mutation that confers resistance in a cell-autonomous manner. Adaptive resistance can be similarly inherent to the cancer cell, but with the genetic or epigenetic change arising upon treatment rather than pre-existing. Importantly, adaptive resistance can also be non-inherent (i.e., non-cell-autonomous) in which resistance relies on the tumor microenvironment. This latter mechanism involving the microenvironment can be viewed as a 'physiological' stress response in which cancer cells are supported by neighboring cells. Understanding the factors that confer intrinsic or adaptive resistance is important for patient stratification and the rational design of combination therapies. Recent studies suggest that sustained mTOR signaling, in cancer cells or cells of the microenvironment, confers resistance to various primary targeted cancer therapies. Thus, mTOR signaling appears to be a major compensatory pathway conferring resistance to targeted therapies.

The mTOR Signaling Pathway

Growth and proliferation are highly regulated. The evolutionarily conserved serine/threonine kinase target of rapamycin (TOR) integrates various stimuli to control the metabolic pathways that drive cell growth and proliferation (Figure 1). TOR forms two structurally and functionally distinct multiprotein complexes termed TOR complex 1 (TORC1) and TORC2 (reviewed in [1,2]). In mammals, mTORC1 contains mTOR, mammalian lethal with sec-13 protein 8 (mLST8), and regulatory associated protein of mammalian target of rapamycin (RAPTOR). mTORC1 is activated by growth factors, nutrients, and cellular energy (reviewed in [3,4]), and is acutely

Trends

The clinical benefit of targeted cancer drugs is limited owing to intrinsic or adaptive resistance. Mechanisms of resistance can be cancer cell-autonomous or non cell-autonomous.

Drugs can alter the tumor microenvironment, resulting in dynamic rewiring of signaling circuits and resistance in neighboring cancer cells.

mTOR signaling is a major compensatory pathway allowing cancer cells to escape the effects of targeted drugs.

mTOR inhibitors should be considered as a co-therapy to prevent resistance to other targeted cancer drugs.

Phosphoproteomics is a novel approach for elucidating mechanisms of resistance to targeted therapies.

[1]Biozentrum, University of Basel, Basel, Switzerland

*Correspondence: m.hall@unibas.ch (M.N. Hall).

 http://dx.doi.org/10.1016/j.trecan.2016.10.006

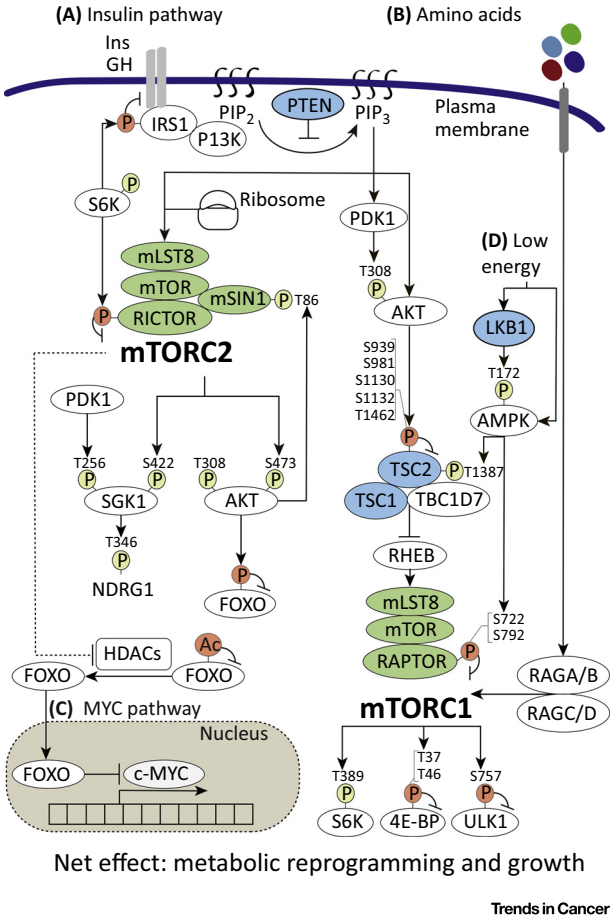

Figure 1. mTOR Signaling Network. mTOR signaling promotes cancer cell growth, survival, and proliferation. (A) Growth factors such as insulin (Ins) stimulate PI3K to convert phosphatidylinositol-4,5-bisphosphate (PIP_2) to phosphatidylinositol-3,4,5-trisphosphate (PIP_3). PIP_3 stimulates PDK1 to phosphorylate (P) AKT at T308. AKT phosphorylates TSC2 on multiple sites, thereby inhibiting its GAP activity toward RHEB. GTP-loaded RHEB binds to and activates mammalian TOR complex 1 (mTORC1). Growth factors also activate mTORC2 in a PI3K- and ribosome-dependent manner. mTORC2 phosphorylates and activates the AGC kinase family members SGK1 and AKT. mTORC2 phosphorylates AKT at Ser473. mTORC2 is not upstream of mTORC1 because AKT Ser473 phosphorylation is not required for mTORC1 activation. (B) Amino acids stimulate mTORC1 by promoting the conversion of RAS-related GTP-binding protein (RAG) heterodimers to the active conformation, in which RAGA or RAGB is loaded with GTP, and RAGC or RAGD is loaded with GDP. Active RAG heterodimer recruits mTORC1 to the surface of the lysosome where mTORC1 encounters its direct activator RHEB. (C) c-MYC, whose expression is repressed by FOXO, mediates cancer cell metabolic reprogramming. In an AKT-independent manner, mTORC2 inhibits class II HDACs, thereby increasing FOXO acetylation (Ac). Ac-FOXO is retained in the cytoplasm, unable to inhibit c-MYC expression. mTORC2 also inhibits FOXO via AKT. (D) In response to low energy (high AMP/ATP ratio), AMP-activated protein kinase (AMPK) inhibits mTORC1 activity by phosphorylating RAPTOR at S792 and S722, and by phosphorylating TSC2. The tumor-suppressor liver kinase B1 (LKB1) activates AMPKα by phosphorylating T172 in the activation loop. Blue-colored proteins are tumor-suppressors that inhibit mTOR activity. Phosphorylation depicted in green is an activation signal and phosphorylation depicted in red is an inhibitory signal. Abbreviations: Ac, acetylation; GH, growth hormone; NDRG1, N-MYC downstream-regulated gene 1.

inhibited by the macrolide rapamycin. Rapamycin (and its analogs known as rapalogs) binds to the cytoplasmic protein FKBP12 (FK506-binding protein 12), and the FKBP12–rapamycin complex then binds to the FRB (FK506-binding protein/rapamycin-binding) domain in mTOR of mTORC1 [5]. Several mTOR inhibitors are approved or in clinical trials for cancer therapy (reviewed in [5–7]). mTORC2 is not acutely inhibited by rapamycin, presumably because the FRB domain in mTOR in mTORC2 is masked [8]. Growth factors and cellular energy stimulate mTORC1 via inhibition of the heterotrimeric protein complex consisting of tuberous sclerosis

complex 1 (TSC1), TSC2, and TRE2–BUB2–CDC16 domain family member 7 (TBC1D7) [9–14], hereafter referred to as the TSC complex. Insulin (or other growth factors) bind to receptor tyrosine kinases (RTKs) to activate phosphatidylinositol-4,5-bisphosphate 3-kinase (PI3K). PI3K phosphorylates the inositol ring of the membrane phospholipid phosphatidylinositol-4,5-bisphosphate (PIP_2) to generate phosphatidylinositol-3,4,5-trisphosphate (PIP_3) [15]. PIP_3 recruits phosphoinositide-dependent kinase 1 (PDK1) and AKT to the plasma membrane [16]. PDK1 phosphorylates Thr308 in the activation loop of AKT and thereby activates AKT [17]. Phosphatase and tensin homolog deleted on chromosome 10 (PTEN) converts PIP_3 to PIP_2, counteracting the activity of PI3K. AKT phosphorylates TSC2, thereby inducing lysosomal release and inhibition of the TSC complex [10,11,18]. The TSC complex is a GTPase-activating protein (GAP) for the lysosomal GTP-binding protein RAS homolog enriched in brain (RHEB). GTP-loaded RHEB interacts with the mTOR catalytic domain and activates mTORC1 [19]. mTORC1 promotes anabolic processes such as protein, lipid, and nucleotide biosynthesis, and inhibits catabolic processes such as autophagy. Notable downstream targets of mTORC1 are ribosomal protein S6 kinase (S6K), eukaryotic translation initiation factor 4E binding proteins (4E-BPs), and the autophagy activating Unc-51-like kinase 1 (ULK1) (reviewed in [20–22]) (Figure 1). mTORC2 contains mTOR, mLST8, mammalian stress-activated mitogen-activated protein kinase (MAPK)-interacting protein 1 (mSIN1), and rapamycin-insensitive companion of mTOR (RICTOR). Growth factors activate mTORC2 by promoting association of mTORC2 with ribosomes in a PI3K-dependent manner [23]. PIP_3 interacts with the PH domain of mSIN1 to trigger mTORC2 activation [24]. mTORC2 regulates several cellular processes via activation of the AGC kinase family members AKT, protein kinase C (PKC), and serum/glucocorticoid-regulated kinase (SGK) (reviewed in [25,26]). mTORC2 phosphorylates Ser473 in AKT. In a positive feedback loop, AKT phosphorylates mSIN1-Thr86 in mTORC2 [27]. In a negative feedback loop, mTORC1 via S6K phosphorylates and inhibits the insulin receptor substrate 1 (IRS-1), thereby dampening PI3K signaling [28–30] (Figure 1). mTORC1 and mTORC2 are frequently activated in human cancers. Genetically engineered mouse models with ectopic activation of mTORC1 or mTORC2 develop cancer [31–34]. mTOR, often in the context of positive and negative feedback loops, is a node for convergence and crosstalk of several oncogenic pathways (Figures 1,2) [30,35–37].

mTOR Signaling in Cell-Autonomous Resistance

Extracellular signal-regulated kinase (ERK) is a MAPK and the major effector of the GTPase Kirsten rat sarcoma viral oncogene homolog (KRAS) (Figure 2). Ligand-mediated activation of RTKs triggers GTP loading of KRAS, which then recruits the kinase BRAF to the plasma membrane for activation [38]. BRAF phosphorylates and activates the MAPK kinase MEK. MEK activates ERK that in turn phosphorylates cytoplasmic signaling proteins, including p90 ribosomal S6 kinase (RSK). ERK and RSK phosphorylate and inhibit TSC2, leading to activation of mTORC1. Furthermore, it has been suggested that RSK phosphorylates several sites in RAPTOR to enhance mTORC1 activity [39]. Finally, ERK and mTORC1 provide distinct activating inputs to eukaryotic translation initiation factor 4E (eIF4E), thereby promoting cap-dependent mRNA translation [40]. Thus, mTOR and ERK signaling are functionally related.

The ERK kinase network is constitutively active in about 40% of human melanomas [41] (Figure 2). Loss of the tumor-suppressor PTEN, which leads to activation of mTOR signaling, confers poor response to BRAF inhibitors in melanoma patients [42–44]. Indeed, these patients define a distinct subset of melanoma that is resistant to BRAF inhibitors. Melanoma cell lines and human patient samples that exhibit resistance to BRAF, MEK, or ERK inhibitors display enhanced S6-S235/236 and S240/244 [45,46] or AKT-Ser473 phosphorylation [47–49], readouts of mTORC1 and mTORC2, respectively. Thus, PI3K–mTOR signaling appears to compensate for loss of ERK signaling and thereby confers resistance to BRAF-MEK-ERK inhibitors. mTOR may compensate by substituting for ERK signaling in phosphorylating particular substrates [50].

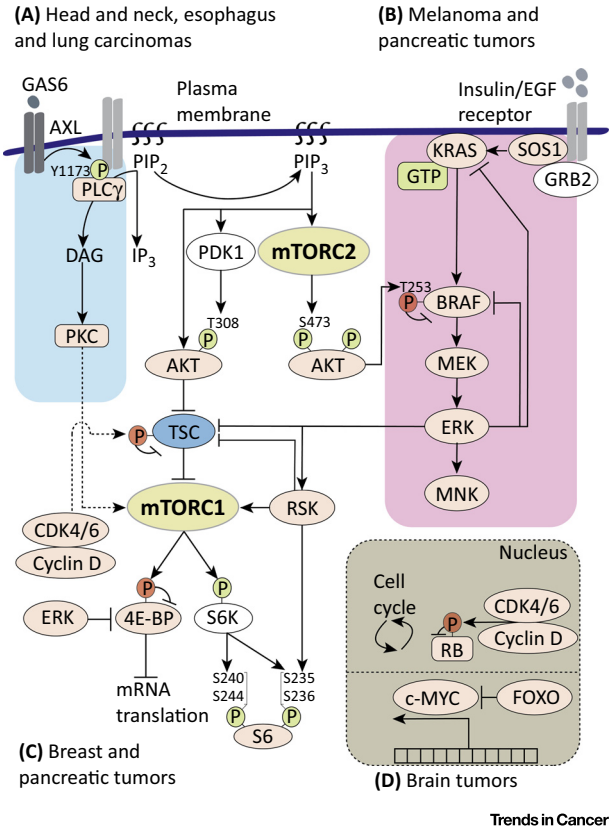

Figure 2. mTOR Signaling and Resistance to Targeted Drugs. (A) AXL is a RTK that is activated through ligand (GAS6)-dependent or -independent dimerization. In head and neck, and esophageal squamous cell carcinomas dimerization of AXL and EGFR contributes to drug resistance via activation of mTORC1. AXL phosphorylates EGFR at Y1173 that in turn serves as a docking site for phospholipase Cγ (PLCγ). PLCγ at the plasma membrane cleaves PIP_2 to produce the second messengers diacylglycerol (DAG) and inositol 1,4,5-trisphosphate (IP_3). DAG activates members of the serine/threonine protein kinase C (PKC) family. By an unknown mechanism, PKC activates mTORC1, thereby promoting resistance to several drugs. (B) The mTOR and ERK pathways respond to extracellular and intracellular cues to control cell survival, proliferation, and metabolism. SOS1 is a guanine nucleotide exchange factor for the GTPase KRAS. GTP-loaded KRAS recruits BRAF kinase to the plasma membrane for activation. BRAF phosphorylates and activates MEK. MEK activates ERK that phosphorylates cytoplasmic signaling proteins, including RSK and MNK. ERK and RSK phosphorylate and inhibit TSC2, thereby activating mTORC1. RSK phosphorylates RAPTOR on several sites to enhance mTORC1 activity. RSK also phosphorylates ribosomal protein S6 at the Ser235 and Ser236. ERK and mTORC1 provide distinct and complementary inputs to eIF4E, thereby promoting mRNA translation (not shown). The ERK pathway is activated in melanoma and pancreatic tumors. In these tumors, targeted inhibition of the ERK pathway promotes both mTORC1 and mTORC2 activation, and thereby resistance to the ERK pathway inhibitors. (C) The cyclin D–cyclin-dependent kinase (CDK) 4/6–retinoblastoma (RB) pathway regulates cell-cycle progression. Unphosphorylated RB binds to and inhibits E2F transcription factors. CDK4/6–cyclin D phosphorylates the tumor-suppressor RB that dissociates from E2F, allowing cell-cycle progression. Resistance to CDK4/6 inhibitors is associated with increased mTORC1 activity in breast and pancreatic cancers. Although the connection between CDK4/6–cyclin D and mTORC1 signaling is poorly understood, mTORC1 activation limits the killing effect of cell-cycle inhibitors. (D) Brain tumor cells containing an EGFRvIII amplification exhibit enhanced mTORC2 activity. mTORC2 mediates metabolic reprogramming and resistance to targeted drugs by increasing expression of c-MYC. Abbreviations: GRB2, growth factor receptor-bound protein 2; RTK, receptor tyrosine kinase; SOS, son of sevenless homolog 1.

PI3K activating mutations are common in various human cancers [51]. In breast cancer cells containing a *PIK3CA* mutation, resistance to the PI3K inhibitor BLY719 correlates with S6 hyperphosphorylation, and mTOR inhibition restores sensitivity to BLY719 [52]. Similarly, mTOR signaling confers resistance to PI3K inhibitors in thyroid tumor cells [53]. Thus, mTOR activation confers resistance to PI3K inhibitors.

The transcription factor c-MYC promotes tumor progression and metabolic adaptation [54] (Figure 2). mTORC2-dependent c-MYC overexpression, and thereby enhanced aerobic glycolysis, confers resistance to a PI3K inhibitor in glioblastoma multiforme (GBM) [47,55]. Thus, mTOR appears to confer resistance to PI3K inhibitors also via upregulation of c-MYC.

The cyclin-dependent kinase (CDK) 4/6–retinoblastoma (RB) pathway regulates cell-cycle progression [56] and is implicated in various cancers [56–58] (Figure 2). Unphosphorylated RB binds and represses E2 family (E2F) transcription factors. CDK4/6 in association with cyclin D1 phosphorylates the tumor-suppressor RB that in turn dissociates from E2F, allowing cell-cycle progression. Resistance to CDK4/6 inhibitors is associated with increased mTORC1 activity in cell lines [59] as well as in mouse models of breast [60] and pancreatic [61] cancers. Although the connection between CDK4/6–cyclin D and mTORC1 signaling is poorly understood, these studies indicate that mTORC1 activation limits the killing effect of cell-cycle inhibitors. Interestingly, phosphorylated RB appears to interact directly with mSIN1 to inhibit mTORC2 [62], suggesting that mTORC2 activation may occur in response to a CDK4/6 inhibitor and confer resistance to the drug. Thus, an ATP competitive pan-mTOR inhibitor that targets both mTORC1 and mTORC2 could be considered as a co-therapy with a CDK4/6 inhibitor.

AXL is a member of the TAM (TYRO, AXL, and MER) family of receptor tyrosine kinases (reviewed in [63,64]) (Figure 2). AXL is activated in many ways including homodimerization or heterodimerization with a non-TAM receptor [65]. AXL activation is associated with acquired resistance to PI3K, RTK, BRAF, and MEK inhibitors [66]. In head and neck, and esophageal squamous cell carcinoma cells treated with a PI3K inhibitor, AXL dimerizes with and phosphorylates EGFR. Phosphorylated EGFR-Y1173 is a docking site for phospholipase Cγ (PLCγ). PLCγ, via the second messenger diacylglycerol (DAG), activates the serine/threonine protein kinase C (PKC). Via an unknown mechanism, PKC activates mTORC1 [67], thereby conferring resistance to the PI3K inhibitor [68] (Figure 2). In cell lines and human lung tumor samples, AXL activation is associated with resistance to the EGFR inhibitors erlotinib [69] and gefitinib [70], respectively. Given the above study demonstrating that AXL can activate EGFR and ultimately mTORC1 to confer resistance to a PI3K inhibitor, AXL-mediated resistance to EGFR inhibitors is possibly also via mTORC1.

The above studies indicate that activation of the mTOR pathway can confer resistance to various targeted therapies. This underscores the complex interplay between mTOR and other major oncogenic pathways, and how such interplay can be exploited for resistance. These studies also suggest that patients should be routinely monitored for mTOR activity, and a co-therapy with an mTOR inhibitor should be considered. Clearly, the clinical application of combination therapies should be evaluated against the risk of side effects, in particular the combination of mTOR and MAPK inhibitors [71,72].

What are the genetic alterations leading to activation of mTOR signaling and cell-autonomous resistance? Cancer cell lines exposed to increasing doses of gefitinib exhibit *MET* (receptor tyrosine kinase) gene amplification, which in turn leads to PI3K–mTOR pathway activation and gefinitib resistance [73]. Although not equivalent to activating a compensatory pathway, mutation of the FRB domain in mTOR in a human thyroid carcinoma conferred resistance to the allosteric mTOR inhibitor everolimus (rapamycin), possibly accounting for the patients' relapse [74]. Although little is known about the mTOR activating mutations that confer cell-autonomous resistance, these studies suggest that such alterations occur within *MTOR* or in a gene encoding an mTOR regulator.

mTOR Signaling in Non-Cell-Autonomous Resistance

mTOR signaling can also confer resistance to targeted drugs in a non-cell-autonomous manner (Figure 3). In this case, activation of mTOR in cells of the tumor microenvironment confers

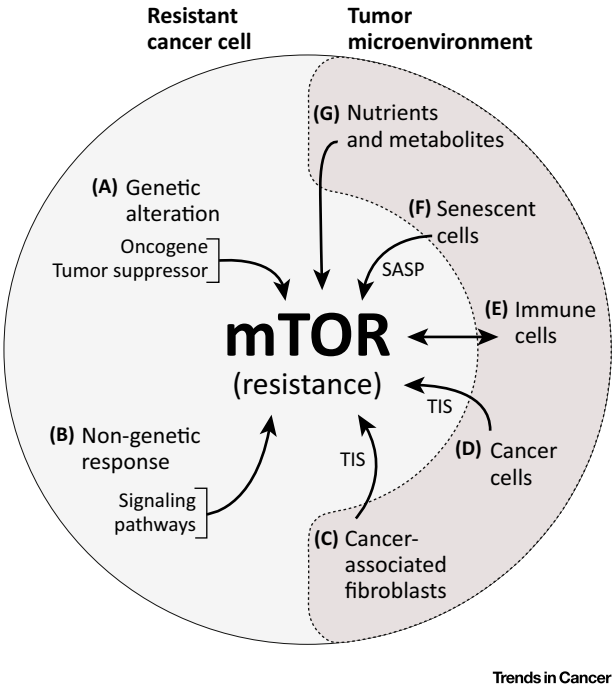

Figure 3. mTOR Confers Resistance in Response to Changes in Cancer Cells or in Stromal Cells (Tumor Microenvironment). Resistance to a targeted therapy can be inherent to the cancer cell or rely on the tumor microenvironment. (A,B) Cancer cell-inherent mechanisms of resistance can be genetically or non-genetically determined. Genetic alterations that activate mTOR to confer resistance may be loss of a tumor-suppressor or acquisition of an oncogene. Non-genetic responses that confer resistance may be dynamic, compensatory signaling changes induced by the drug.

A tumor is a mixture of transformed and non-transformed cells supported by an extracellular matrix, which together form the so-called tumor microenvironment. (C,D) Cells of the tumor microenvironment, in addition to cancer cells, include immune, vasculature, and lymphatic cells as well as cancer-associated fibroblasts (CAFs). Antitumor drugs affect both cancer cells and other cells of the microenvironment. In response to a drug the cells of the tumor microenvironment, such as CAFs or cancer cells that respond to the drug, secrete poorly defined factors referred to as the TIS (therapy-induced secretome). The TIS can act in a paracrine manner to promote resistance. (E) Immune cells play an important role in tumor eradication. mTOR in cancer cells promotes the expression of PD-L1 to suppress tumor-invading immune cells. (F) mTOR in senescent cells regulates the senescence-associated secretory phenotype (SASP). SASP is composed of various cytokines, growth factors, and proteases that modulate the tumor microenvironment. mTORC1 mediates SASP secretion from senescent cells that promotes the resistance and proliferation of nearby cancer cells. (G) Cancer cells operate in different metabolic compartments and secrete metabolites in response to targeted drugs. Nutrients and metabolites in the tumor microenvironment may activate mTORC1 to confer resistance.

resistance on nearby cancer cells. The cells of the microenvironment that confer resistance in a paracrine manner can be stromal cells or cancer cells. Non-autonomous resistance is a drug-induced stress response that is context-dependent and may disappear once the drug (stress) is removed.

Tumors are a heterogeneous population of cells, composed of cancer cells and supporting stromal cells. The therapy-induced secretome (TIS) is a collection of ill-defined factors that are secreted in response to therapy. Stromal TIS can induce extensive changes in the tumor niche to confer drug resistance on nearby cancer cells [75–77]. In this case, the TIS from cancer-associated fibroblasts (CAFs) promotes RTK phosphorylation and thereby mTOR activation in neighboring colorectal or pancreatic cancer cells. In melanoma, the cancer cells respond to the targeted therapy and secrete the TIS component mitogen FOS-related antigen 1 (FRA1). FRA1 activates PI3K–mTOR signaling and promotes resistance in neighboring cancer cells [78]. Finally, mTORC1–4EBP1 signaling controls the TIS in CAFs derived from human pancreatic

tumors [79]. Thus, mTOR plays a dual role in controlling the tumor microenvironment, in other words in sending and receiving the TIS signal to promote cancer resistance to targeted drugs.

Therapy also induces a so-called senescence-associated secretory phenotype (SASP) that can modulate the tumor microenvironment. Therapy may induce cancer cells to secrete SASP factors that are tumorigenic by blunting the effect of the drug on other (non-senescent) cancer cells [80,81]. Two recent studies showed that mTORC1 in senescent cancer cells mediates SASP. Rapamycin selectively abrogates SASP, and thereby improves therapy response in prostate [82] and liver [83] tumor xenografts. This suggests that mTOR can modulate the cancer microenvironment by promoting SASP, and thereby confer therapy resistance in a non-cell-autonomous manner.

Cancer cells present programmed death ligand 1 (PD-L1) to the T cell-borne receptor PD-1. This results in suppression of the T cell, thereby allowing tumor cells to evade killing by the immune system. PD-1 or PD-L1 inhibition, so-called immunotherapy, prevents cancer cells from evading the immune system and is thus an anticancer therapy, particularly effective in the treatment of melanoma. However, PTEN deficient melanomas in which PI3K–mTOR signaling is hyperactive are resistant to immunotherapy. In this context, co-treatment with a PI3K inhibitor improves the efficacy of at least PD-1 inhibition [84]. Furthermore, mTORC1 signaling drives PD-L1 expression in a rapamycin-sensitive manner in mouse models of non-small cell lung carcinoma [85]. Thus, PI3K–mTOR signaling in cancer cells mediates immune evasion and thereby tumor resistance to immunotherapy.

Tumors display complex spatial organization. Cancer cells operate in different metabolic compartments within a tumor and communicate through released metabolites or nutrients. Sonveaux *et al.* [86] showed that cancer cells in hypoxic regions of a tumor perform aerobic glycolysis and consequently excrete lactate. Neighboring cancer cells in normoxic regions of the tumor take up the lactate, via monocarboxylate transporter 1 (MCT1), and utilize it for oxidative respiration. This phenomenon in which tumor cells feed other tumor cells is referred to as metabolic symbiosis. Anti-angiogenic cancer therapy partly disrupts blood vessels, thereby creating hypoxic and normoxic compartments in tumors. Recently, three groups demonstrated that angiogenesis inhibitors induce metabolic symbiosis [87–89]. Importantly, the drug-induced metabolic symbiosis is mTOR-dependent and confers drug resistance [87,88]. Glutamine-activated mTORC1 promotes MCT1 expression and, in turn, lactate uptake in normoxic cells [87,90]. Thus, the normoxic cells utilize lactate as a carbon source, sparing the available glucose for the hypoxic, glycolytic cells that symbiotically feed the normoxic, oxidative cells. The net effect is that cancer cells both near and far from blood vessels survive anti-angiogenic therapy. Rapamycin administration disrupts therapy-induced metabolic symbiosis, leading to tumor regression [87,88]. Furthermore, mTORC1 confers resistance to the glycolysis inhibitor 2-deoxyglucose (2-DG), in a glutaminolysis-dependent manner [91]. In summary, mTORC1 promotes metabolic symbiosis to confer adaptive resistance to angiogenesis inhibitors in a non-cell-autonomous manner.

Concluding Remarks

mTOR signaling is emerging as a major compensatory pathway allowing tumors to escape targeted cancer therapies. mTOR may be a common escape route because it is a central signaling hub functionally related to other oncogenic pathways. Resistance mechanisms can be cell-autonomous or non-cell-autonomous. Non-cell-autonomous resistance is generally adaptive, reversible, and dependent on the tumor microenvironment. Drugs modify the tumor microenvironment, not only the targeted cancer cells. In particular, they stimulate stromal cells and cancer cells to secrete factors that can confer drug resistance to neighboring tumor cells. Importantly, mTOR can mediate both the secretion of such factors and the response to the

Outstanding Questions

What are the cell-autonomous genetic alterations that lead to the activation of mTOR in response to a targeted drug, thereby conferring resistance?

What are the mTOR-dependent non-cell-autonomous changes that could be clinically exploited to limit resistance in cancer cells?

Resistance to a targeted drug is also determined by the spatial and cellular complexity of the tumor. What approaches should be taken to decipher tumor complexity, especially in human tumors?

How can one monitor mTOR activity longitudinally in human patients undergoing targeted therapy?

What regimen should be used for an mTOR inhibitor as a co-therapy?

Box 1. The Use of Phosphoproteomics To Study Mechanisms of Resistance to Targeted Cancer Drugs

Genomic analysis of various human cancers has identified key driver and resistance-conferring mutations, often affecting kinases in signaling pathways [92]. Whereas genomic analysis has been very effective, it only indirectly examines oncogenic signaling pathways. To elucidate signaling changes in response to targeted drugs, phosphorylation cascades can be monitored directly. Mass spectrometry (MS)-based proteomics, in particular phosphoproteomics, is a powerful tool to monitor directly the effect of targeted drugs on oncogenic signaling pathways [93]. However, caution should be taken when performing phosphoproteomics to avoid complications due to rapid dephosphorylation [94]. Phosphoproteins belonging to the MAPK and mTOR signaling pathways are particularly sensitive to ischemia [95] or hypoglycemia. Dynamic signaling cascades are best monitored by analyzing immediately snap-frozen needle biopsies in which tumor conditions are preserved [96].

The usefulness of phosphoproteomics in elucidating resistance mechanisms is underscored by a recent study by Wei *et al.* [97]. Mice transplanted with patient-derived GBM cells were treated with mTOR inhibitors. Cancer cells that developed resistance were then subjected to genomic and phosphoproteomic analyses. Phosphoproteomics revealed marked deregulation of mTOR-related signaling pathways in resistant tumors, suggesting a rewiring of protein signaling networks. However, in-depth genomic analysis did not identify significant genetic changes in resistant tumors versus non-resistant tumors. In another recent study, Dazert *et al.* [50] performed phosphoproteomics on serial biopsies from a sorafenib-treated hepatocellular carcinoma (HCC) patient, taken before and during treatment, to identify mechanisms of resistance to sorafenib. Sorafenib acts by inhibiting RAF (B and C), vascular endothelial growth factor receptor (VEGFR), and platelet-derived growth factor receptor (PDGFR) [98]. Sorafenib is the only approved targeted drug for HCC, with median enhanced survival of <3 months [99]. Dazert and colleagues demonstrated that sorafenib was effective in inhibiting its target in the tumor, based on reduced RSK phosphorylation downstream of BRAF–MEK–ERK signaling. However, phosphorylation of the putative MAPK target Filamin A S2152 and the mTORC1 target S6-S240 was increased in the sorafenib-treated tumor, indicating that a compensatory pathway(s) may have been active in the sorafenib-resistant tumor. Phosphoproteomic analysis of a cohort of patients will provide a more complete picture of the mechanisms of sorafenib resistance.

factors in a recipient cancer cell. The seemingly central role of mTOR in conferring therapy resistance suggests that effective therapy may require combination of an inhibitor of the primary tumor driver and an mTOR inhibitor as co-therapy. To prevent resistance to the co-therapy, intermittent administration should be considered.

Mechanisms of adaptive or intrinsic resistance to targeted drugs are poorly characterized (see Outstanding Questions). The identities of the compensatory signaling pathways and the functional interconnections that underlie resistance are largely unknown. Whereas genomic analysis has been very effective in identifying oncogenic pathways, elucidating the dynamic pathways that confer resistance may require a combination of genomic and phosphoproteomic analyses (Box 1). In particular, tumor biopsies obtained before and during treatment in a longitudinal study should be assessed by mass spectrometry to determine drug-related changes in dynamic phosphorylation cascades. Tumor heterogeneity is a major limitation, especially when human biopsy specimens are limited. Efforts from computational biologists will be important in resolving this complexity.

Acknowledgments

We acknowledge support from Swiss Cancer Research, the European Research Council (MERiC), SystemsX.ch, the Swiss National Science Foundation, and the Canton of Basel.

References

1. Wullschleger, S.R. *et al.* (2006) TOR signaling in growth and metabolism. *Cell* 124, 471–484
2. Laplante, M. and Sabatini, D.M. (2012) mTOR signaling in growth control and disease. *Cell* 149, 274–393
3. Shimobayashi, M. and Hall, M.N. (2016) Multiple amino acid sensing inputs to mTORC1. *Cell Res.* 26, 7–20
4. Dibble, C.C. and Manning, B.D. (2013) Signal integration by mTORC1 coordinates nutrient input with biosynthetic output. *Nat. Cell Biol.* 15, 555–564
5. Benjamin, D. *et al.* (2011) Rapamycin passes the torch: a new generation of mTOR inhibitors. *Nat. Rev. Drug. Discov.* 10, 868–880
6. Ilagan, E. and Manning, B.D. (2016) Emerging role of mTOR in the response to cancer therapeutics. *Trends Cancer* 2, 241–251
7. Liko, D. and Hall, M.N. (2015) mTOR in health and in sickness. *J. Mol. Med.* 93, 1061–1073
8. Gaubitz, C. *et al.* (2015) Molecular basis of the rapamycin insensitivity of target of rapamycin complex 2. *Mol. Cell* 58, 977-898
9. Kenerson, H.L. *et al.* (2002) Activated mammalian target of rapamycin pathway in the pathogenesis of tuberous sclerosis complex renal tumors. *Cancer Res.* 62, 5645–5650
10. Inoki, K. *et al.* (2002) TSC2 is phosphorylated and inhibited by Akt and suppresses mTOR signalling. *Nat. Cell Biol.* 4, 648–657

11. Manning, B.D. *et al.* (2002) Identification of the tuberous sclerosis complex-2 tumor suppressor gene product tuberin as a target of the phosphoinositide 3-kinase/Akt pathway. *Mol. Cell* 10, 151–162
12. Tee, A.R. *et al.* (2002) Tuberous sclerosis complex-1 and -2 gene products function together to inhibit mammalian target of rapamycin (mTOR)-mediated downstream signaling. *Proc. Natl. Acad. Sci. U.S.A.* 99, 13571–13576
13. Kwiatkowski, D.J. *et al.* (2002) A mouse model of TSC1 reveals sex-dependent lethality from liver hemangiomas, and up-regulation of p70S6 kinase activity in Tsc1 null cells. *Hum. Mol. Genet.* 11, 525–534
14. Dibble, C.C. *et al.* (2012) TBC1D7 is a third subunit of the TSC1–TSC2 complex upstream of mTORC1. *Mol. Cell* 47, 535–546
15. Dibble, C.C. and Cantley, L.C. (2015) Regulation of mTORC1 by PI3K signaling. *Trends Cell Biol.* 25, 545–555
16. Pearce, L.R. *et al.* (2010) The nuts and bolts of AGC protein kinases. *Nat. Rev. Mol. Cell Biol.* 11, 9–22
17. Alessi, D.R. *et al.* (1997) Characterization of a 3-phosphoinositide-dependent protein kinase which phosphorylates and activates protein kinase B alpha. *Curr. Biol.* 7, 261–269
18. Menon, S. *et al.* (2014) Spatial control of the TSC complex integrates insulin and nutrient regulation of mTORC1 at the lysosome. *Cell* 156, 771–785
19. Long, X. *et al.* (2005) Rheb binds and regulates the mTOR kinase. *Curr. Biol.* 15, 702–713
20. Ma, X.M. and Blenis, J. (2009) Molecular mechanisms of mTOR-mediated translational control. *Nat. Rev. Mol. Cell Biol.* 10, 307–318
21. Mamane, Y. *et al.* (2006) mTOR, translation initiation and cancer. *Oncogene* 25, 6416–6422
22. Kim, J. *et al.* (2011) AMPK and mTOR regulate autophagy through direct phosphorylation of Ulk1. *Nat. Cell Biol.* 13, 132–141
23. Zinzalla, V. *et al.* (2011) Activation of mTORC2 by association with the ribosome. *Cell* 144, 757–768
24. Liu, P. *et al.* (2015) PtdIns(3,4,5)P3-dependent activation of the mTORC2 kinase complex. *Cancer Discov.* 5, 1194–1209
25. Cybulski, N. and Hall, M.N. (2009) TOR complex 2: a signaling pathway of its own. *Trends Biochem. Sci.* 34, 620–627
26. Sparks, C.A. and Guertin, D.A. (2010) Targeting mTOR: prospects for mTOR complex 2 inhibitors in cancer therapy. *Oncogene* 29, 3733–3744
27. Yang, G. *et al.* (2015) A positive feedback loop between Akt and mTORC2 via SIN1 phosphorylation. *Cell Rep.* 12, 937–943
28. Takano, T. *et al.* (2001) Mammalian target of rapamycin pathway regulates insulin signaling via subcellular redistribution of insulin receptor substrate 1 and integrates nutritional signals and metabolic signals of insulin. *Mol. Cell. Biol.* 21, 5050–5062
29. Um, S.H. *et al.* (2004) Absence of S6K1 protects against age- and diet-induced obesity while enhancing insulin sensitivity. *Nature* 431, 200–205
30. Efeyan, A. and Sabatini, D.M. (2010) mTOR and cancer: many loops in one pathway. *Curr. Opin. Cell Biol.* 22, 169–176
31. Menon, S. *et al.* (2012) Chronic activation of mTOR complex 1 is sufficient to cause hepatocellular carcinoma in mice. *Sci. Signal.* 5, ra24
32. Stiles, B. *et al.* (2004) Liver-specific deletion of negative regulator Pten results in fatty liver and insulin hypersensitivity. *Proc. Natl. Acad. Sci. U.S.A.* 101, 2082–2087
33. Horie, Y. *et al.* (2004) Hepatocyte-specific Pten deficiency results in steatohepatitis and hepatocellular carcinomas. *J. Clin. Invest.* 113, 1774–1783
34. Guertin, D.A. *et al.* (2009) mTOR complex 2 is required for the development of prostate cancer induced by Pten loss in mice. *Cancer Cell* 15, 148–159
35. Shimobayashi, M. and Hall, M.N. (2014) Making new contacts: the mTOR network in metabolism and signalling crosstalk. *Nat. Rev. Mol. Cell Biol.* 15, 155–162
36. Eltschinger, S. and Loewith, R. (2016) TOR complexes and the maintenance of cellular homeostasis. *Trends Cell Biol.* 26, 148–159
37. Chandarlapaty, S. *et al.* (2011) AKT inhibition relieves feedback suppression of receptor tyrosine kinase expression and activity. *Cancer Cell* 19, 58–71
38. Dhillon, A.S. *et al.* (2007) MAP kinase signalling pathways in cancer. *Oncogene* 26, 3279–3290
39. Romeo, Y. *et al.* (2012) Regulation and function of the RSK family of protein kinases. *Biochem. J.* 441, 553–569
40. She, Q.B. *et al.* (2010) 4E-BP1 is a key effector of the oncogenic activation of the AKT and ERK signaling pathways that integrates their function in tumors. *Cancer Cell* 18, 39–51
41. Davies, M.A. and Samuels, Y. (2010) Analysis of the genome to personalize therapy for melanoma. *Oncogene* 29, 5545–5555
42. Aguissa-Toure, A.H. and Li, G. (2012) Genetic alterations of PTEN in human melanoma. *Cell Mol. Life Sci.* 69, 1475–1491
43. Bucheit, A.D. *et al.* (2014) Complete loss of PTEN protein expression correlates with shorter time to brain metastasis and survival in stage IIIB/C melanoma patients with BRAFV600 mutations. *Clin. Cancer Res.* 20, 5527–5536
44. Trunzer, K. *et al.* (2013) Pharmacodynamic effects and mechanisms of resistance to vemurafenib in patients with metastatic melanoma. *J. Clin. Oncol.* 31, 1767–1774
45. Corcoran, R.B. *et al.* (2013) TORC1 suppression predicts responsiveness to RAF and MEK inhibition in BRAF-mutant melanoma. *Sci. Transl. Med.* 5, 196ra98
46. Wee, S. *et al.* (2009) PI3K pathway activation mediates resistance to MEK inhibitors in KRAS mutant cancers. *Cancer Res.* 69, 4286–4293
47. Hayes, T.K. *et al.* (2016) Long-term ERK inhibition in KRAS-mutant pancreatic cancer is associated with MYC degradation and senescence-like growth suppression. *Cancer Cell* 29, 75–89
48. Villanueva, J. *et al.* (2010) Acquired resistance to BRAF inhibitors mediated by a RAF kinase switch in melanoma can be overcome by cotargeting MEK and IGF-1R/PI3K. *Cancer Cell* 18, 683–695
49. Gopal, Y.N.V. *et al.* (2010) Basal and treatment-induced activation of AKT mediates resistance to cell death by AZD6244 (ARRY-142886) in Braf-mutant human cutaneous melanoma cells. *Cancer Res.* 70, 8736–8747
50. Dazert, E. *et al.* (2016) Quantitative proteomics and phosphoproteomics on serial tumor biopsies from a sorafenib-treated HCC patient. *Proc. Natl. Acad. Sci. U.S.A.* 113, 1381–1386
51. Liu, P.X. *et al.* (2009) Targeting the phosphoinositide 3-kinase pathway in cancer. *Nat. Rev. Drug Discov.* 8, 627–644
52. Elkabets, M. *et al.* (2013) mTORC1 inhibition is required for sensitivity to PI3K p110 alpha inhibitors in PIK3CA-mutant breast cancer. *Sci. Transl. Med.* 5
53. Liu, D.X. *et al.* (2009) Genetic alterations in the phosphoinositide 3-kinase/Akt signaling pathway confer sensitivity of thyroid cancer cells to therapeutic targeting of Akt and mammalian target of rapamycin. *Cancer Res.* 69, 7311–7319
54. Dang, C.V. (2013) MYC, Metabolism, cell growth, and tumorigenesis. *Cold Spring Harb. Perspect. Med.* 3
55. Masui, K. *et al.* (2013) mTOR complex 2 controls glycolytic metabolism in glioblastoma through FoxO acetylation and upregulation of c-Myc. *Cell Metab.* 18, 726–739
56. Narasimha, A.M. *et al.* (2014) Cyclin D activates the Rb tumor suppressor by mono-phosphorylation. *Elife* 3
57. Hamilton, E. and Infante, J.R. (2016) Targeting CDK4/6 in patients with cancer. *Cancer Treat Rev.* 45, 129–138
58. Sherr, C.J. *et al.* (2016) Targeting CDK4 and CDK6: from discovery to therapy. *Cancer Discov.* 6, 353–367
59. Zacharek, S.J. *et al.* (2005) Negative regulation of TSC1–TSC2 by mammalian D-type cyclins. *Cancer Res.* 65, 11354–11360
60. Goel, S. *et al.* (2016) Overcoming therapeutic resistance in HER2-positive breast cancers with CDK4/6 inhibitors. *Cancer Cell* 29, 255–269
61. Franco, J. *et al.* (2016) Metabolic reprogramming of pancreatic cancer mediated by CDK4/6 Inhibition elicits unique vulnerabilities. *Cell Rep.* 14, 979–990
62. Zhang, J. *et al.* (2016) Inhibition of Rb phosphorylation leads to mTORC2-mediated activation of Akt. *Mol Cell.* 62, 929–942

63. Graham, D.K. *et al.* (2014) The TAM family: phosphatidylserine sensing receptor tyrosine kinases gone awry in cancer. *Nat. Rev. Cancer* 14, 769–785
64. Lemke, G. (2013) Biology of the TAM receptors. *Cold Spring Harb. Perspect. Biol.* 5, a009076
65. Wu, X.L. *et al.* (2014) AXL kinase as a novel target for cancer therapy. *Oncotarget* 5, 9546–9576
66. Tirosh, I. *et al.* (2016) Dissecting the multicellular ecosystem of metastatic melanoma by single-cell RNA-seq. *Science* 352, 189–196
67. Byers, L.A. *et al.* (2013) An epithelial–mesenchymal transition gene signature predicts resistance to EGFR and PI3K inhibitors and identifies Axl as a therapeutic target for overcoming EGFR inhibitor resistance. *Clin. Cancer Res.* 19, 279–290
68. Elkabets, M. *et al.* (2015) AXL mediates resistance to PI3K alpha inhibition by activating the EGFR/PKC/mTOR axis in head and neck and esophageal squamous cell carcinomas. *Cancer Cell* 27, 533–546
69. Zhang, Z. *et al.* (2012) Activation of the AXL kinase causes resistance to EGFR-targeted therapy in lung cancer. *Nat. Genet.* 44, 852–860
70. Ji, W. *et al.* (2013) Mechanisms of acquired resistance to EGFR-tyrosine kinase inhibitor in Korean patients with lung cancer. *BMC Cancer* 13, 606
71. Shimizu, T. *et al.* (2012) The clinical effect of the dual-targeting strategy involving PI3K/AKT/mTOR and RAS/MEK/ERK pathways in patients with advanced cancer. *Clin. Cancer Res.* 18, 2316–2325
72. Tolcher, A.W. *et al.* (2015) Antitumor activity in RAS-driven tumors by blocking AKT and MEK. *Clin. Cancer Res.* 21, 739–748
73. Engelman, J.A. *et al.* (2007) MET amplification leads to gefitinib resistance in lung cancer by activating ERBB3 signaling. *Science* 316, 1039–1043
74. Wagle, N. *et al.* (2014) Response and acquired resistance to everolimus in anaplastic thyroid cancer. *N. Engl. J. Med.* 371, 1426–1433
75. Liles, J.S. *et al.* (2011) Targeting ErbB3-mediated stromal–epithelial interactions in pancreatic ductal adenocarcinoma. *Br. J. Cancer* 105, 523–533
76. De Boeck, A. *et al.* (2013) Bone marrow-derived mesenchymal stem cells promote colorectal cancer progression through paracrine neuregulin 1/HER3 signalling. *Gut* 62, 550–560
77. Noguchi, H. *et al.* (1999) Expression of heregulin alpha, erbB2, and erbB3 and their influences on proliferation of gastric epithelial cells. *Gastroenterology* 117, 1119–1127
78. Obenauf, A.C. *et al.* (2015) Therapy-induced tumour secretomes promote resistance and tumour progression. *Nature* 520, 368–372
79. Duluc, C. *et al.* (2015) Pharmacological targeting of the protein synthesis mTOR/4E-BP1 pathway in cancer-associated fibroblasts abrogates pancreatic tumour chemoresistance. *EMBO Mol. Med.* 7, 735–753
80. Canino, C. *et al.* (2012) SASP mediates chemoresistance and tumor-initiating-activity of mesothelioma cells. *Oncogene* 31, 3148–3163
81. Di Mitri, D. and Alimonti, A. (2016) Non-cell-autonomous regulation of cellular senescence in cancer. *Trends Cell Biol.* 26, 215–226
82. Laberge, R.M. *et al.* (2015) MTOR regulates the pro-tumorigenic senescence-associated secretory phenotype by promoting IL1A translation. *Nat. Cell Biol.* 17, 1049–1061
83. Herranz, N. *et al.* (2015) mTOR regulates MAPKAPK2 translation to control the senescence-associated secretory phenotype. *Nat. Cell Biol.* 17, 1205–1217
84. Peng, W. *et al.* (2016) Loss of PTEN promotes resistance to T cell-mediated immunotherapy. *Cancer Discov.* 6, 202–216
85. Lastwika, K.J. *et al.* (2016) Control of PD-L1 expression by oncogenic activation of the AKT–mTOR pathway in non-small cell lung cancer. *Cancer Res.* 76, 227–238
86. Sonveaux, P. *et al.* (2008) Targeting lactate-fueled respiration selectively kills hypoxic tumor cells in mice. *J. Clin. Invest.* 118, 3930–3942
87. Allen, E. *et al.* (2016) Metabolic symbiosis enables adaptive resistance to anti-angiogenic therapy that is dependent on mTOR signaling. *Cell Rep.* 15, 1144–1160
88. Jimenez-Valerio, G. *et al.* (2016) Resistance to antiangiogenic therapies by metabolic symbiosis in renal cell carcinoma PDX models and patients. *Cell Rep.* 15, 1134–1143
89. Pisarsky, L. *et al.* (2016) Targeting metabolic symbiosis to overcome resistance to anti-angiogenic therapy. *Cell Rep.* 15, 1161–1174
90. Duran, R.V. *et al.* (2012) Glutaminolysis activates Rag–mTORC1 signaling. *Mol. Cell* 47, 349–358
91. Pusapati, R.V. *et al.* (2016) mTORC1-dependent metabolic reprogramming underlies escape from glycolysis addiction in cancer cells. *Cancer Cell* 29, 548–562
92. Vogelstein, B. *et al.* (2013) Cancer genome landscapes. *Science* 339, 1546–1558
93. Zanivan, S. *et al.* (2013) In vivo SILAC-based proteomics reveals phosphoproteome changes during mouse skin carcinogenesis. *Cell Rep.* 3, 552–566
94. Baker, A.F. *et al.* (2005) Stability of phosphoprotein as a biological marker of tumor signaling. *Clin. Cancer Res.* 11, 4338–4340
95. Mertins, P. *et al.* (2014) Ischemia in tumors induces early and sustained phosphorylation changes in stress kinase pathways but does not affect global protein levels. *Mol. Cell Proteomics* 13, 1690–1704
96. Zahari, M.S. *et al.* (2015) Phosphoproteomic profiling of tumor tissues identifies HSP27 Ser82 phosphorylation as a robust marker of early ischemia. *Sci. Rep.* 5, 13660
97. Wei, W. *et al.* (2016) Single-cell phosphoproteomics resolves adaptive signaling dynamics and informs targeted combination therapy in glioblastoma. *Cancer Cell* 29, 563–573
98. Wilhelm, S.M. *et al.* (2004) BAY 43-9006 exhibits broad spectrum oral antitumor activity and targets the RAF/MEK/ERK pathway and receptor tyrosine kinases involved in tumor progression and angiogenesis. *Cancer Res.* 64, 7099–7109
99. Llovet, J.M. *et al.* (2008) Sorafenib in advanced hepatocellular carcinoma. *N. Engl. J. Med.* 359, 378–390